Formulation and Validation of Vertically Two-Dimensional Shallow-Water Wave Model

by

Bradley D. Johnson, Nobuhisa Kobayashi
and
Daniel T. Cox

RESEARCH REPORT NO. CACR-96-05
July, 1996

CENTER FOR APPLIED COASTAL RESEARCH

Ocean Engineering Laboratory
University of Delaware
Newark, Delaware 19716

DISCLAIMER NOTICE

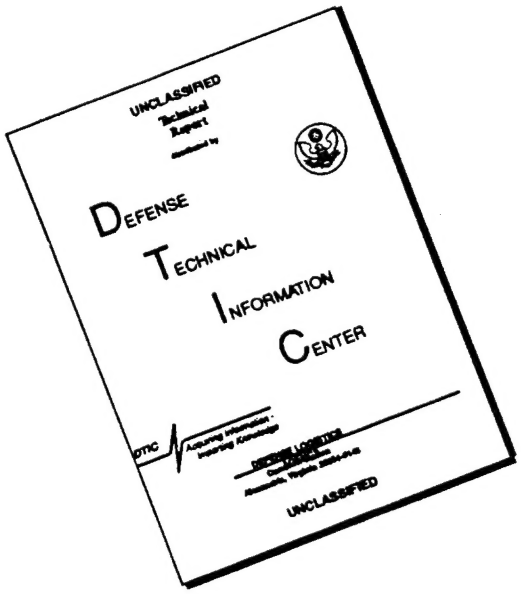

THIS DOCUMENT IS BEST QUALITY AVAILABLE. THE COPY FURNISHED TO DTIC CONTAINED A SIGNIFICANT NUMBER OF PAGES WHICH DO NOT REPRODUCE LEGIBLY.

SF 298 MASTER COPY KEEP THIS COPY FOR REPRODUCTION PURPOSES

REPORT DOCUMENTATION PAGE

Form Approved
OMB NO. 0704-0188

1. AGENCY USE ONLY *(Leave blank)*	2. REPORT DATE	3. REPORT TYPE AND DATES COVERED
	July 1996	Technical

4. TITLE AND SUBTITLE

FORMULATION AND VALIDATION OF VERTICALLY TWO-DIMENSIONAL SHALLOW-WATER WAVE MODEL

5. FUNDING NUMBERS

DAAL03-92-G-0116

6. AUTHOR(S)

Bradley D. Johnson, Nobuhisa Kobayashi and
Daniel T. Cox

7. PERFORMING ORGANIZATION NAMES(S) AND ADDRESS(ES)

UNIVERSITY OF DELAWARE
CENTER FOR APPLIED COASTAL RESEARCH
OCEAN ENGINEERING LABORATORY
NEWARK, DE 19716

8. PERFORMING ORGANIZATION REPORT NUMBER

CACR-96-05

9. SPONSORING / MONITORING AGENCY NAME(S) AND ADDRESS(ES)

U.S. Army Research Office
P.O. Box 12211
Research Triangle Park, NC 27709-2211

10. SPONSORING / MONITORING AGENCY REPORT NUMBER

ARO 30379.45-GS-URI

11. SUPPLEMENTARY NOTES

The views, opinions and/or findings contained in this report are those of the author(s) and should not be construed as an official Department of the Army position, policy or decision, unless so designated by other documentation.

12a. DISTRIBUTION / AVAILABILITY STATEMENT

Approved for public release; distribution unlimited.

12 b. DISTRIBUTION CODE

13. ABSTRACT *(Maximum 200 words)*

Not Furnished

14. SUBJECT TERMS

15. NUMBER IF PAGES

16. PRICE CODE

17. SECURITY CLASSIFICATION OR REPORT	18. SECURITY CLASSIFICATION OF THIS PAGE	19. SECURITY CLASSIFICATION OF ABSTRACT	20. LIMITATION OF ABSTRACT
UNCLASSIFIED	UNCLASSIFIED	UNCLASSIFIED	UL

ACKNOWLEDGMENTS

This work was sponsored by the US Army Research Office, University Research Initiative under contract No. DAAL03-92-G-0116 and by the National Science Foundation under grant No. CTS-9407827.

This work was originally submitted by Bradley D. Johnson in the Spring of 1996 as a thesis at the University of Delaware in partial fulfillment of the requirements for the degree of Master of Civil Engineering.

TABLE OF CONTENTS

LIST OF FIGURES

LIST OF TABLES

ABSTRACT

The computer program VBREAK is developed to predict the time-dependent, two-dimensional velocity field under normally incident breaking waves on beaches and coastal structures. To reduce computation time considerably, use is made of the depth-integrated continuity and horizontal momentum equations. The momentum equation includes the momentum flux correction due to the vertical variation of the horizontal velocity. The bottom shear stress is expressed in terms of the near-bottom horizontal velocity immediately outside the thin wave boundary layer. The third equation for the momentum flux correction is derived from the depth-integrated wave energy equation. In order to express these three one-dimensional, time-dependent equations in terms of the three unknown variables of the water depth, depth-averaged horizontal velocity, and near-bottom horizontal velocity, the normalized vertical profile of the horizontal velocity is assumed to be cubic on the analogy between turbulent bores and hydraulic jumps. Furthermore, the turbulent shear stress is assumed to be expressed using the turbulent eddy viscosity whose mixing length is proportional to the water depth.

The three governing equations are solved using the MacCormack finite difference method for its simplicity and success in the computation of hydraulic jumps. The seaward and landward boundary algorithms are extensions of those used in the previous one-dimensional models such as IBREAK. The developed model VBREAK can function as a one-dimensional model if the momentum flux correction term is assigned to be zero at the seaward boundary. To assess the applicability of the MacCormack method to the shallow-water continuity and momentum equations,

VBREAK is reduced to a one-dimensional model and compared with the previously developed model IBREAK. The differences in the computed depth averaged velocity and free surface are minimal. The MacCormack method is hence considered to be efficient and accurate in the solution of the shallow-water continuity and momentum equations.

The quasi two-dimensional model VBREAK is compared with two laboratory data sets. The first is from the experiment conducted by Stive and outlined in Stive (1980) and Stive and Wind (1982). Finally, the model is compared with the data collected and analyzed by Cox *et al.* (1995). VBREAK predicts the free surface and depth averaged velocity well. The addition of the momentum flux correction in the governing equations has little effect on these quantities as anticipated by Kobayashi and Wurjanto (1992). However, the vertical variation of the horizontal velocity is sensitive to this momentum flux correction because there would be no vertical variation without this correction term. The phase speed is predicted reasonably well. The agreement between the measured and computed vertical variation of the horizontal velocity is effected by the mismatch of the measured and computed phase speed. Although the energy dissipation due to wave breaking is modeled explicitly in VBREAK, energy dissipation in the model is primarily numerical for breaking waves on gentle slopes. This is likely due to the fact that the energy dissipation and associated landward mass flux in the surface roller are not accounted for in VBREAK. Nevertheless, VBREAK predicts the vertical variation of the horizontal velocity measured below the trough reasonably well.

Originally, this work was submitted by Bradley D. Johnson in the Spring of 1996 as a thesis (Johnson 1996) at the University of Delaware in partial fulfillment of the requirements for the degree of Master of Civil Engineering. A summary of this report is being presented at the 25^{th} International Conference of Coastal Engineering(Johnson *et al.* 1996).

Chapter 1

INTRODUCTION

Available time-dependent, one-dimensional and other numerical models for breaking and nonbreaking waves on inclined structures and beaches were reviewed by Kobayashi and Poff (1994). The one-dimensional shallow-water models (e.g., Kobayashi and Wurjanto 1989; Kobayashi and Poff 1994) are relatively simple and robust. Generally, these models predict the free surface elevation fairly accurately, within about 20% errors. Raubenheimer *et al.* (1995) showed that the one-dimensional, shallow-water model was in good agreement with the variations of wave spectra and shapes (e.g., wave skewness) measured across the inner surf and swash zones on a gently sloping natural beach.

The one-dimensional models predict only the depth-averaged horizontal velocity. The vertical velocity may be estimated using the two-dimensional continuity equation together with the computed depth-averaged velocity, while the bottom shear stress may be expressed by a quadratic friction equation based on the depth-averaged velocity. The comparisons with the experiment for regular waves spilling on a rough, impermeable 1:35 slope conducted by Cox *et al.* (1995) indicated that the horizontal velocity measured below the wave trough level was represented by the computed depth-averaged velocity reasonably well. The computed vertical velocity represented the measured vertical velocity at least qualitatively except under the wave crest. The temporal variation of the bottom shear stress was predicted poorly because errors in the computed horizontal velocity were magnified in the computed

bottom shear stress and because the bottom friction factor was not really constant. These limited comparisons suggest that a vertically two-dimensional model will be required to predict the detailed vertical variations of the fluid velocities and shear stress which are essential for predicting cross-shore sediment transport on beaches and hydrodynamic forces acting on armor units on coastal structures (e.g., Tørum 1994).

A simplified two-dimensional model is developed in this report. To reduce computational efforts considerably, the normalized vertical variation of the horizontal velocity outside the wave boundary layer is assumed to be cubic. The vertically two-dimensional problem is then reduced to a depth-integrated one-dimensional problem in which the three time-dependent, one-dimensional differential equations for the water depth h, depth-averaged horizontal velocity U and near-bottom horizontal velocity u_b need to be solved numerically. The simplified two-dimensional model called VBREAK is computationally as efficient as the previous one-dimensional models such as RBREAK2 (Kobayashi and Poff 1994). As a result, VBREAK can be applied easily and routinely using workstations.

1.1 Outline of Report

The approximate governing equations adopted for VBREAK are derived in Chapter 2. First, approximate two-dimensional equations for shallow-water waves on relatively gentle slopes are derived from the continuity and Reynolds equations. The approximate two-dimensional equations are then integrated vertically to obtain the depth-integrated continuity and horizontal momentum equations. This momentum equation includes the unknown momentum flux correction m due to the vertical variation of the horizontal velocity u. An equation for the momentum flux correction m is derived from the depth-integrated wave energy equation (Kobayashi and Wurjanto 1992). The bottom shear stress and wave energy dissipation inside the thin wave boundary layer are expressed in terms of the near-bottom horizontal

velocity u_b and the wave friction factor (Jonsson 1966; Cox *et al.* 1995). The vertical variation of the normalized horizontal velocity u outside the wave boundary layer is assumed to be cubic on the analogy between turbulent bores and hydraulic jumps (Madsen and Svendsen 1983; Svendsen and Madsen 1984). The momentum flux correction m and the wave energy dissipation rate outside the wave boundary layer due to wave breaking are then expressed in terms of h, U and u_b. The three depth-integrated continuity, horizontal momentum, and momentum flux correction equations may thus be solved numerically to obtain the temporal and cross-shore variations of h, U and u_b.

The numerical procedures adopted to solve the three governing equations with appropriate initial and boundary conditions are explained in detail in Chapter 3 of this report. The MacCormack finite difference method (MacCormack 1969) is selected because of its simplicity and success in the computation of unsteady open channel flows with hydraulic jumps (Chaudhry 1993). The computation is initiated at the time $t = 0$ when the specified incident wave train arrives at the seaward boundary and no wave action exists in the computation domain. The interval Δt of each time step for the time-marching computation is calculated using an approximate stability criterion of the adopted explicit finite difference method. Approximate seaward boundary conditions are used to compute the boundary values of h, U and u_b as well as the reflected wave train using the method of characteristics (Kobayashi *et al.* 1987, 1989). The landward boundary algorithm used in RBREAK2 (Kobayashi and Poff 1994) is modified to compute wave runup on the slope which is assumed to be impermeable. The details of the computer program VBREAK have been published separately in the report by Kobayashi and Johnson (1995).

In Chapter 4, the model VBREAK is initially compared with a previously developed one-dimensional model IBREAK (Kobayashi and Wurjanto 1989). The

model VBREAK is reduced to the corresponding one-dimensional model through the appropriate simplification of the boundary condition for the momentum flux correction. The two models are then based on the same governing equations. The MacCormack method is assesed using one of the tests conducted by Ahrens (1975) with regular waves on a rough 1:2.5 slope. Finally, The numerical model VBREAK is compared with two sets of regular wave data in Chapter 4. One data set is the comprehensive measurements of test 1 presented by Stive (1980) and Stive and Wind (1982) in which the incident regular waves broke as spilling breakers on a concrete 1:40 beach. The other data set is the detailed velocity, bottom shear stress and free surface measurements by Cox *et al.* (1995) for the case of regular waves spilling on a rough, impermeable 1:35 slope.

The summary and conclusions of this report are given in Chapter 5

Chapter 2

MATHEMATICAL FORMULATION

2.1 Two-Dimensional Equations in Shallow Water

The approximate governing equations adopted in the numerical model VBREAK are derived from the two-dimensional continuity and Reynolds equations (e.g., Rodi 1980)

$$\frac{\partial u_j'}{\partial x_j'} = 0 \tag{2.1}$$

$$\frac{\partial u_i'}{\partial t'} + u_j' \frac{\partial u_i'}{\partial x_j'} = -\frac{1}{\rho}\frac{\partial p'}{\partial x_i'} - g\delta_{i2} + \frac{1}{\rho}\frac{\partial \tau_{ij}'}{\partial x_j'} \tag{2.2}$$

in which the prime indicates the physical variables and the summation convention is used with respect to repeated indexes. The symbols used in (2.1) and (2.2) are depicted in Figure 2.1 where t' = time; x_1' = horizontal coordinate taken to be positive landward; x_2' = vertical coordinate taken to be positive upward with $x_2' = 0$ at the still water level (SWL); u_1' = horizontal velocity; u_2' = vertical velocity; ρ = fluid density which is assumed constant; p' = pressure; g = gravitational acceleration; δ_{i2} = Kronecker delta; and τ_{ij}' = sum of turbulent and viscous stresses. Assuming that the viscous stresses are negligible, τ_{ij}' may be expressed as (e.g., Rodi 1980)

$$\tau_{ij}' = \rho\left[\nu_t'\left(\frac{\partial u_i'}{\partial x_j'} + \frac{\partial u_j'}{\partial x_i'}\right) - \frac{2}{3}k'\delta_{ij}\right] \tag{2.3}$$

in which ν_t' = turbulent eddy viscosity; and k' = turbulent kinetic energy per unit mass.

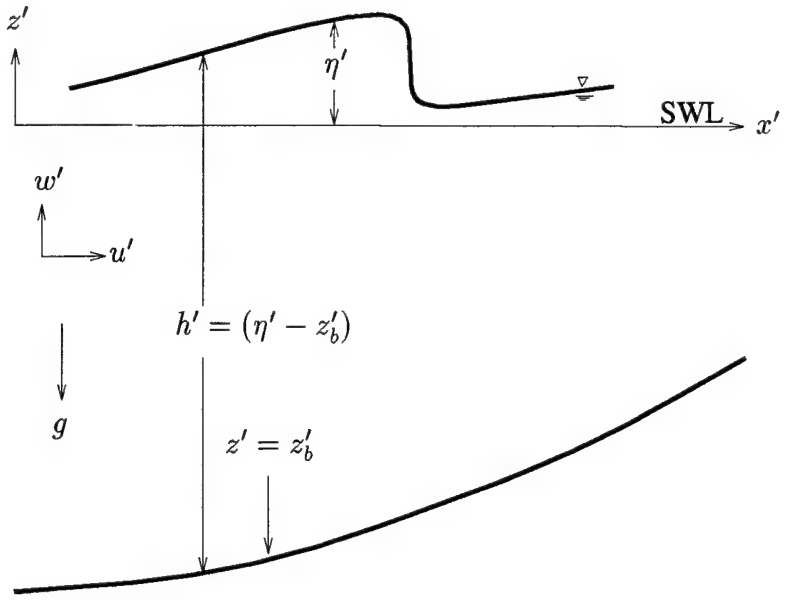

Figure 2.1: Definition sketch.

To simplify (2.1) and (2.2) with (2.3) in shallow water, the dimensional variables may be normalized as

$$t = \frac{t'}{T'} \quad ; \quad x_1 = \frac{x_1'}{T'\sqrt{gH'}} \quad ; \quad x_2 = \frac{x_2'}{H'} \tag{2.4}$$

$$u_1 = \frac{u_1'}{\sqrt{gH'}} \quad ; \quad u_2 = \frac{u_2'}{H'/T'} \quad ; \quad p = \frac{p'}{\rho g H'} \tag{2.5}$$

$$\nu_t = \frac{\nu_t'}{H'^2/T'} \quad ; \quad k = \frac{k'}{\sqrt{gH'}H'/T'} \quad ; \quad \sigma = T'\sqrt{\frac{g}{H'}} \tag{2.6}$$

in which T' and H' are the reference wave period and height used for the normalization. The parameter σ defined in (2.6) is the ratio between the horizontal and vertical length scales. The normalized variables in (2.4) and (2.5) are assumed to

be on the order of unity in shallow water. The normalization of ν_t' and k' in (2.6) is based on the turbulence measurements in a wave flume by Cox *et al.* (1994) which have indicated that ν_t and k are on the order of unity or less inside and immediately outside the surf zone, respectively.

Substituting (2.4)–(2.6) into (2.1)–(2.3), the normalized continuity and momentum equations are obtained. The conventional notations of $x = x_1$, $z = x_2$, $u = u_1$ and $w = u_2$ are used in the following. The normalized continuity equation is given by

$$\frac{\partial u}{\partial x} + \frac{\partial w}{\partial z} = 0 \tag{2.7}$$

The momentum equations are simplified under the assumption of $\sigma^2 \gg 1$ for shallow water waves. The approximate horizontal momentum equation is expressed as

$$\frac{\partial u}{\partial t} + u\,\frac{\partial u}{\partial x} + w\,\frac{\partial u}{\partial z} = -\frac{\partial}{\partial x}\left(p + \frac{2k}{3\sigma}\right) + \frac{\partial \tau}{\partial z} \tag{2.8}$$

with

$$\tau = \nu_t\,\frac{\partial u}{\partial z} \tag{2.9}$$

The approximate vertical momentum equation is written as

$$0 = -\frac{\partial}{\partial z}\left(p + z + \frac{2k}{3\sigma}\right) \tag{2.10}$$

The free surface and bottom are located at $z' = \eta'$ and $z' = z_b'$ as shown in Figure 2.1 where the bottom is assumed to be fixed and impermeable. The water depth h' is given by $h' = (\eta' - z_b')$. The dimensional variables η', z_b' and h' are normalized by the vertical length scale H'

$$\eta = \frac{\eta'}{H'} \quad ; \quad z_b = \frac{z_b'}{H'} \quad ; \quad h = \frac{h'}{H'} \tag{2.11}$$

The kinematic boundary conditions at the free surface and bottom are expressed as

$$\frac{\partial \eta}{\partial t} + u\,\frac{\partial \eta}{\partial x} - w = 0 \qquad \text{at } z = \eta \tag{2.12}$$

$$u\,\frac{\partial z_b}{\partial x} - w = 0 \qquad \text{at } z = z_b \tag{2.13}$$

The normal and tangential stresses at the free surface are assumed to be zero. These boundary conditions for $\sigma^2 \gg 1$ can be shown to yield

$$p + \frac{2k}{3\sigma} = 0 \qquad \text{at } z = \eta \tag{2.14}$$

$$\tau = 0 \qquad \text{at } z = \eta \tag{2.15}$$

Integration of (2.10) with respect to z using (2.14) gives

$$p = \eta - z - \frac{2k}{3\sigma} \tag{2.16}$$

The pressure is approximately hydrostatic in shallow water where k is on the order of unity or less and σ is relatively large to satisfy $\sigma^2 \gg 1$. Substituting (2.16) into (2.8), the horizontal momentum equation is rewritten as

$$\frac{\partial u}{\partial t} + u\,\frac{\partial u}{\partial x} + w\,\frac{\partial u}{\partial z} = -\frac{\partial \eta}{\partial x} + \frac{\partial \tau}{\partial z} \tag{2.17}$$

Eqs. (2.7) and (2.17) together with (2.9), (2.12), (2.13) and (2.15) may be solved numerically but considerable numerical difficulties are expected because the unknown free surface elevation η varies rapidly in space and time. In addition, such a numerical model will be too time-consuming to compute breaking wave motions of long duration.

2.2 Depth-Integrated Equations

To reduce computational efforts significantly, (2.7) and (2.17) are integrated from $z = z_b$ to $z = \eta$ using (2.12), (2.13) and (2.15). No additional approximation is introduced in this integration. The depth-integrated continuity equation is expressed as

$$\frac{\partial h}{\partial t} + \frac{\partial q}{\partial x} = 0 \tag{2.18}$$

where h = water depth given by $h = (\eta - z_b)$; and q = volume flux per unit width defined as

$$q = \int_{z_b}^{\eta} u\, dz \tag{2.19}$$

The depth-integrated horizontal momentum equation is written as

$$\frac{\partial q}{\partial t} + \frac{\partial}{\partial x}\left(qU + m + \frac{1}{2}h^2\right) = -\theta h - \tau_b \tag{2.20}$$

with

$$m = \int_{z_b}^{\eta} (u - U)^2 \, dz \tag{2.21}$$

in which U = depth-averaged horizontal velocity defined as $U = q/h$; θ = normalized bottom slope defined as $\theta = dz_b/dx$; τ_b = bottom shear stress; and m = momentum flux correction due to the vertical variation of the horizontal velocity u where $m = 0$ if $u = U$.

The previous one-dimensional models IBREAK (Kobayashi and Wurjanto 1989), RBREAK (Wurjanto and Kobayashi 1991), and RBREAK2 (Kobayashi and Poff 1994) assumed $m = 0$ and expressed τ_b in terms of U. Eqs. (2.18) and (2.20) with $m = 0$ were solved using the dissipative Lax-Wendroff finite difference method to compute h and q as a function of t and x. These one-dimensional models do not predict the vertical variations of the fluid velocities u and w. Furthermore, these models do not account for energy dissipation due to wave breaking explicitly.

Boussinesq equations have been extended to predict breaking waves on gentle slopes (Zelt 1991; Schäffer *et al.* 1992). Boussinesq equations without the dispersive terms correspond to (2.18) and (2.20) if the bottom friction is included in Boussinesq equations (Zelt 1991). Gharangik and Chaudhry (1991) computed hydraulic jumps using Boussinesq equations with and without the dispersive terms and found that the dispersive terms had little effect on the computed hydraulic jumps. This indicates that the dispersive terms may be negligible for breaking waves inside the surf zone. Moreover, the dispersive terms derived under the assumption of potential flow may not be valid for breaking waves. To include energy dissipation due to wave breaking in Boussinesq equations, Zelt (1991) and Schäffer *et al.* (1992) added a term corresponding to the term for the momentum flux correction m in (2.20). Zelt (1991) expressed this additional term in the form of horizontal momentum diffusion

with an artificial viscosity proposed by Heitner and Housner (1970). The artificial viscosity was calibrated for breaking solitary waves where the diffusion term was activated using a semi-empirical criterion for solitary wave breaking. On the other hand, Schäffer *et al.* (1992) expressed the additional momentum flux using a simple approach based on a surface roller that represented a passive bulk of water riding on the front of a breaking wave. An empirical geometric method was used to determine the shape and location of the surface rollers during the computation. These models do not predict the vertical variations of the fluid velocities. It is also not certain whether the computed energy dissipation was truly caused by the term added to the momentum equation because they did not check whether the computed results satisfied the energy equation as will be elaborated in the following.

In this report, the equation for the momentum flux correction m is derived from the depth-integrated instantaneous wave energy equation (Kobayashi and Wurjanto 1992)

$$\frac{\partial E}{\partial t} + \frac{\partial}{\partial x}\left(E_F\right) = -D \tag{2.22}$$

which is obtained by integrating (2.17) multiplied by u from $z = z_b$ to $z = \eta$ by use of (2.12), (2.13), (2.15) and (2.18). The specific energy E defined as the sum of kinetic and potential energy per unit horizontal area is given by

$$E = \frac{1}{2}\left(qU + m + \eta^2\right) \qquad \text{for } z_b < 0 \tag{2.23}$$

$$E = \frac{1}{2}\left(qU + m + \eta^2 - z_b^2\right) \qquad \text{for } z_b > 0 \tag{2.24}$$

in which the potential energy is taken to be relative to the potential energy in the absence of wave action with SWL at $z = 0$. The energy flux E_F per unit width is expressed as

$$E_F = \eta q + \frac{1}{2}\left(qU^2 + 3mU + m_3\right) \tag{2.25}$$

with

$$m_3 = \int_{z_b}^{\eta} \left(u - U\right)^3 dz \tag{2.26}$$

in which m_3 = kinetic energy flux correction due to the third moment of the velocity deviation $(u - U)$ over the depth where $m_3 = 0$ if $u = U$. The energy dissipation rate D per unit horizontal area in (2.22) is given by

$$D = \int_{z_b}^{\eta} \tau \frac{\partial u}{\partial z} \, dz \tag{2.27}$$

where use is made of the no slip condition $u = 0$ at $z = z_b$.

The wave boundary layer is not analyzed explicitly in this numerical model. The energy dissipation rate D_f inside the wave boundary layer may be estimated by (Jonsson and Carlsen 1976)

$$D_f = \tau_b \, u_b \tag{2.28}$$

where u_b = near-bottom horizontal velocity immediately outside the wave boundary layer. The normalized bottom shear stress τ_b may be expressed as

$$\tau_b = f_w \mid u_b \mid u_b \quad ; \quad f_w = \frac{1}{2} \sigma f'_w \tag{2.29}$$

in which f'_w = wave friction factor (Jonsson 1966). The value of f'_w specified as input is allowed to vary spatially to accommodate the spatial variation of bottom roughness (Kobayashi and Raichle 1994). The previous one-dimensional models (e.g., Kobayashi and Wurjanto 1992) employed (2.27) and (2.28) in which the depth-averaged velocity U and the corresponding friction factor f' were used instead of the near-bottom velocity u_b and the wave friction factor f'_w. Cox *et al.* (1995) showed that the bottom shear stress and near-bottom velocity measured inside the surf zone could be related fairly well by the quadratic friction equation (2.28) with the wave friction factor f'_w estimated using the formula of Jonsson (1966).

The energy dissipation rate D given by (2.26) may be expressed as

$$D = D_f + D_B \tag{2.30}$$

in which D_B = energy dissipation rate outside the wave boundary layer due to wave breaking. Assuming that the thickness of the wave boundary layer is much smaller than the water depth, D_B may be estimated using (2.26) together with (2.9)

$$D_B = \int_{z_b}^{\eta} \nu_t \left(\frac{\partial u}{\partial z}\right)^2 dz \quad \text{outside boundary layer} \tag{2.31}$$

where the vertical variations of u and ν_t outside the wave boundary layer will be assumed in the following.

Rearranging the instantaneous wave energy equation (2.22) with (2.27) and (2.29) by use of (2.18) and (2.20), the equation for the momentum flux correction m is derived

$$\frac{\partial m}{\partial t} + \frac{\partial}{\partial x}\left(3mU + m_3\right) = 2U\,\frac{\partial m}{\partial x} - 2\left(\tau_b \tilde{u}_b + D_B\right) \tag{2.32}$$

with

$$\tilde{u}_b = u_b - U \tag{2.33}$$

in which $\tilde{u}_b$ = near-bottom horizontal velocity correction due to the vertical variation of the horizontal velocity u outside the wave boundary layer. If $u = U$, $\tilde{u}_b = 0$, $m = 0$ and $m_3 = 0$. As a result, (2.31) yields $D_B = 0$ if $u = U$, whereas D_B given by (2.30) outside the wave boundary layer is also zero if u is independent of z. This proves that the energy dissipation due to wave breaking in the previous one-dimensional models based on the assumptions of $\tilde{u}_b = 0$, $m = 0$ and $m_3 = 0$ is solely numerical (Kobayashi and Wurjanto 1992).

In order to express m, m_3 and D_B in terms of $\tilde{u}_b$, the horizontal velocity u outside the wave boundary layer is assumed to be expressible in the form

$$u(t,x,z) = U(t,x) + \tilde{u}_b(t,x)F(\zeta) \tag{2.34}$$

with

$$\zeta = \left[z - z_b(x)\right]/h(t,x) \quad \text{for } 0 \le \zeta \le 1 \tag{2.35}$$

in which F = normalized function expressing the vertical variation of the velocity deviation $(u-U)$ from $\zeta = 0$ immediately outside the wave boundary layer to $\zeta = 1$ at the free surface. Furthermore, the dimensional turbulent eddy viscosity ν_t' outside the wave boundary layer is assumed to be given by

$$\nu_t' = (C_\ell h')^2 \left|\frac{\partial u'}{\partial z'}\right| \tag{2.36}$$

in which C_ℓ = mixing length parameter. The turbulence measurements inside the surf zone by Cox *et al.* (1994) have indicated that (2.35) is a reasonable first approximation outside the wave boundary layer and that C_ℓ is on the order of 0.1. Using (2.4)–(2.6) and (2.11), the normalized turbulent eddy viscosity ν_t corresponding to (2.35) is expressed as

$$\nu_t = C_\ell^2 \sigma\, h^2 \left|\frac{\partial u}{\partial z}\right| \tag{2.37}$$

Substitution of (2.33) with (2.34) and (2.36) into (2.21), (2.25) and (2.30) yields

$$m = C_2 h \tilde{u}_b^2 \quad ; \quad C_2 = \int_0^1 F^2 d\zeta \tag{2.38}$$

$$m_3 = C_3 h \tilde{u}_b^3 \quad ; \quad C_3 = \int_0^1 F^3 d\zeta \tag{2.39}$$

$$D_B = C_B C_\ell^2 \sigma \left|\tilde{u}_b\right|^3 \quad ; \quad C_B = \int_0^1 \left|\frac{dF}{d\zeta}\right|^3 d\zeta \tag{2.40}$$

in which m and D_B are positive or zero.

Madsen and Svendsen (1983) and Svendsen and Madsen (1984) assumed a cubic velocity profile for their analyses of a hydraulic jump and a turbulent bore on a beach. Accordingly, the function F in (2.33) outside the wave boundary layer is assumed to be cubic and expressed as

$$F = 1 - (3 + 0.75a)\zeta^2 + a\zeta^3 \quad \text{for } 0 \le \zeta \le 1 \tag{2.41}$$

in which a = cubic velocity profile parameter. The function F given by (2.40) satisfies (2.19) with $q = Uh$ and (2.32). The shear stress τ given by (2.9) with (2.36) must satisfy (2.15). However, (2.40) yields $\tau = 0$ at $\zeta = 1$ only if $a = 4$.

Moreover, (2.40) results in $\tau = 0$ at $\zeta = 0$ immediately outside the wave boundary layer in contradiction with the turbulence measurements inside the surf zone by Cox *et al.* (1994). Consequently, (2.40) with the single empirical parameter a may not predict the shear stress accurately in the vicinity of the free surface and bottom. Comparison of (2.40) with the cubic profile assumed by Svendsen and Madsen (1984) suggests that the parameter a is approximately 3. The range of a = 3–4 is considered in the following. Substitution of (2.40) into the equations for C_2, C_3 and C_B in (2.37)–(2.39) yields

$$C_2 = 1 + \frac{2b}{3} + \frac{a}{2} + \frac{b^2}{5} + \frac{ab}{3} + \frac{a^2}{7} \tag{2.42}$$

$$C_3 = 1 + b + \frac{3a}{4} + \frac{3b^2}{5} + ab + \frac{3a^2 + b^3}{7} + \frac{3ab^2}{8} + \frac{a^2 b}{3} + \frac{a^3}{10} \tag{2.43}$$

$$C_B = -\left(2b^3 + \frac{36ab^2}{5} + 9a^2 b + \frac{27a^3}{7}\right) \tag{2.44}$$

in which $b = -(3 + 0.75a)$.

Figure 2.2 shows the cubic velocity profile function F given by (2.40) as a function of ζ for a = 3.0, 3.5 and 4.0. The abscissa in Figure 2.2 is the value of $-F$ because $\tilde{u}_b$ in (2.33) is expected to be negative under the wave crest. Figure 2.2 hence depicts the normalized vertical variation of the horizontal velocity deviation $(u - U)$ under the wave crest. The assumed cubic profile is not sensitive to the parameter a in the range of a = 3–4 except in the vicinity of the free surface where no velocity data is available inside the surf zone. Figure 2.3 shows the parameters C_2, C_3 and C_B as a function of the cubic profile parameter a. These parameters vary little for a = 3–4. Figure 2.3 indicates that $C_2 \simeq 0.5$, $C_3 \simeq -0.03$ and $C_B \simeq 13$. In short, Figures 2.2 and 2.3 imply that the computed results will not be sensitive to the empirical parameter a. The mixing length parameter C_ℓ affects only D_B given by (2.39) but will modify the computed magnitude of D_B more than the cubic profile parameter a because D_B is proportional to C_ℓ^2.

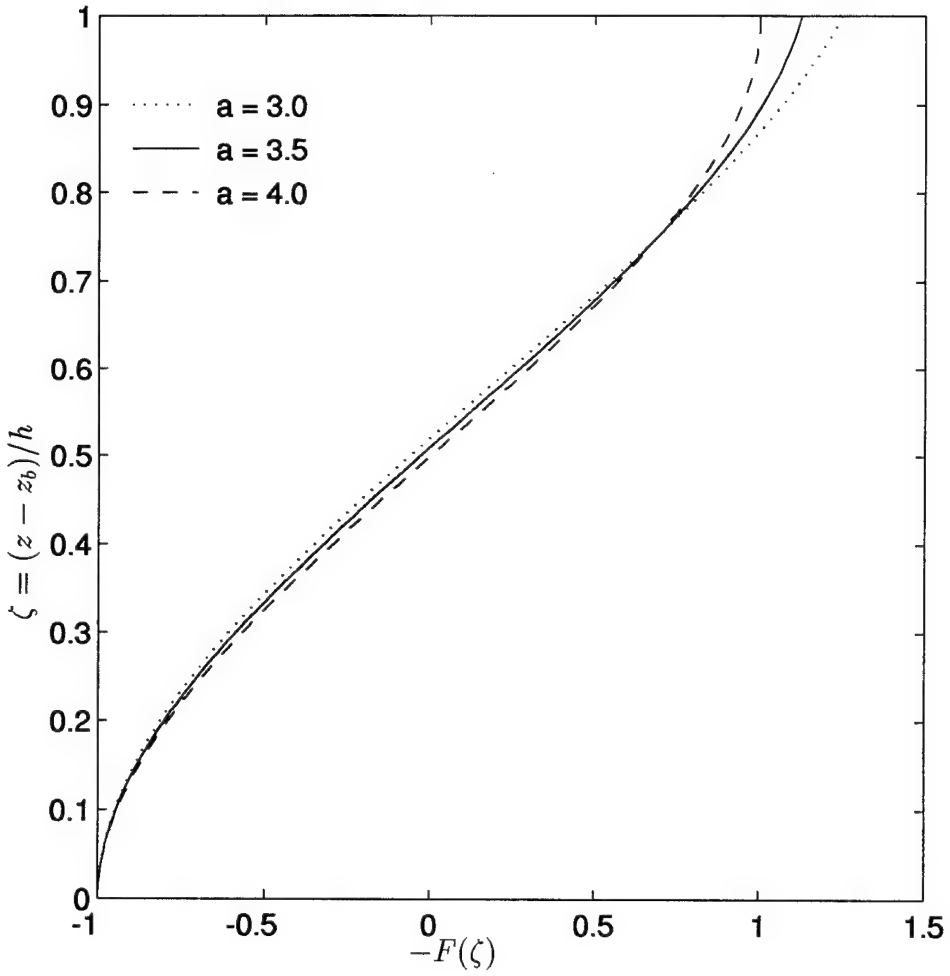

Figure 2.2: Cubic velocity profile function $-F$ as a function of ζ with $\zeta = 0$ at bottom and $\zeta = 1$ at free surface for $a = 3.0$, 3.5, and 4.0.

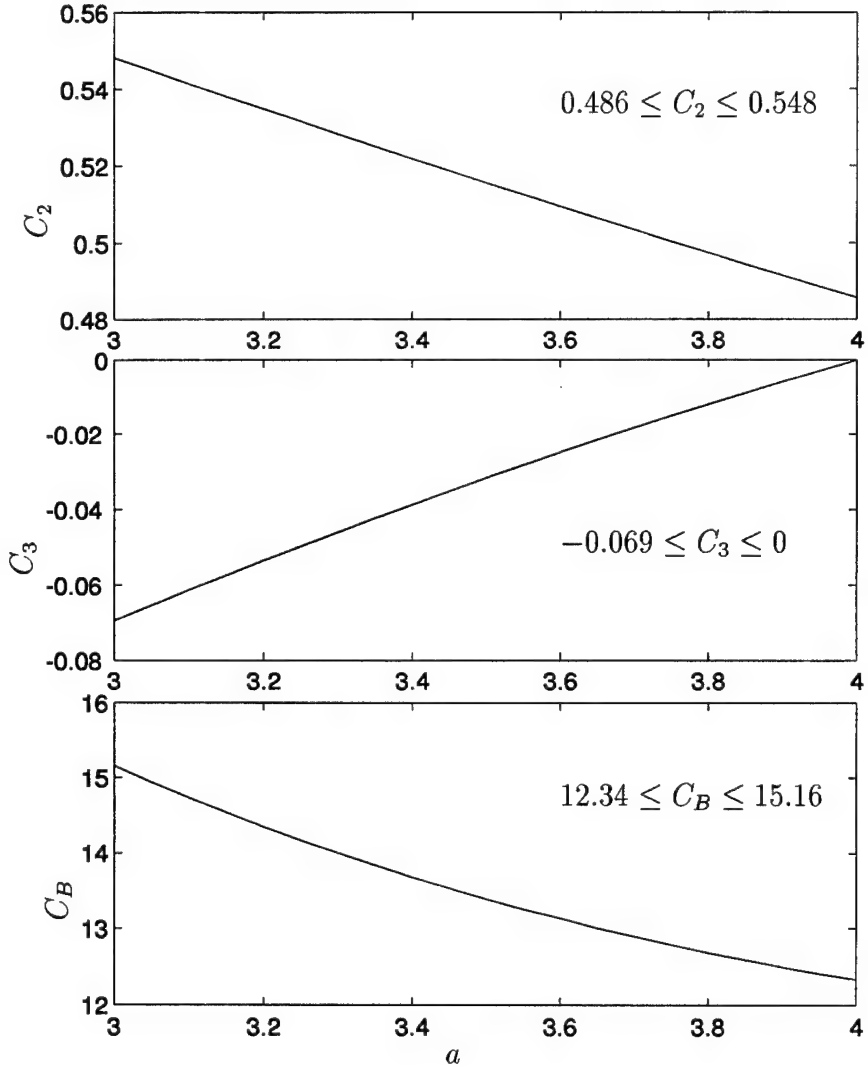

Figure 2.3: C_2, C_3, and C_B as a function of cubic profile parameter a.

Eqs. (2.18), (2.20), and (2.31) together with (2.28), (2.32), and (2.37)–(2.39) will be solved numerically in the next section to compute h, q and m as a function of t and x. To obtain $\tilde{u}_b$ using (2.37) for the computed h and m, it is assumed that

$$\tilde{u}_b = -\left(\frac{m}{C_2 h}\right)^{1/2} \qquad \text{for } U \geq 0 \tag{2.45}$$

$$\tilde{u}_b = \left(\frac{m}{C_2 h}\right)^{1/2} \qquad \text{for } U < 0 \tag{2.46}$$

which ensures that $|u_b| \leq |U|$ with $u_b = (U + \tilde{u}_b)$. It is required in (2.44) that $m \geq 0$. For the computed h, $U = q/h$ and $\tilde{u}_b$, the horizontal velocity u can be obtained using (2.33). The vertical velocity w can be found using the continuity equation (2.7).

$$w = -(z - z_b)\frac{\partial U}{\partial x} - h\frac{\partial \tilde{u}_b}{\partial x}\left[\zeta - \left(1 + \frac{a}{4}\right)\zeta^3 + \frac{a}{4}\zeta^4\right] \tag{2.47}$$

in which ζ is given by (2.34) and use is made of $w = 0$ at $z = z_b$.

To examine the degree of numerical dissipation hidden in the computed results, the instantaneous energy equation (2.22) with (2.29) is averaged from $t = t_{\text{stat}}$ to $t = t_{\max}$

$$\Delta E + \frac{\partial}{\partial x}\left(\overline{E_F}\right) = -\overline{D_f} - \overline{D_B} \tag{2.48}$$

with

$$\Delta E = \frac{E(t = t_{\max}) - E(t = t_{\text{stat}})}{t_{\max} - t_{\text{stat}}} \tag{2.49}$$

in which the overbar denotes the time averaging from the starting time t_{stat} of the statistical calculations to the ending time $t_{\max}$ of the computation as will be explained in Section 3.4. For the computed h, q and m, E, E_F, D_f and D_B are computed using (2.23), (2.24), (2.27) and (2.39), respectively, during $t_{\text{stat}} \leq t \leq t_{\max}$. The computed E, E_F, D_f and D_B will satisfy the time- averaged energy equation (2.46) in the absence of numerical dissipation in the adopted numerical procedures. In the previous one-dimensional models, $\overline{D_B}$ was calculated using (2.46) because these models did not include any physical dissipation mechanism associated with wave breaking.

Chapter 3

NUMERICAL MODEL

3.1 MacCormack Method

To solve (2.18), (2.20) and (2.31) for h, q and m, these equations are combined and expressed in the following vector form:

$$\frac{\partial \mathbf{U}}{\partial t} + \frac{\partial \mathbf{F}}{\partial x} + \mathbf{G} = 0 \tag{3.1}$$

with

$$\mathbf{U} = \begin{bmatrix} h \\ q \\ m \end{bmatrix} \quad ; \quad \mathbf{F} = \begin{bmatrix} q \\ F_2 \\ F_3 \end{bmatrix} \quad ; \quad \mathbf{G} = \begin{bmatrix} 0 \\ G_2 \\ G_3 \end{bmatrix} \tag{3.2}$$

and

$$F_2 = qU + m + \frac{1}{2}h^2 \quad ; \quad G_2 = \theta h + \tau_b \tag{3.3}$$

$$F_3 = 3mU + m_3 \quad ; \quad G_3 = 2\left(\tau_b \tilde{u}_b + D_B - U\frac{\partial m}{\partial x}\right) \tag{3.4}$$

in which $U = q/h$. τ_b is given by (2.28) with $u_b = (U + \tilde{u}_b)$ and $\tilde{u}_b$ is calculated using (2.44). m_3 and D_B are obtained from (2.38) and (2.39), respectively. Eq. (3.1) is solved numerically using the MacCormack method (MacCormack 1969) which is a simplified variation of the two-step Lax-Wendroff method (e.g., Anderson *et al.* 1984) and has been applied successfully for the computation of unsteady open channel flows with hydraulic jumps (e.g., Fennema and Chaudhry 1986; Gharangik

and Chaudhry 1991). The use of the Lax-Wendroff method for (3.1) would be very difficult because this method requires the Jacobian of $\mathbf{F}$ with respect to $\mathbf{U}$.

The initial time $t = 0$ for the computation marching forward in time is taken to be the time when the incident wave arrives at the seaward boundary located at $x = 0$ and there is no wave action in the computation domain $x \geq 0$. The initial conditions for the computation are thus given by

$$h = -z_b \quad \text{at } t = 0 \quad \text{for } z_b < 0 \quad \text{(below SWL)} \tag{3.5}$$

$$h = 0 \quad \text{at } t = 0 \quad \text{for } z_b \geq 0 \quad \text{(above SWL)} \tag{3.6}$$

$$q = 0 \quad ; \quad m = 0 \quad \text{at } t = 0 \tag{3.7}$$

in which z_b = normalized bottom elevation taken to be negative below SWL.

A finite difference grid of constant nodal interval Δx and variable time step Δt is used in the numerical model VBREAK. The spatial nodes are located at $x = (j-1)\Delta x$ with $j = 1,\ 2,\ \ldots,\ j_{\max}$ where $j_{\max}$ = number of the spatial nodes in the computation domain. The computational shoreline is defined as the location where the normalized instantaneous water depth h equals a small value δ such as $\delta = 10^{-3}$ as in the previous one-dimensional models (e.g., Kobayashi and Poff 1994). The integer s is used to indicate the wet node next to the moving shoreline such that $h_{s+1} \leq \delta < h_s$ where h_s and h_{s+1} are the values of h_j at the node $j = s$ and $(s+1)$, respectively. It is noted that no wave overtopping and transmission are allowed in the present form of VBREAK unlike the previous one-dimensional models. It is hence required that $s < j_{\max}$.

The values of $\mathbf{U}_j$ at the node j with $j = 1, 2, \ldots, s$ and at the present time t are known in the following where $\mathbf{U}_j = \mathbf{0}$ with $j = (s+1),\ (s+2),\ \ldots,\ j_{\max}$ landward of the shoreline node s. The unknown values of $\mathbf{U}_j^*$ at the node j and

at the next time level $t^* = (t + \Delta t)$ are denoted by the superscript asterisk. The predictor, corrector and final steps of the MacCormack method are expressed as

$$\dot{\mathbf{U}}_j = \mathbf{U}_j - \frac{\Delta t}{\Delta x}(\mathbf{F}_{j+1} - \mathbf{F}_j) - \Delta t \mathbf{G}_j \quad \text{for } j = 1, 2, \ldots, s \tag{3.8}$$

$$\ddot{\mathbf{U}}_j = \dot{\mathbf{U}}_j - \frac{\Delta t}{\Delta x}\left(\dot{\mathbf{F}}_j - \dot{\mathbf{F}}_{j-1}\right) - \Delta t \dot{\mathbf{G}}_j \quad \text{for } j = 2, 3, \ldots, s \tag{3.9}$$

$$\mathbf{U}_j^* = \frac{1}{2}\left(\mathbf{U}_j + \ddot{\mathbf{U}}_j\right) \quad \text{for } j = 2, 3, \ldots, s \tag{3.10}$$

in which a forward spatial difference is used for the second term on the right hand side of the predictor equation (3.8), and a backward spatial difference is used for this term in the corrector equation (3.9). This is because the spatial difference in the predictor equation is recommended to be in the direction of propagation of wave fronts (Anderson *et al.* 1984). Accordingly, the term $\partial m/\partial x$ in the function G_3 defined in (3.4) is expressed by the forward and backward spatial differences in (3.8) and (3.9), respectively. The values of $\dot{\mathbf{U}}_j$ computed by (3.8) and the corresponding values of $\dot{\mathbf{F}}_j$ and $\dot{\mathbf{G}}_j$ in (3.9) are temporary values at the next time level t^*. In the computer program VBREAK, the three equations corresponding to each of (3.8), (3.9) and (3.10) are used for clarity. The values of $\mathbf{U}_1^*$ are computed using the seaward boundary conditions in Section 3.5. The numerical procedures for the moving shoreline in Section 3.6 are used to improve the computed values of $\mathbf{U}_s^*$ and find the shoreline node s^* at the next time level t^*.

3.2 Numerical Stability and Smoothing

The constant nodal interval Δx needs to be small enough to resolve steep wave fronts in the surf zone. The variable time step size Δt for numerically stable computation is estimated at the beginning of each time step using the following approximate equation:

$$\Delta t = \frac{C_n \Delta x}{\max\left(|U_j| + \sqrt{h_j}\right)} \quad \text{for } j = 1, 2, \ldots, s \tag{3.11}$$

in which C_n is the Courant number and the denominator in (3.11) is the maximum value of $(|U_j| + \sqrt{h_j})$ at all the wet nodes at the present time t. The value of Δt for each time step is selected using (3.11) except for the last time step that is chosen such that $t^* = (t + \Delta t) = t_{\max}$ for given t and $t_{\max}$. The numerical stability of the MacCormack method applied to (3.1) with $m = 0$ and $G_2 = 0$ requires that $C_n \leq 1$ (e.g., Anderson *et al.* 1984). Eq. (3.11) is approximate because the characteristic equations corresponding to (3.1) with $m \neq 0$ can not be expressed in simple analytical forms. Moreover, (3.11) does not account for the shoreline algorithm which tends to suffer numerical difficulties. Consequently, the value of C_n less than unity is specified as input to adjust Δt for the successful computation of each case. This manual adjustment of Δt through the specification of C_n on the order of 0.4 appears to be sufficient because the computation time of VBREAK is relatively short.

Use of the MacCormack method results in numerical high-frequency oscillations which tend to appear at the rear of a breaking wave, especially on a gentle slope. For open-channel flows, Chaudhry (1993) summarized a procedure presented by Jameson *et al.* (1981) to smooth these high-frequency oscillations without disturbing the rest of the computed variations. To apply this procedure for breaking waves on slopes, the computed water depth h_j^* at the node j and at the next time level t^* is used to calculate the parameter ν_j at the node j defined as

$$\nu_j = \frac{|h_{j+1}^* - 2h_j^* + h_{j-1}^*|}{|h_{j+1}^*| + 2|h_j^*| + |h_{j-1}^*|} \qquad \text{for } j = 2,\ 3,\ \ldots,\ (s^* - 1) \tag{3.12}$$

The parameter $\epsilon_{j+0.5}$ at the midpoint of the nodes j and $(j+1)$ is given by

$$\epsilon_{j+0.5} = \kappa \left(\frac{h_j^* + h_{j+1}^*}{2}\right)^{0.5} \max(\nu_j,\ \nu_{j+1}) \qquad \text{for } j = 2,\ 3,\ \ldots,\ (s^* - 2) \tag{3.13}$$

in which κ = numerical damping coefficient for regulating the amount of damping the high-frequency oscillations. The computed water depth h_j^* is modified as

$$h_j^* = h_j^* + \epsilon_{j+0.5}\left(h_{j+1}^* - h_j^*\right) - \epsilon_{j-0.5}\left(h_j^* - h_{j-1}^*\right) \quad \text{for } j = 3,\ 4,\ \ldots,\ (s^* - 2) \tag{3.14}$$

which should be considered as a FORTRAN replacement statement. Likewise, U_j^* and m_j^* are smoothed using (3.14) with h_j^* being replaced by U_j^* and m_j^*, respectively, where $\epsilon_{j+0.5}$ is the same. The smoothed h_j^* and U_j^* are used to calculate $q_j^* = h_j^* U_j^*$.

Chaudhry (1993) suggested the expressions of ν_j at the end points $j = 1$ and s^* in (3.12) for open-channel flows. Addition of these expressions in (3.13) and (3.14) is found to produce spurious fluid motions even in the absence of waves on slopes. As a result, the smoothing at the end points is not recommended for breaking waves on slopes.

The numerical damping coefficient κ is specified as input to VBREAK. For breaking waves on gentle beach slopes, the value of κ on the order of unity is found to be necessary to damp the high-frequency oscillations adequately. For waves surging on steep slopes of coastal structures, the value of κ on the order of 0.1 appears to be sufficient. However, the smoothing procedure based on (3.12) tends to cause more damping near the shoreline where the water depth h is very small. To remedy this uneven damping, the term $[(h_j^* + h_{j+1}^*)/2]^{0.5}$ is added in (3.13) to reduce the damping near the shoreline.

3.3 Incident or Measured Wave Profile

The required wave input for the numerical model VBREAK is the normalized incident or measured wave profile at the seaward boundary of the computation domain, that is, $\eta_i(t) = \eta_i'(t')/H'$ or $\eta(t) = \eta'(t')/H'$ at $x = 0$ with $t = t'/T'$ where H' and T' are the reference wave height and period used for the normalization in (2.4)–(2.6). The specification of $\eta_i(t)$ or $\eta(t)$ at $x = 0$ for $t \geq 0$ needs to satisfy the condition $\eta_i = 0$ or $\eta = 0$ at $x = 0$ at the initial time $t = 0$ to be consistent with the assumed initial conditions of no wave action in the region of $x \geq 0$ at $t = 0$.

The temporal variation of the incident wave profile $\eta_i(t)$ at $x = 0$ can be

1. the incident monochromatic wave profile computed (by the computer program VBREAK) using an appropriate wave theory, or

2. a user-specified incident irregular or transient wave train including the incident wave profile measured in the absence of wave reflection, measured in the presence of wave reflection but separated from the reflected wave using linear wave theory, or generated numerically for given frequency spectrum.

For convenience, the former will be referred to as the case of *regular* waves, while the latter is simply called the case of *irregular* waves, although this case can also include monochromatic transient waves.

The temporal variation of the normalized free surface elevation $\eta(t)$ at $x = 0$ can be specified as input if $\eta(t)$ at $x = 0$ is measured in the presence of wave reflection. This option eliminates uncertainties associated with the separation of incident and reflected waves using linear wave theory in laboratory and field measurements.

3.3.1 Incident Regular Wave

For the case of incident regular waves, the periodic variation of $\eta_i(t)$ is computed by the computer program using either cnoidal or Stokes second-order wave theory. The height and period of the incident regular waves at the seaward boundary located at $x = 0$ are denoted by H_i' and T_i'. The reference wave period T' is taken as $T' = T_i'$ for the incident regular waves. The reference wave height H' specified as input may be in deeper water depth. Since the numerical model is based on the assumption of shallow water waves, the seaward boundary should be located in relatively shallow water. As a result, it is not always possible to take $H' = H_i'$. Defining $K_s = H_i'/H'$, the height and period of the regular wave profile $\eta_i(t)$ at $x = 0$ is K_s and unity, respectively.

For Stokes second-order wave theory, the incident wave profile $\eta_i(t)$ at $x = 0$ is given by (e.g., Kobayashi and Poff 1994)

$$\eta_i(t) = K_s \left\{ \frac{1}{2} cos\left[2\pi(t + t_0)\right] + a_2 cos\left[4\pi(t + t_0)\right] \right\} \quad \text{for } t \geq 0 \tag{3.15}$$

with

$$a_2 = \frac{2\pi}{L} cosh\left(\frac{2\pi}{L}\right)\left[2 + cosh\left(\frac{4\pi}{L}\right)\right]\left[16\frac{d_t}{K_s} sinh^3\left(\frac{2\pi}{L}\right)\right]^{-1} \tag{3.16}$$

$$L = L_0 \, tanh\frac{2\pi}{L} \tag{3.17}$$

where t_0 = time shift computed to satisfy the conditions that $\eta_i = 0$ at $t = 0$ and η_i decreases initially; a_2 = normalized amplitude of the second-order harmonic; $L = L'/d'_t$; $d_t = d'_i/H'$; $L_0 = L'_0/d'_i$; d'_t = water depth below SWL at $x = 0$; L' = dimensional wavelength at $x = 0$; and L'_0 = dimensional linear wavelength in deep water. The normalized wavelength L satisfying (3.17) for given L_0 is computed using a Newton-Raphson iteration method. Eq. (3.16) yields the value of a_2 for given $d_t = d'_t/H'$, K_s, and L. Since (3.15) satisfies $\eta_i(t+1) = \eta_i(t)$ and $\eta_i(-t - t_0) = \eta_i(t + t_0)$, it is sufficient to compute the profile $\eta_i(t)$ for $0 \leq (t + t_0) \leq 0.5$ to obtain $\eta_i(t)$ for $0 \leq t \leq t_{\max}$ where $t_{\max}$ = specified computation duration. Eq. (3.15) may be appropriate if the Ursell parameter $U_r < 26$ where $U_r = [H'_i(L')^2/(d'_i)^3] = (K_s L^2/d_t)$ at $x = 0$. It is noted that the value of U_r based on the normalized wavelength L computed from (3.17) is simply used to decide whether cnoidal or Stokes second-order wave theory is applied.

For the case of $U_r \geq 26$, cnoidal wave theory is used to compute the incident wave profile $\eta_i(t)$ at $x = 0$ (e.g., Kobayashi and Poff 1994)

$$\eta_i(t) = \eta_{min} + K_s \, cn^2\left[2K(t + t_0)\right] \quad \text{for } t \geq 0 \tag{3.18}$$

with

$$\eta_{min} = \frac{K_s}{m}\left(1 - \frac{E}{K}\right) - K_s \tag{3.19}$$

where $\eta_{\min}$ = normalized trough elevation below SWL; cn = Jacobian elliptic function; K = complete elliptic integral of the first kind; E = complete elliptic integral of the second kind, which should be differentiated from the specific wave energy E given by (2.23); and m = parameter determining the complete elliptic integrals

$K(m)$ and $E(m)$. It is noted that this parameter m is different from the momentum flux correction m used in the previous sections. The notation of m for cnoidal wave theory is standard and therefore used here. The parameter m for cnoidal wave theory is related to the Ursell parameter U_r

$$U_r = \frac{K_s L^2}{d_t} = \frac{16}{3} m K^2 \tag{3.20}$$

For $U_r \geq 26$, the parameter m is in the range $0.8 < m < 1$. The parameter m for given σ, d_t, and K_s, where σ is defined in (2.6), is computed from

$$\frac{\sigma}{L\sqrt{d_t}} \sqrt{\left[1 + \frac{K_s}{m\, d_t}\left(-m + 2 - 3\frac{E}{K}\right)\right]} - 1 = 0 \tag{3.21}$$

where the normalized wavelength L is given by (3.20) as a function of m for given d_t and K_s. The left hand side of (3.21) is a reasonably simple function of m in the range $0.8 < m < 1$. As a result, (3.21) can be solved using an iteration method which successively narrows down the range of m bracketing the root of (3.21). After the value of m is computed for given σ, d_t, and K_s, the values of U_r and L are computed using (3.20), while (3.19) yields the value of η_{min}. The incident wave profile $\eta_i(t)$ is computed using (3.18) for $0 \leq (t + t_0) \leq 0.5$ where the time shift t_0 and the periodicity and symmetry of the cnoidal wave profile are used in the same manner as the Stokes second-order wave profile given by (3.15). It should be mentioned that the Jacobian elliptic function and the complete elliptic integrals of the first and second kinds are computed using the subroutines given by Press *et al.* (1986).

3.3.2 Incident Irregular Wave

The specification of incident irregular waves as input to VBREAK is the same as in the previous one-dimensional model RBREAK2 (Kobayashi and Poff 1994). Various examples of user-specified irregular wave trains were given by Wurjanto and Kobayashi (1991).

The incident wave train $\eta_i(t)$ normalized by the reference wave height H' is read at the following sampling rate

$$\delta t_i = \frac{t_{\max}}{\text{NPINP–1}} \tag{3.22}$$

in which NPINP = specified number of points in the input wave train for $0 \leq t \leq t_{\max}$ with t and $t_{\max}$ being normalized by the reference wave period T'. The reference wave height and period can be chosen as any height and period that are convenient for the analysis of computed normalized results. The normalized wave height K_s specified as input for case of incident regular waves is not required when an irregular wave time series is used. It is noted that the normalized incident regular wave train given by (3.15) and (3.18) is also computed at the rate δt_i given by (3.22).

The sampling rate δt_i must be small enough to resolve the temporal variation of $\eta_i(t)$ but is normally much larger than the finite difference time step Δt calculated by (3.11) for the numerically stable computation. A simple linear interpolation of $\eta_i(t)$ sampled at the rate δt_i is performed to find the value of $\eta_i(t^*)$ at the time level $t^* = (t + \Delta t)$ during the time-marching computation.

3.3.3 Measured Wave Profile

If the free surface oscillation is measured at the seaward boundary of the computation, it is more direct and straightforward to specify the measured free surface oscillation as input to VBREAK . This option eliminates the uncertainty associated with the separation of incident and reflected waves using linear wave theory.

The measured free surface elevation above SWL at the seaward boundary is normalized by the values of H' and T' specified as input. The normalized input time series of $\eta(t)$ at $x = 0$ is read at the sampling rate δt_i given by (3.22) and interpolated linearly in the same way as $\eta_i(t)$ at $x = 0$ for case of specified irregular waves.

3.4 Statistical Calculations

The *statistical calculations* in this report imply the calculations of the mean, root-mean-square (rms), maximum and minimum values of computed time-series for the duration of $t_{\rm stat} \leq t \leq t_{\rm max}$. For example, the rms value of η is defined as

$$\eta_{\rm rms} = \left[\ \overline{(\eta - \bar{\eta})^2} \ \right]^{1/2} = \left[\ \overline{\eta^2} - (\bar{\eta})^2 \right]^{1/2} \tag{3.23}$$

in which the overbar denotes the time averaging for $t_{\rm stat} \leq t \leq t_{\rm max}$.

For the case of *regular* waves, the statistical calculations should be executed over the last wave period, assuming that the computation duration $t_{\rm max}$ is large enough to reach the periodicity of time-varying quantities during $t_{\rm stat} \leq t \leq t_{\rm max}$ with $t_{\rm stat} = (t_{\rm max} - 1)$. This duration ranges from approximately five wave periods for coastal structures (Kobayashi and Wurjanto 1989) to about 30 wave periods for beaches (Kobayashi *et al.* 1989).

For *irregular* wave computations, the statistical calculations are conducted over most or all of the computation duration. The initial transient waves may be excluded by specifying an appropriate value of $t_{\rm stat}$ estimated from the corresponding regular wave computation.

3.5 Wave Reflection

The normalized reflected wave train $\eta_r(t)$ at the seaward boundary needs to be computed to estimate the degree of wave reflection from the computation domain. It is also required to find the unknown value of the vector $\mathbf{U}_1^*$ at $x = 0$ and at the next time level $t^* = (t + \Delta t)$ which can not be computed using (3.10). The seaward boundary algorithm needs to be developed for the cases of IWAVE=1 and 2 where the incident wave profile $\eta_i(t)$ at $x = 0$ is specified as input and for IWAVE=3 where the total free surface profile $\eta(t)$ at $x = 0$ is specified as input.

In order to derive approximate seaward boundary conditions for h and q, (2.18) and (2.20) are expressed in the following characteristic forms:

$$\frac{d\alpha}{dt} = \frac{\partial \alpha}{\partial t} + (U+c)\frac{\partial \alpha}{\partial x} = -\theta - \frac{\tau_b}{h} - \frac{1}{h}\frac{\partial m}{\partial x} \quad \text{along} \quad \frac{dx}{dt} = U + c \tag{3.24}$$

$$\frac{d\beta}{dt} = \frac{\partial \beta}{\partial t} + (U-c)\frac{\partial \beta}{\partial x} = \theta + \frac{\tau_b}{h} + \frac{1}{h}\frac{\partial m}{\partial x} \quad \text{along} \quad \frac{dx}{dt} = U - c \tag{3.25}$$

with

$$c = \sqrt{h} \quad ; \quad \alpha = U + 2c \quad ; \quad \beta = -U + 2c \tag{3.26}$$

in which c is the normalized phase velocity, whereas α and β are the characteristic variables.

Assuming that $U < c$ and the flow is subcritical in the vicinity of the seaward boundary where the normalized water depth below SWL is d_t, α and β represent the characteristics advancing landward and seaward, respectively, in the vicinity of the seaward boundary. The total water depth at the seaward boundary is expressed in the form (Kobayashi *et al.* 1987).

$$h(t) = d_t + \eta(t) \quad \text{at} \quad x = 0 \tag{3.27}$$

with

$$\eta(t) = \eta_i(t) + \eta_r(t) \quad \text{at} \quad x = 0 \tag{3.28}$$

where η_i and η_r are the free surface elevations normalized by H' at $x = 0$ due to the incident and reflected waves, respectively. The incident wave train may be specified by prescribing the variation of η_i with respect to t for $t \geq 0$. Alternatively, the free surface elevation measured at $x = 0$ may be specified as input by prescribing the variation of η with respect to t for $t \geq 0$. The normalized reflected wave train η_r is approximately expressed in terms of the seaward advancing characteristic β at $x = 0$

$$\eta_r(t) \simeq \frac{1}{2}\sqrt{d_t}\beta(t) - d_t - C_t \quad \text{at} \quad x = 0 \tag{3.29}$$

where β is obtained using (3.25) and linear long wave theory is used to derive (3.29). For $h(t)$ at $x = 0$ calculated using (3.27), $U = (2\sqrt{h} - \beta)$ using (3.26) and $q = hU$.

The correction term C_t in (3.29) introduced by Kobayashi *et al.* (1989) to predict wave set-down and setup on a beach may be expressed as

$$C_t = \frac{1}{2}\sqrt{d_t}\,\frac{\overline{(\eta - \bar{\eta})(U - \bar{U})}}{\bar{h}} \qquad \text{at} \quad x = 0 \tag{3.30}$$

For incident regular waves on gentle slopes, C_t may be estimated by (Kobayashi *et al.* 1989)

$$C_t = \frac{K_s^2}{16 d_t} \qquad \text{for gentle slopes} \tag{3.31}$$

where the assumptions of linear long wave and negligible wave reflection were made in (3.30) to derive (3.31). For coastal structures, wave reflection may not be negligible but the location of the seaward boundary may be chosen such that $C_t \simeq 0$ on the basis of (3.31). For incident irregular waves, (3.31) may still be used as a first approximation to improve the prediction of wave set-down and setup on a beach. When the measured time series of $\eta(t)$ at $x = 0$ specified as input includes the wave set-down or setup at $x = 0$, the reflected wave train $\eta_r(t)$ is computed using (3.29) with $C_t = 0$.

On the other hand, the value of m at the seaward boundary needs to be found using (2.31). The initial condition for m is specified as $m = 0$ at $t = 0$ in the computation domain $x \geq 0$. The value of m at $x = 0$ might be taken as $m = 0$ at $x = 0$ if the seaward boundary is located outside the surf zone. This is because the vertical variation of the horizontal velocity assumed in (2.33) is caused by wave breaking in this numerical model for shallow water waves. However, the boundary condition of $m = 0$ at $x = 0$ will yield $m = 0$ for $t > 0$ and $x > 0$ because $m = 0$ is a trivial solution of (2.31). It is hence required to introduce $m \geq 0$ at $x = 0$ so

that $m \geq 0$ for $t > 0$ and $x > 0$. One option is to rewrite (2.31) in terms of $\tilde{u}_b$ using (2.37), (2.38) and (2.39)

$$\frac{\partial \tilde{u}_b}{\partial t} + \frac{\partial}{\partial x}(U\tilde{u}_b) = -\frac{C_3\tilde{u}_b}{2C_2}\left(\frac{\tilde{u}_b}{h}\frac{\partial h}{\partial x} + 3\frac{\partial \tilde{u}_b}{\partial x}\right) - \frac{\tau_b + C_{B\ell}|\tilde{u}_b|\tilde{u}_b}{C_2 h} \tag{3.32}$$

with

$$C_{B\ell} = C_B C_\ell^2 \sigma \tag{3.33}$$

in which τ_b is given by (2.28) with $u_b = (U + \tilde{u}_b)$ and $\tilde{u}_b = 0$ is not a trivial solution of (3.32). The value of $m = C_2 h \tilde{u}_b^2$ at $x = 0$ may be obtained using the value of $\tilde{u}_b$ at $x = 0$ computed using (3.32) as explained in the following.

3.5.1 Seaward Boundary Algorithm for Specified Incident Regular and Irregular Waves

An explicit first-order finite difference equation corresponding to (3.25) is used to find the value of β_1^* at $x = 0$ and the next time t^* for the cases of specified incident regular and irregular waves

$$\beta_1^* = \beta_1 - \frac{\Delta t}{\Delta x}(U_1 - c_1)(\beta_2 - \beta_1) + \Delta t\left[\theta_1 + \frac{(\tau_b)_1}{h_1}\right] + \frac{\Delta t}{\Delta x}\frac{m_2 - m_1}{h_1} \tag{3.34}$$

where $\beta_1 = (-U_1 + 2c_1)$ and $\beta_2 = (-U_2 + 2c_2)$. The right hand side of (3.34) can be computed for the known values of $\mathbf{U}_j$ with $j = 1$ and 2 at the present time t where the spatial nodes are located at $x = (j-1)\Delta x$. The value of η_r^* at the time t^* is calculated using (3.29). The incident wave profile $\eta_i(t)$ specified as input together with (3.27) and (3.28) yields the value of h_1^*, while $U_1^* = [2\sqrt{(h_1^*)} - \beta_1^*]$ using the definition of β given in (3.26). Thus, the values of h_1^*, U_1^*, and $q_1^* = U_1^* h_1^*$ at $x = 0$ and the time t^* are obtained.

As for the value of m_1^* at $x = 0$ and the next time t^*, an explicit first-order finite difference approximation of (3.32) is used to obtain the value of $(\tilde{u}_b)_1^*$ as follows:

$$(\tilde{u}_b)_1^* = (\tilde{u}_b)_1 - \frac{\Delta t}{\Delta x}\left[U_2\,(\tilde{u}_b)_2 - U_1\,(\tilde{u}_b)_1\right] - \frac{\Delta t}{C_2}\left\{\frac{C_3(\tilde{u}_b)_1}{2\Delta x}\left[(\tilde{u}_b)_1\left(\frac{h_2}{h_1} - 4\right)\right.\right.$$
$$\left.\left. +3\,(\tilde{u}_b)_2\right] + h_1^{-1}\left[(\tau_b)_1 + C_{B\ell}\mid(\tilde{u}_b)_1\mid(\tilde{u}_b)_1\right]\right\} \quad (3.35)$$

The value of m_1^* is then calculated using (2.37)

$$m_1^* = C_2 h_1^*\left[(\tilde{u}_b)_1^*\right]^2 \quad (3.36)$$

3.5.2 Seaward Boundary Algorithm for Specification of Total Incident and Reflected Waves

When the total free surface comprised of both incident and reflected waves $\eta(t)$ at $x = 0$ in (3.27) is specified as input, the values of η_1^* and h_1^* at $x = 0$ and the time t^* are known. The value of U_1^* at $x = 0$ and the time t^* is computed using (3.25) for the characteristic variable β advancing seaward from the computation domain.

A simple first-order finite difference approximation of (3.25) along the straight line, $dx/dt = (U_1^* - c_1^*) < 0$, originating from the point at node 1 and the time $t^* = (t + \Delta t)$ may be expressed as

$$\beta_1^* = \beta_{12} + \Delta t\left[\theta_1 + \frac{(\tau_b)_1}{h_1}\right] + \frac{\Delta t}{\Delta x}\,\frac{m_2 - m_1}{h_1} \quad (3.37)$$

where β_{12} is the value of β at the time t and at the location of $x = \delta x$ given by

$$\delta x = -\,(U_1^* - c_1^*)\,\Delta t > 0 \quad (3.38)$$

The numerical stability criterion given by (3.11) requires that $\delta x < \Delta x$. As a result, the point of $x = \delta x$ is located between nodes 1 and 2. The linear interpolation between the known values of β_1 and β_2 at the time t yields

$$\beta_{12} = \beta_1 + \frac{\delta x}{\Delta x}\,(\beta_2 - \beta_1) \quad (3.39)$$

Using (3.38) and (3.39), (3.37) may be rewritten as

$$\beta_1^* = \beta_1 - \frac{\Delta t}{\Delta x}\left(U_1^* - c_1^*\right)\left(\beta_2 - \beta_1\right) + \Delta t\left[\theta_1 + \frac{(\tau_b)_1}{h_1}\right] + \frac{\Delta t}{\Delta x}\,\frac{m_2 - m_1}{h_1} \qquad (3.40)$$

which corresponds to (3.34) except that $(U_1 - c_1)$ in (3.34) is replaced by $(U_1^* - c_1^*)$. Eq. (3.40) for $\beta_1^* = (2c_1^* - U_1^*)$ is an implicit scheme for U_1^* for the known value of $c_1^* = \sqrt{(h_1^*)}$. Solving (3.40) for U_1^* yields

$$U_1^* = \left[1 - \frac{\Delta t}{\Delta x}\left(\beta_2 - \beta_1\right)\right]^{-1}\left\{2c_1^* - \beta_1 - \frac{\Delta t}{\Delta x}\left[c_1^*\left(\beta_2 - \beta_1\right) + \frac{m_2 - m_1}{h_1}\right] - \Delta t\left[\theta_1 + \frac{(\tau_b)_1}{h_1}\right]\right\} \qquad (3.41)$$

If the absolute value of the denominator on the right hand side of (3.41) becomes almost zero, this implicit algorithm may not be appropriate. This problem has never been encountered so far partly because the numerical stability criterion expressed as (3.11) generally requires a value of $\Delta t/\Delta x$ that is much less than unity.

After U_1^* is computed using (3.41), the value of β_1^* is obtained from $\beta_1^* = (2c_1^* - U_1^*)$. The value of η_r^* for the reflected wave profile is then calculated using (3.29) at the time t^*. The value of η_i^* for the incident wave profile is obtained from $\eta_i^* = (\eta_1^* - \eta_r^*)$ based on (3.28). The value of m_1^* is computed using (3.36) with (3.35).

3.5.3 Wave Reflection Coefficient

The average reflection coefficient r for regular and irregular waves may be estimated using the root-mean-square values of the time series of η_r and η_i as defined by (3.23)

$$r = (\eta_r)_{\text{rms}} \,/\, (\eta_i)_{\text{rms}} \qquad (3.42)$$

which is equal to the square root of the ratio between the time-averaged reflected wave energy as compared to the time-averaged incident wave energy on the basis of linear wave theory. The reflection coefficient as a function of the frequency for

irregular waves can be calculated using the reflected and incident wave spectra computed from the time series of η_r and η_i (*e.g.*, Kobayashi *et al.* 1990).

3.6 Wave Runup

For the case of no wave overtopping, the landward boundary of the numerical model is located at the moving shoreline on the slope where the water depth is essentially zero. The kinematic boundary condition requires that the horizontal shoreline velocity be the same as the horizontal fluid velocity. In reality, it is difficult to pinpoint the exact location of the moving shoreline on the slope. For the computation, the shoreline is defined as the location where the normalized instantaneous water depth equals a small value δ such as $\delta = 10^{-3}$ as explained in Section 3.1.

The following numerical procedure dealing with the moving shoreline located at $h = \delta$ is used to obtain the values of $\mathbf{U}_j^*$ at the next time $t^* = (t + \Delta t)$ for the nodes $j \geq s$ where $s =$ integer indicating the wet node next to the moving shoreline at the present time t such that $h_{s+1} \leq \delta < h_s$. It is noted that the procedure is somewhat intuitive and may be improved since the moving shoreline tends to cause numerical instability.

1. After computing $\mathbf{U}_j^*$ with $j = 2,\ 3,\ \ldots,\ s$ using (3.10), it is checked whether $h_{s-1}^* \leq \delta$, which may be encountered during a downrush. This is considered a computation failure since the shoreline should not move more than Δx because of the numerical stability criterion of the adopted explicit method given by (3.11).

2. If $h_s^* \geq h_{s-1}^*$, use $h_s^* = (2h_{s-1}^* - h_{s-2}^*)$, and $U_s^* = (2U_{s-1}^* - U_{s-2}^*)$, so that the water depth near the shoreline decreases landward. The following adjustments are made

   - if $|U_s^*| > |U_{s-1}^*|$, set $U_s^* = 0.9U_{s-1}^*$;

- if $h_s^* < 0$, set $h_s^* = 0.5h_{s-1}^*$;
- and if $h_s^* > h_{s-1}^*$, set $h_s^* = 0.9h_{s-1}^*$.

Then, obtain $q_s^* = h_s^* U_s^*$ based on the *adjusted* values of h_s^* and U_s^*.

3. If $h_s^* \leq \delta$, set $s^* = (s-1)$ and go to Step 11. The integer s^* indicates the wet node next to the shoreline at the next time t^*.

4. If $h_s^* > \delta$, compute $h_{s+1}^* = (2h_s^* - h_{s-1}^*)$, $U_{s+1}^* = (2U_s^* - U_{s-1}^*)$, and $q_{s+1}^* = h_{s+1}^* U_{s+1}^*$.

5. If $h_{s+1}^* \leq \delta$, set $s^* = s$ and go to Step 11.

6. If $h_{s+1}^* > \delta$, compute $\mathbf{U}_s^{**}$ at the time $t^{**} = (t^* + \Delta t)$ using (3.10) with $m = 0$ where $\mathbf{U}_j^*$ and $\mathbf{U}_j$ in (3.10) are replaced by $\mathbf{U}_s^{**}$ and $\mathbf{U}_s^*$, respectively. The vertical variation of the horizontal velocity may be assumed to be small in the vicinity of the moving shoreline. Improve the linearly extrapolated values in Step 4 using the following finite difference equations derived from (2.18) and (2.20) with $m = 0$ at $\tau_b = 0$:

$$q_{s+1}^* = q_{s-1}^* - \frac{\Delta x}{\Delta t}(h_s^{**} - h_s) \tag{3.43}$$

$$U_{s+1}^* = U_{s-1}^* - \frac{1}{U_s^*}\left[\frac{\Delta x}{\Delta t}(U_s^{**} - U_s) + h_{s+1}^* - h_{s-1}^* + 2\Delta x\, \theta_s\right] \tag{3.44}$$

The upper limit of the absolute value of $(U_s^*)^{-1}$ in (3.44) is taken as δ^{-1} to avoid the division by the very small value. Calculate $h_{s+1}^* = q_{s+1}^*/U_{s+1}^*$.

7. If $|U_{s+1}^*| \leq \delta$, set $s^* = s$ and go to Step 11.

8. If $h_{s+1}^* \leq h_s^*$ and $h_{s+1}^* \leq \delta$, set $s^* = s$ and go to Step 11.

9. If $h_{s+1}^* \leq h_s^*$ and $h_{s+1}^* > \delta$, set $s^* = (s+1)$ and go to Step 11.

10. If $h^*_{s+1} > h^*_s$, the linearly extrapolated values of h^*_{s+1}, U^*_{s+1}, and q^*_{s+1} in Step 4 are adopted in the following instead of those computed in Step 6. Furthermore, set $s^* = (s+1)$ if $h^*_{s+1} \leq h^*_s$ and $U^*_{s+1} \geq \delta$ and set $s^* = s$ otherwise where h^*_{s+1} and U^*_{s+1} are the adopted values.

11. After $s*$ is obtained, set $h^*_j = 0$, $U^*_j = 0$, $q^*_j = 0$ and $m^*_j = 0$ for $j \geq (s^* + 1)$ since no water is present above the computational shoreline. If $s^* = (s + 1)$, set $m^*_{s+1} = 0$. It is noted that the smoothing procedure given by (3.14) does not affect this shoreline algorithm.

Once the normalized water depth h at the given time is known as a function of x, the normalized free surface elevation, $Z_r = Z'_r/H'$, where the physical water depth equals a specified value δ'_r, can be computed as long as $\delta_r = (\delta'_r/H') > \delta$. The use of the physical depth δ'_r is related to the use of a runup wire to measure the shoreline oscillation on the slope (*e.g.*, Raubenheimer *et al.* 1995). The specified depth δ'_r can be regarded as the vertical distance between the runup wire and the slope, while the corresponding elevation Z'_r is the elevation above SWL of the intersection between the runup wire and the free surface. The computed oscillations of $Z_r(t)$ for different values of δ'_r can be used to examine the sensitivity to δ'_r of wave runup and run-down, which are normally defined as the maximum and minimum elevations relative to SWL reached by uprushing and downrushing water on the slope, respectively. The normalized runup R, run-down R_d, and setup $\overline{Z_r}$ as well as the root-mean-square value (standard deviation) of $Z_r(t)$ for given δ'_r are obtained from the computed oscillation of $Z_r(t)$.

Chapter 4

COMPARISON OF MODEL VBREAK TO DATA AND PREVIOUS MODEL

4.1 Comparison of Model to Previously Developed One Dimensional Model

To demonstrate the effectiveness of the MacCormack method in the numerical solutions of the continuity and momentum equations, the model VBREAK is reduced to a one-dimensional model and compared with a previously developed one-dimensional model. VBREAK implements the explicit first order finite difference of (3.32) to obtain the value of $(\tilde{u}_b)_1^*$ and thus m_1^*, the momentum correction factor at the next time level at the seaward boundary. When the value of m_1^* is set to zero at all times, the computed values of m_j^* at any j are zero for all times everywhere inside the computational domain. Thus the computed horizontal velocity has no vertical variation. For the entirety of this Section 4.1, VBREAK is reduced to a one-dimensional model through the specification of zero vertical variation at the seaward boundary.

The model VBREAK as a a one-dimensional model is compared with the previously developed IBREAK; the two models employ different numerical methods to solve the same governing equations. Use is made of the 1:2.5 riprap revetment test conducted by Ahrens (1975). The comparison of VBREAK to IBREAK is the only example of a steep slope computed in this report. The seaward boundary for the computation is taken at the toe of the 1:2.5 slope where the water depth below

SWL d_t' is 15 ft. Cnoidal waves of 8.5 s period with a height of 3.06 ft are the time series of the incident wave at the seaward boundary. A friction factor of 0.3 for the riprap slope (Kobayashi *et al.* 1987) and a Courant number of 0.4 are used for the computation. Although the numerical model VBREAK is found to be stable for Courant numbers up to 0.7, the value $C_n = 0.4$ is used so as to be consistent with other comparisons throughout this report. A numerical damping coefficient κ of 0.1 is sufficient for damping high frequency oscillations throughout the six wave periods from $t = 0$ to $t = t_{max} = 6$. The steep slope case suffers less numerical oscillation problem at the rear of the steep front than the gently sloped cases computed in the subsequent sections. Tables 4.1 and 4.2 are the primary input and output from the model VBREAK as explained by Kobayashi and Johnson (1995). The resultant dimensionless parameters for this case are: surf similarity parameter $\xi = 4.4$; the ratio of horizontal to vertical length scales $\sigma = 27.6$; Ursell number = 30.1. As evident in the primary output file, the reflection coefficient ($r = 0.55$) is large as expected for the steep slope and surf similarity parameter $\xi = 4.4$. Although information on the cubic profile parameter a is included, it is not utilized in the computations until the following sections.

Figure 4.1 depicts the six Cnoidal waves used as input to the models VBREAK and IBREAK as well as the reflected wave. Incident and reflected waves are found to be essentially the same for both models. The reflected wave is of considerable size relative to the incident wave and periodicity is reached within two wave periods.

The runup for the computational shoreline based on the water depth $\delta_r' = 0.787$ in is shown in Figure 4.2 where the incident wave train arrives at the shoreline at $t \simeq 0.5$. The computed runup Z is the normalized shoreline elevation above the SWL and is plotted against the normalized time. Following an initial depression of the free surface, the runup consists of the setup $\bar{\eta} \simeq 1.0$ above the SWL and a periodic component of amplitude $\simeq 1.0$. Figure 4.2 shows that the two models yield

Table 4.1: Primary input data file for VBREAK in comparison with IBREAK .

```
  3                    = number of comment lines
-------------------------------------------------------------
Ahren (1975)  Test 12
-------------------------------------------------------------
2            <--ISYST
1    <--IWAVE
2    <--IBOT
0    <--INCLCT
1    <--IENERG
1    <--ITEMVA
1    <--ISPAEU
5.                6.              <--TSTAT,TMAX
100                               <--STILL
0.001             0.400            0.1      <--DELTA,COURNO,DKAPPA
3.06              8.5             <--HREF,TREF
1.0                               <--KS
24001                             <--NPINP
4.0                .10             <--APROFL,CMIXL
15.               0.4             <--DSEAP,SLSURF
1                                 <--NBSEG
  60.000          9.000       .30
1201                              <--NPOUT
3                                 <--NDELR
0.157480
0.787402
1.574803
4                                 <--NONODS
91    101    111   121            <--NODLOC(1)  (2)  (3)  (4)
5                                 <--NOTIML
5.0         5.25         5.50        5.75         6.0   <--TIMSPA
```

Table 4.2: Primary output file for VBREAK in comparison with IBREAK.

```
------------------------------------------------------------
Ahren (1975)  Test 12
------------------------------------------------------------

WAVE CONDITION

Cnoidal Incident Wave at Seaward Boundary
Normalized wave height KS      =       1.000000
1-m =       0.112815261D+00
E   =       0.111509461D+01
K   =       0.252149782D+01
Reference Wave Period          =     8.500000 sec.
Reference Wave Height          =     3.060000 feet
Depth at Seaward Boundary      =    15.000000 feet
Norm. Depth at Seaw. Bdr.      =     4.902
Included Correction Term   CT
0 = no; 1 = yes         INCLCT =     0
Normalized Wave Length         =    12.144
"Sigma"                        =    27.573
Ursell Number                  =    30.084
Surf Similarity Parameter      =     4.400
Input Wave Train from Time=0 to TMAX
Computed or Read at Normalized Rate DELTI =      0.000250

Parameters of Vertical Velocity Variations
Cubic Profile Parameter      APROFL =     4.000000
Mixing Length Parameter      CMIXL  =     0.100000
Momentum Flux Coefficient    C2     =     0.485714
Kinetic Energy Flux Coeff.   C3     =     0.000000
Energy Dissipation Coeff.    CB     =    12.342857
Coefficient of DB            CBL    =     3.403313


BOTTOM GEOMETRY

Norm. Horiz. Length of
      Computation Domain   =     0.711121
Number of Segments         =        1
-------------------------------------------
 SEGMENT    XBSEG(I)    ZBSEG(I)    BFFSEG(I)
       I      feet        feet
-------------------------------------------
.....X=0    0.000000  -15.000000
       1   60.000000    9.000000    0.300000
```

Table 4.2: – Continued

```
COMPUTATION PARAMETERS

Normalized DX                          =   0.444451D-02
Normalized DELTA                       =   0.100000E-02
Courant Number                         =     0.400
 Must not exceed unity
Numerical Damping Coefficient          =    0.1000
 Must be zero or positive
Normalized Computation Duration  TMAX =      6.000000
Statistical Calculations Start
 when Time is equal to           TSTAT      5.000000
Total Number of Spatial Nodes    JMAX =       161
Number of Nodes Along Bottom Below SWL
                                 STILL =      100
Storing Temporal Variations from Time = 0
 to TMAX at Normalized Rate      DELTO =     0.005000
Wave Runup Time Series Stored for
                                  NDER =   3 Water Depths
Time Series of ETA, U, and UB
          Stored at              NONODS =        4 Nodes
Spacial Variations of ETA, U, and UB
         Stored at               NOTIML =       5 Time Levels

Maximum time step        =    0.82969E-03
Minimum time step        =    0.50928E-03

REFLECTION COEFFICIENT

ETARRMS/ETAIRMS =     0.550

INCIDENT AND REFLECTED WAVES

            Max           Min          Mean          RMS
Inc.      0.6287       -0.3713       0.0000       0.3472
Ref.      0.2790       -0.2720       0.0143       0.1910
SHORELINE OSCILLATIONS

Largest Node Number Reached by Computational Shoreline
                                          SMAX =      138
-------------------------------------------------------------------
      I   DELTAR(I)    RUNUP(I)  RUNDOWN(I)  SETUP(I) RMS(I)
            [inch]         Ru          Rd          Zr      Rrms
-------------------------------------------------------------------
      1      0.157      1.831       0.641       1.295      0.365
      2      0.787      1.811      -0.322       0.874      0.668
      3      1.575      1.803      -0.746       0.670      0.813
```

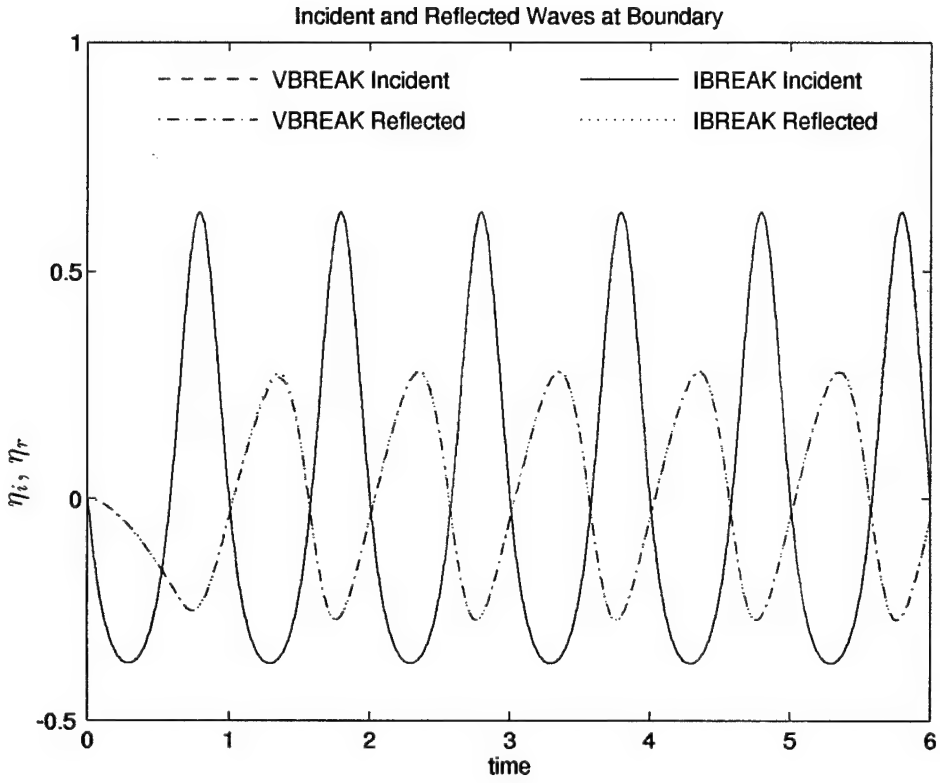

Figure 4.1: Incident and reflected waves at the seaward boundary: Incident(—); Reflected(···).

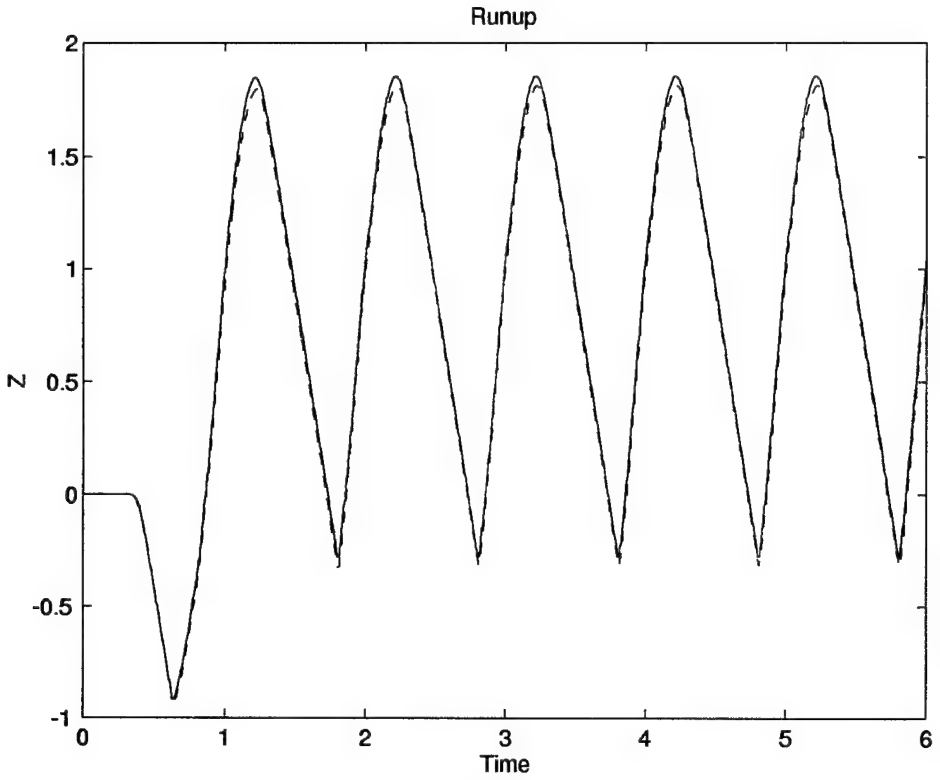

Figure 4.2: Computed time series of normalized runup with $\delta_r' = 0.787$ in : IBREAK(—); VBREAK(- - -).

results that are almost indistinguishable. Two additional computational shoreline depths are also specified but are not shown here as the results are basically similar.

Figures 4.3 and 4.4 depict the computed spatial variation of the normalized free surface η and the normalized depth averaged velocity U at five times throughout the final wave period. The plots for $t = 5$ and $t = 6$ are identical because of the periodicity. In each panel, the variations of η computed by VBREAK and IBREAK match almost exactly. The planar bottom is shown in each panel as a straight line. On the other hand, the spatial variations of the depth averaged horizontal velocities computed by the two models differ only slightly. The greatest difference occurs at the shoreline where the slight irregularity of the results of IBREAK seems physically

implausible.

The cross-shore variations of the maximum, minimum, and mean of the normalized free surface with the planar bottom profile and the depth averaged velocity are depicted in Figure 4.5. The free surface statistics are practically the same. The wave height increases as the wave shoals and is reflected from the steep slope. The mean free surface reveals a small set-down before wave uprush occurs at approximately $x = 0.3$. A significant setup occurs at the shoreline as shown in Table 4.2. The depth averaged velocity statistics are, again, essentially the same for the two numerical models. A small discrepancy is apparent in the maximum depth averaged velocity near the shore as the model VBREAK predicts a value that is approximately 20% larger than the prediction of IBREAK. The mean of the horizontal velocity U is a small negative value throughout the domain. This is a return current caused by forward velocities under the crest with larger water depth.

The cross-shore variation of the mean volume flux is cited as an indicator of the computational accuracy (Kobayashi *et al.* 1989). Theoretically, the no flux condition into the impermeable beach would dictate a net volume flux of zero. The time averaged continuity equation corresponding to (2.18) indicates that the time averaged volume flux would be zero throughout the domain. Figure 4.6 demonstrates that the flux is indeed very much less than one for both models. IBREAK demonstrates a greater accuracy than the developed model for this case. However, the net volume flux computed by VBREAK of approximately 0.003 or less is still acceptably small.

The normalized energy quantities for both models are shown in Figure 4.7. The normalized mean specific wave energy shown in the first panel increases as the waves shoal then falls to zero at the shoreline. The normalized mean energy flux as defined in Chapter 2 falls monotonically to zero at the shoreline as energy is dissipated through bottom friction and wave breaking. Panel three shows the energy

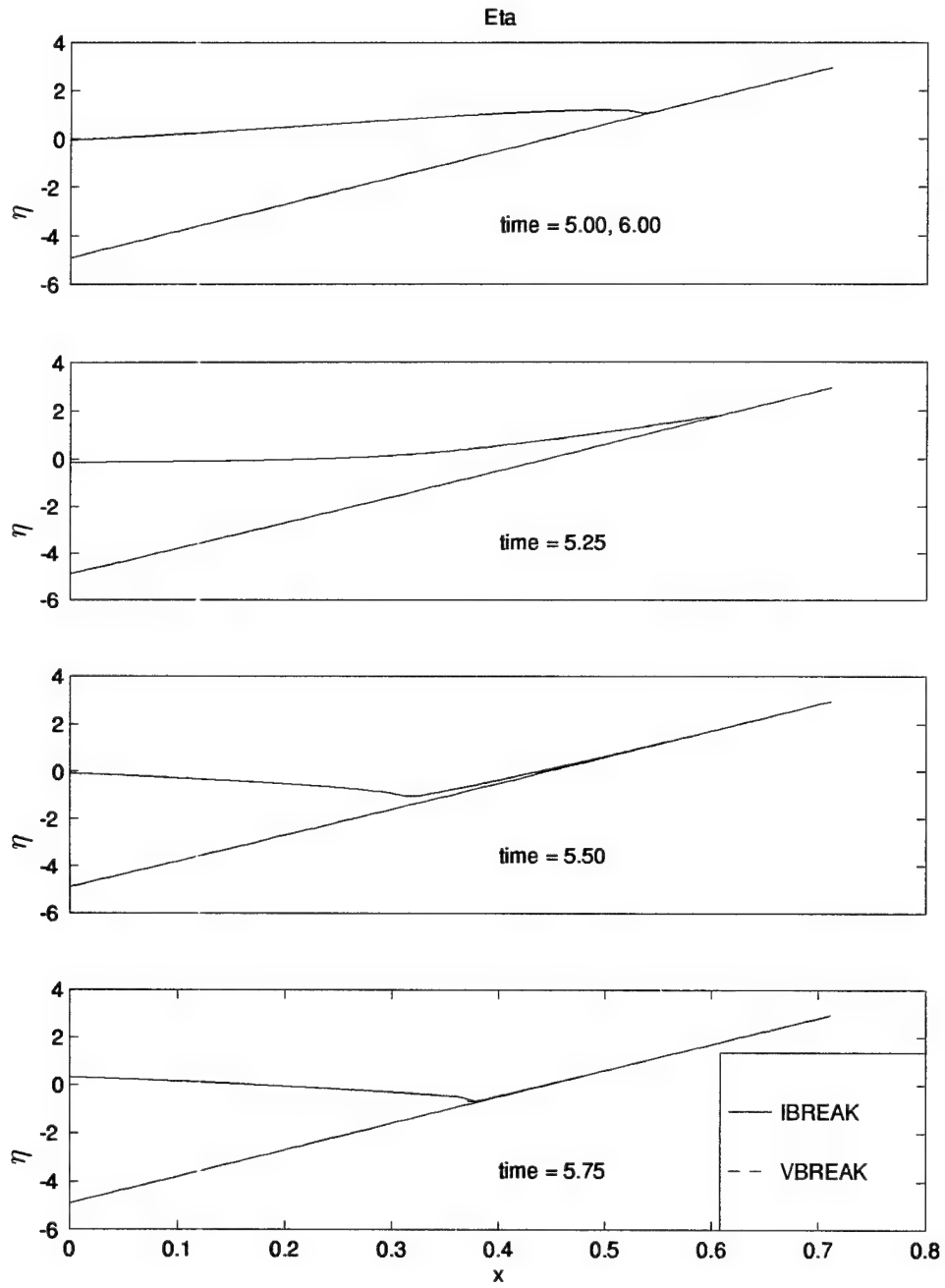

Figure 4.3: Computed cross-shore variation of normalized free surface η taken as zero at SWL at 5 time levels, t = 5.00, 5.25, 5.50, 5.75, and 6.00: IBREAK(—); VBREAK(- - -).

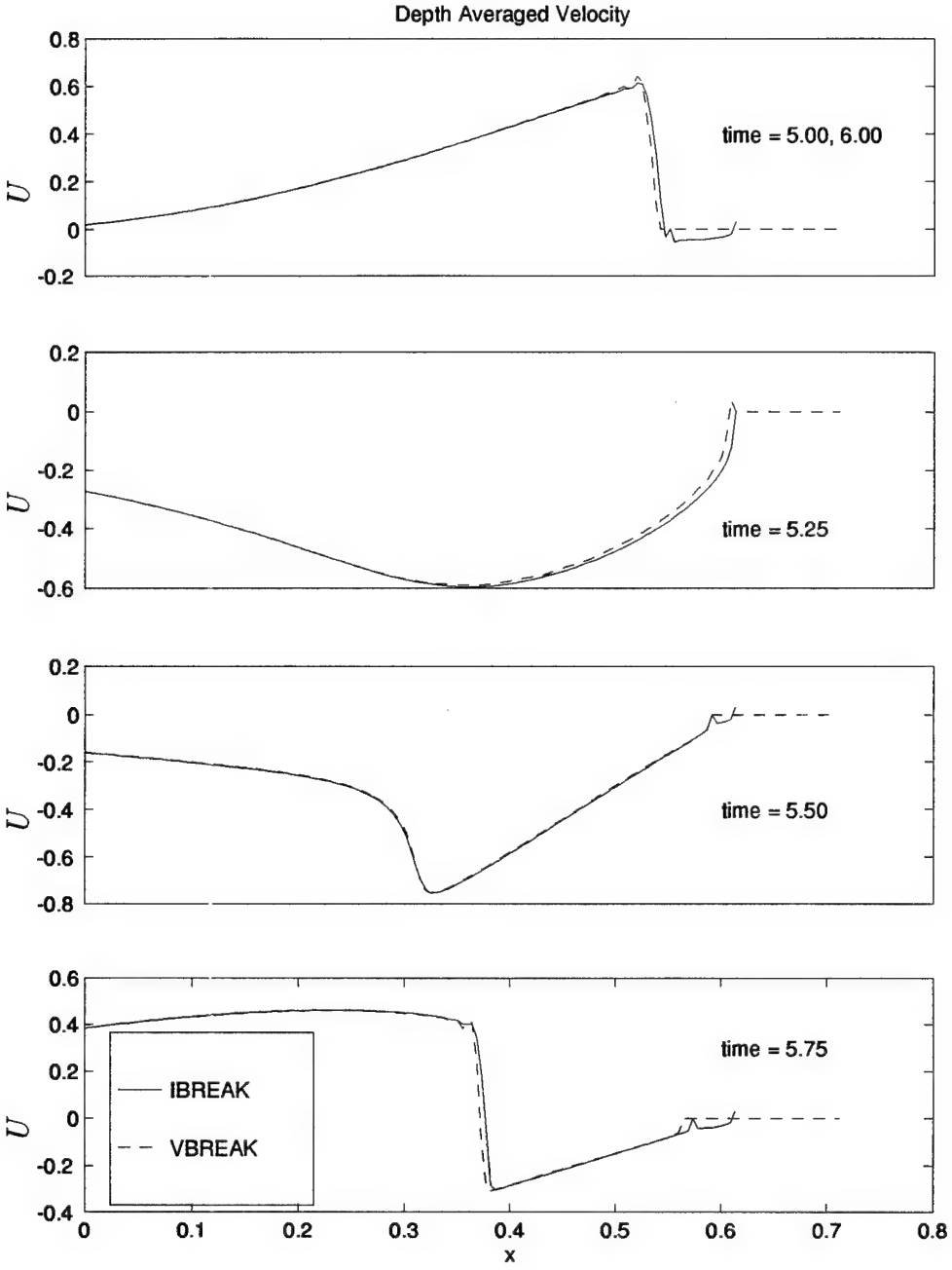

Figure 4.4: Computed cross-shore variation of normalized depth averaged velocity U at 5 time levels, $t = 5.00$, 5.25, 5.50, 5.75, and 6.00: IBREAK(—); VBREAK(- - -).

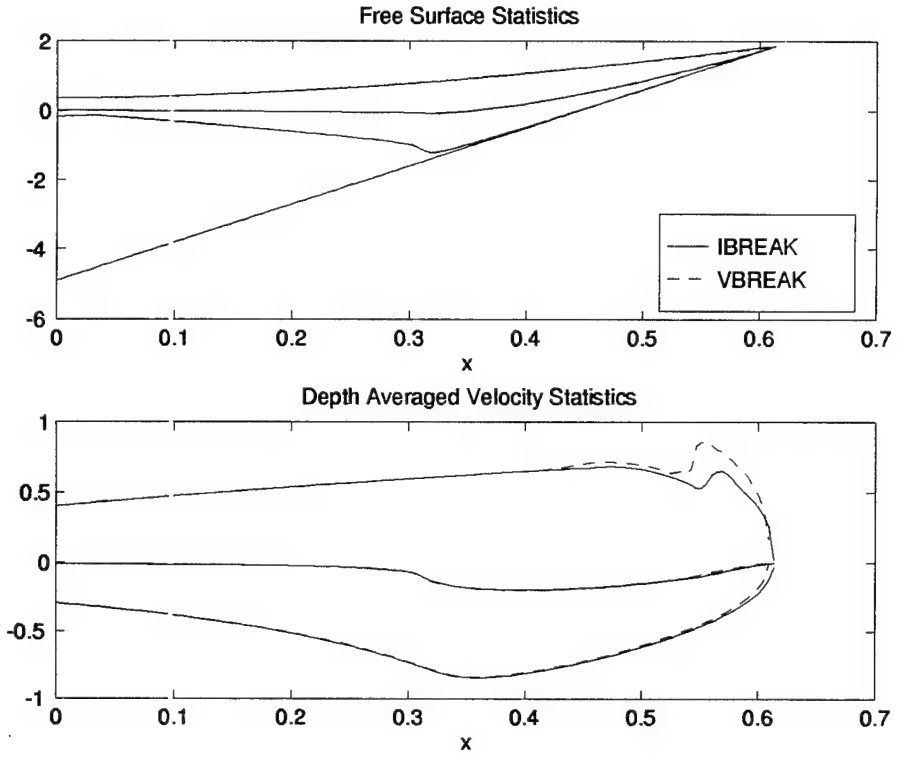

Figure 4.5: Computed cross-shore variation of maximum, minimum, and mean of the normalized free surface η and depth averaged velocity U: IBREAK(—); VBREAK(- - -).

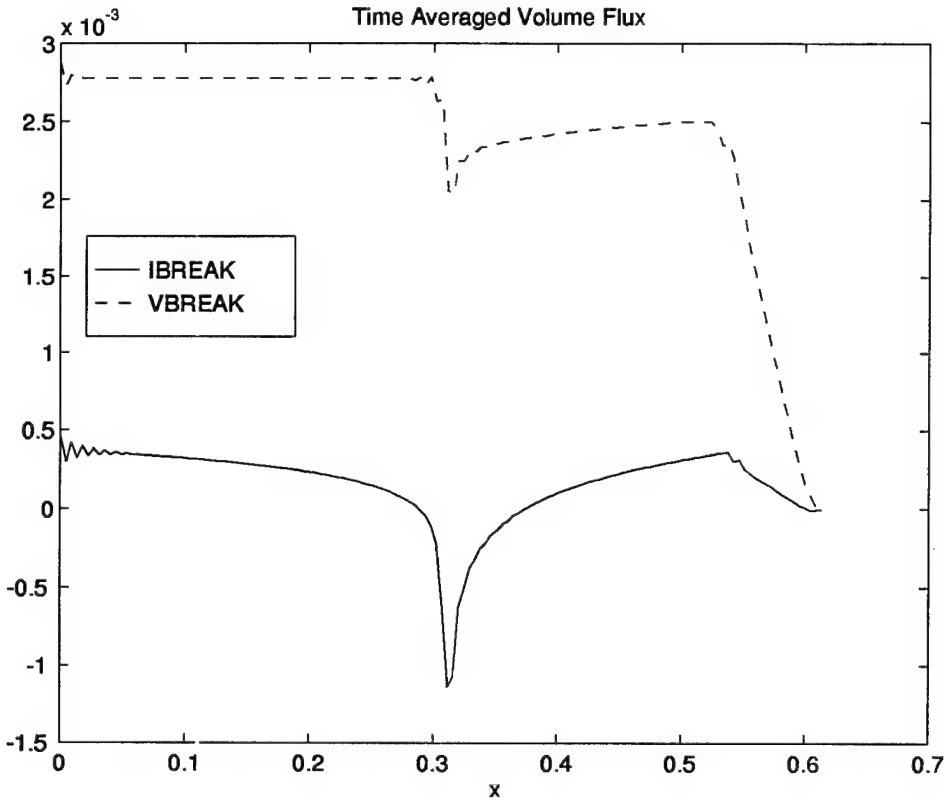

Figure 4.6: Computed cross-shore variation of normalized, time averaged volume flux: IBREAK(—); VBREAK(- - -).

dissipated in the bottom boundary layer as explained in Section 2. For the non-breaking waves on the steep riprap slope, the wave energy dissipation by the bottom friction is dominant. Panel four indicates that VBREAK dissipates only a small fraction of energy in breaking while IBREAK does not include energy dissipation due to the vertical shear. This is expected as the breaking dissipation is dependent on a vertical structure as addressed in Section 2.2. The final panel depicts the numerical dissipation from both models. The numerical dissipation is calculated through an energy balance as outlined in (2.46) and (2.47) where discrepancies are attributed to numerical dissipation related to no explicit wave breaking modeling in IBREAK and the deficiency of the simplified wave breaking modeling adopted in VBREAK. It should be noted that the numerical dissipation is small relative to the physical dissipation due to the bottom friction.

4.2 Comparison of Model to Data of Stive (1980)

The model VBREAK is compared with the comprehensive measurements of test 1 presented by Stive (1980) and Stive and Wind (1982). Because the numerical model VBREAK predicts the vertical variations of the horizontal velocity, the comparison of the measured and computed velocities can be made without any ambiguity. Likewise, the free surface characteristics might demonstrate greater agreement with the measured data as a result of a realistic vertical structure. In Stive's test 1, the incident regular waves with the period $T' = 1.79$ s broke as spilling breakers on the 1:40 concrete beach. The seaward boundary for the computation is taken to be at the still water depth $d'_t = 0.2375$ m, where the near-breaking wave profile was shown to be similar to the cnoidal wave profile as explained by Kobayashi *et al.* (1989). The measured wave height at the seaward boundary was $H' = 0.172$ m. The free surface and velocity characteristics have been found to be relatively insensitive to the choice of the cubic velocity profile parameter, a. In this particular comparison, the parameter a is set to 3.0. The friction factor of 0.05 is used as in

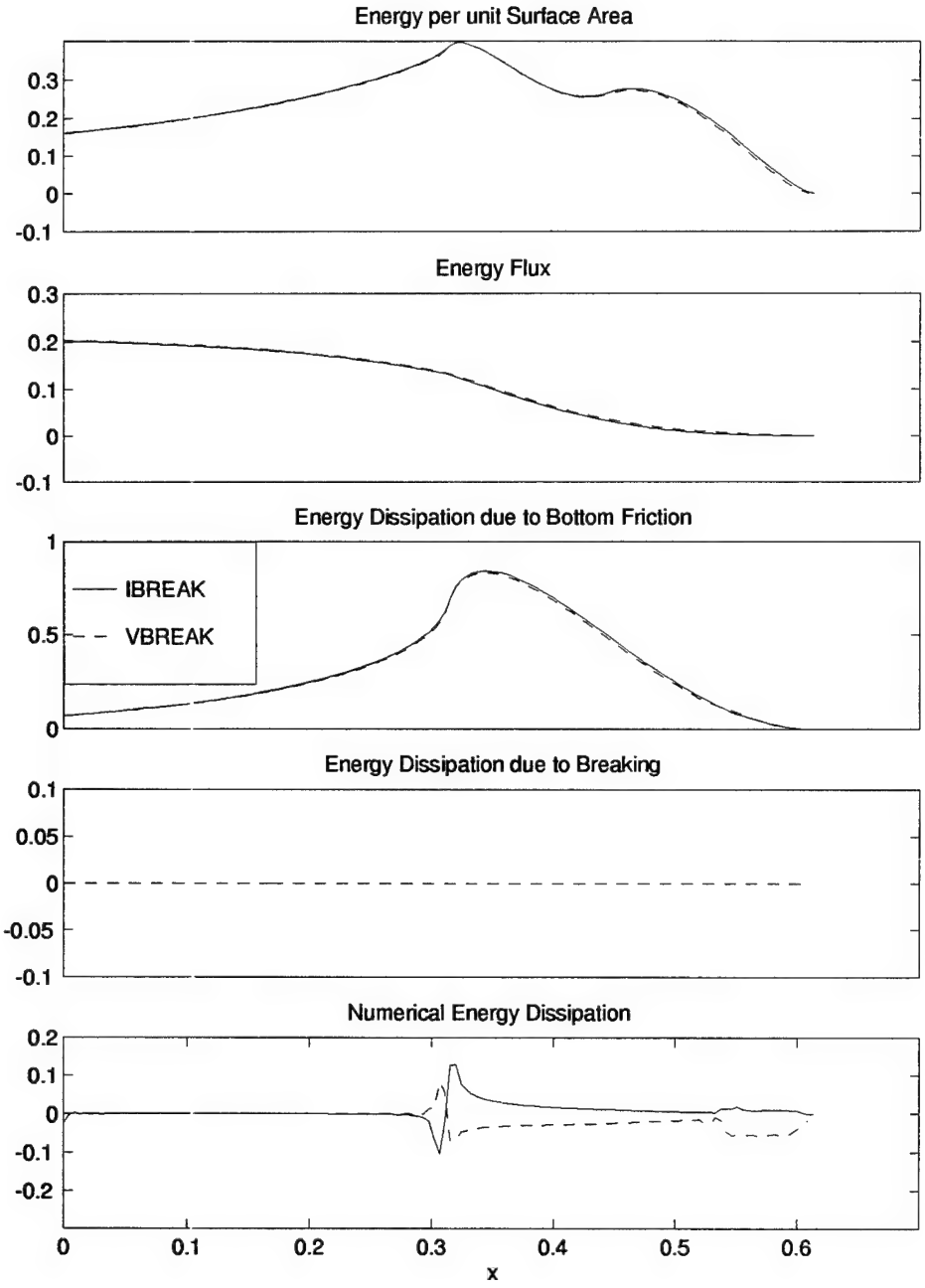

Figure 4.7: Computed cross-shore variation of normalized specific wave energy, energy flux, bottom dissipation, breaking dissipation, and numerical dissipation: IBREAK(—); VBREAK(- - -).

the previous computation by Kobayashi *et al.* (1989). A Courant number of 0.3 is adopted for the stable computation. Numerical stability is more difficult to maintain during the longer computation for the gentle slope of Stive compared with the steep slope case in Section 4.1. The numerical damping coefficient κ is taken to be 1.0 in an effort to suppress the high frequency oscillations that occur at the rear of the breaking wave crest. Tables 4.3 and 4.4 represent the primary input and output files of the numerical model VBREAK. The resultant dimensionless parameters were: surf similarity parameter $\xi = 0.135$; the ratio of horizontal to vertical length scales $\sigma = 13.5$; and Ursell number = 121.7.

The normalized incident wave specified as input to the model and the computed reflected wave are depicted in Figure 4.8. The reflection coefficient $r = 0.008$ is very small as expected from the small surf similarity parameter $\xi = 0.135$.

With a computational shoreline based on the water depth $\delta_r' = 1$ cm, the computed runup is shown in Figure 4.9 where the incident wave train arrives at the shoreline at $t \simeq 5$. The periodic runup consists of the steady setup $\bar{\eta} \simeq 0.06$ from the SWL and a relatively small oscillatory component of amplitude $\simeq 0.015$. The swash is much smaller than the swash on the steep slope presented in Section 4.1.

Figures 4.10 and 4.11 depict the computed spatial variation of the normalized free surface η and the depth averaged velocity U at five times throughout the final wave period. The plots for $t = 29$ and $t = 30$ are identical because of the periodicity. As the wave propagates shoreward, the saw tooth profile develops. The high frequency numerical oscillations are apparent following the crest of the wave; The numerical smoothing described in Section 3.2 is intended to reduce these oscillations. The previous one-dimensional models based on the Lax-Wendroff scheme also developed these unrealistic numerical irregularities. Figure 4.11 also shows the near bottom velocity calculated by model VBREAK. The horizontal velocity $u_b = (U + \tilde{u_b})$ immediately outside the bottom boundary layer is attenuated due to

Table 4.3: Primary input data file for Stive's test 1.

```
  3                    = number of comment lines
-------------------------------------------------------------
Stive 1980 Test 1
-------------------------------------------------------------
1                                              <--ISYST
1                                              <--IWAVE
1                                              <--IBOT
1                                              <--INCLCT
1                                              <--IENERG
1                                              <--ITEMVA
1                                              <--ISPAEU
29.                 30.                        <--TSTAT,TMAX
190                                            <--STILL
0.001               0.300              1.0     <--DELTA,COURNO,DKAPPA
.172                1.79                       <--HREF,TREF
1.0                                            <--KS
9001                                           <--NPINP
3.0                  .10                       <--APROFL,CMIXL
.2375                0.025                     <--DSEAP,SLSURF
1                                              <--NBSEG
  18.000            .025        .05            <--WBSEG(1),TBSLOP(1),BFFSEG(1)
3001                                           <--NPOUT
1                                              <--NDELR
1.                                             <--DELRP(1)
6                                              <--NONODS
1     41    61    81    101                    <--NODLOC(1,2,3,4,5)
141                                            <--NODLOC(6)
5                                              <--NOTIML
29.0        29.25       29.50       29.75       30.00       <--TIMSPA(1,2,3,4,5)
```

Table 4.4: Primary output file for Stive's test 1.

```
------------------------------------------------------------
Stive 1980 Test 1
------------------------------------------------------------

WAVE CONDITION

Cnoidal Incident Wave at Seaward Boundary
Normalized wave height KS     =       1.000000
1-m =       0.113153458D-02
E   =       0.100242146D+01
K   =       0.477945412D+01
Reference Wave Period          =     1.790000 sec.
Reference Wave Height          =     0.172000 meters
Depth at Seaward Boundary      =     0.237500 meters
Norm. Depth at Seaw. Bdr.      =     1.381
Included Correction Term   CT
0 = no; 1 = yes         INCLCT =     1
Normalized Wave Length         =    12.963
"Sigma"                        =    13.518
Ursell Number                  =   121.692
Surf Similarity Parameter      =     0.135
Input Wave Train from Time=0 to TMAX
Computed or Read at Normalized Rate DELTI =     0.003333

Parameters of Vertical Velocity Variations
Cubic Profile Parameter     APROFL =     3.000000
Mixing Length Parameter     CMIXL  =     0.100000
Momentum Flux Coefficient   C2     =     0.548214
Kinetic Energy Flux Coeff.  C3     =    -0.069420
Energy Dissipation Coeff.   CB     =    15.163393
Coefficient of DB           CBL    =     2.049839


BOTTOM GEOMETRY

Norm. Horiz. Length of
      Computation Domain   =     7.741422
Number of Segments         =        1
---------------------------------------------
 SEGMENT     WBSEG(I)    TBSLOP(I)    BFFSEG(I)
       I       meters
---------------------------------------------
       1    18.000000     0.025000     0.050000
```

Table 4.4: – Continued

```
COMPUTATION PARAMETERS

Normalized DX                          =     0.215040D-01
Normalized DELTA                       =     0.100000E-02
Courant Number                         =     0.300
 Must not exceed unity
Numerical Damping Coefficient          =     1.0000
 Must be zero or positive
Normalized Computation Duration  TMAX =    30.000000
Statistical Calculations Start
 when Time is equal to           TSTAT=    29.000000
Total Number of Spatial Nodes    JMAX =      361
Number of Nodes Along Bottom Below SWL
                                 STILL =     190
Storing Temporal Variations from Time = 0
 to TMAX at Normalized Rate      DELTO =     0.010000
Wave Runup Time Series Stored for
                                  NDER =   1 Water Depths
Time Series of ETA, U, and UB
          Stored at              NONODS =       6 Nodes
Spacial Variations of ETA, U, and UB
         Stored at               NOTIML =      5 Time Levels

Maximum time step       =    0.73200E-02
Minimum time step       =    0.27400E-02

REFLECTION COEFFICIENT

ETARRMS/ETAIRMS =     0.008

INCIDENT AND REFLECTED WAVES

            Max          Min          Mean          RMS
Inc.      0.7906      -0.2088       0.0000       0.3096
Ref.     -0.0354      -0.0427      -0.0388       0.0024

SHORELINE OSCILLATIONS

Largest Node Number Reached by Computational Shoreline
                                          SMAX =      204
-------------------------------------------------------------
      I   DELTAR(I)    RUNUP(I)  RUNDOWN(I)  SETUP(I) RMS(I)
            [cm]         Ru          Rd          Zr      Rrms
-------------------------------------------------------------
      1     1.000      0.074       0.047       0.059      0.009
```

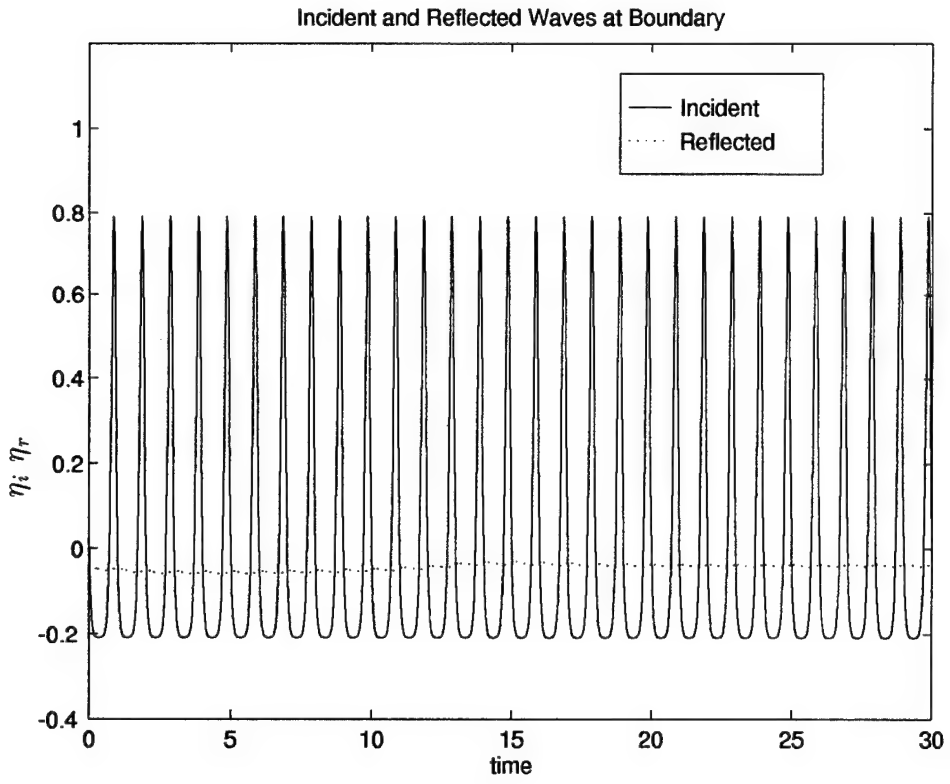

Figure 4.8: Normalized incident and reflected waves at the seaward boundary.

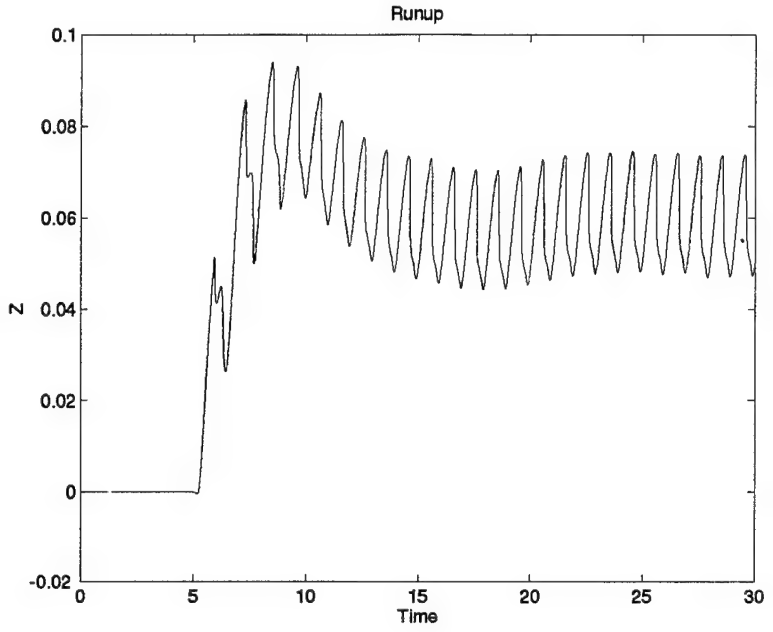

Figure 4.9: Computed normalized time series of runup with $\delta_r' = 1$ cm.

bottom friction. The magnitude of the computed bottom velocity is slightly smaller than that of the depth averaged velocity because $\tilde{u}_b$ is assumed to be out of phase with the depth averaged velocity U in (2.44). Near the bottom, the horizontal velocity develops a kink as the depth averaged velocity U changes sign and the value of $\tilde{u}_b$ changes abruptly. This unrealistic kink, which is apparent in Figure 4.11, suggests the shortcoming of the vertical variation of the horizontal velocity assumed in (2.33).

Figure 4.12 shows the computed and measured maximum free surface elevations throughout the domain for the final wave period. The measured and computed minimum free surface elevations are depicted in Figure 4.13. The wave height comparison is shown in Figure 4.14, defined as the difference between the maximum and minimum elevations. The data of Stive presented in these plots is read from Figure 4 of Stive and Wind (1982). The wave height prediction, appears to be better in

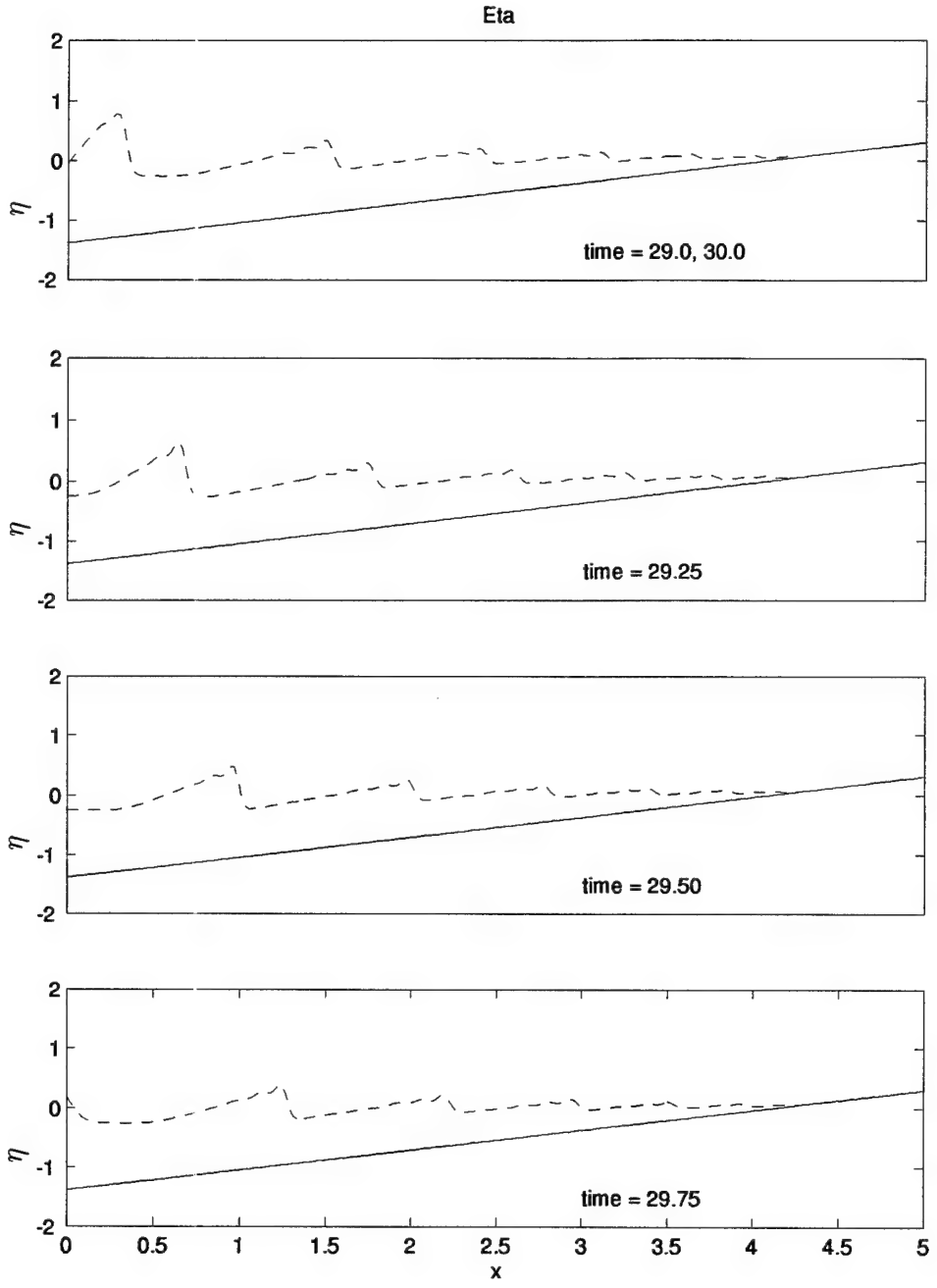

Figure 4.10: Computed cross-shore variation of normalized free surface η at 5 time levels, $t = 29.00$, 29.25, 29.50, 29.75, and 30.00.

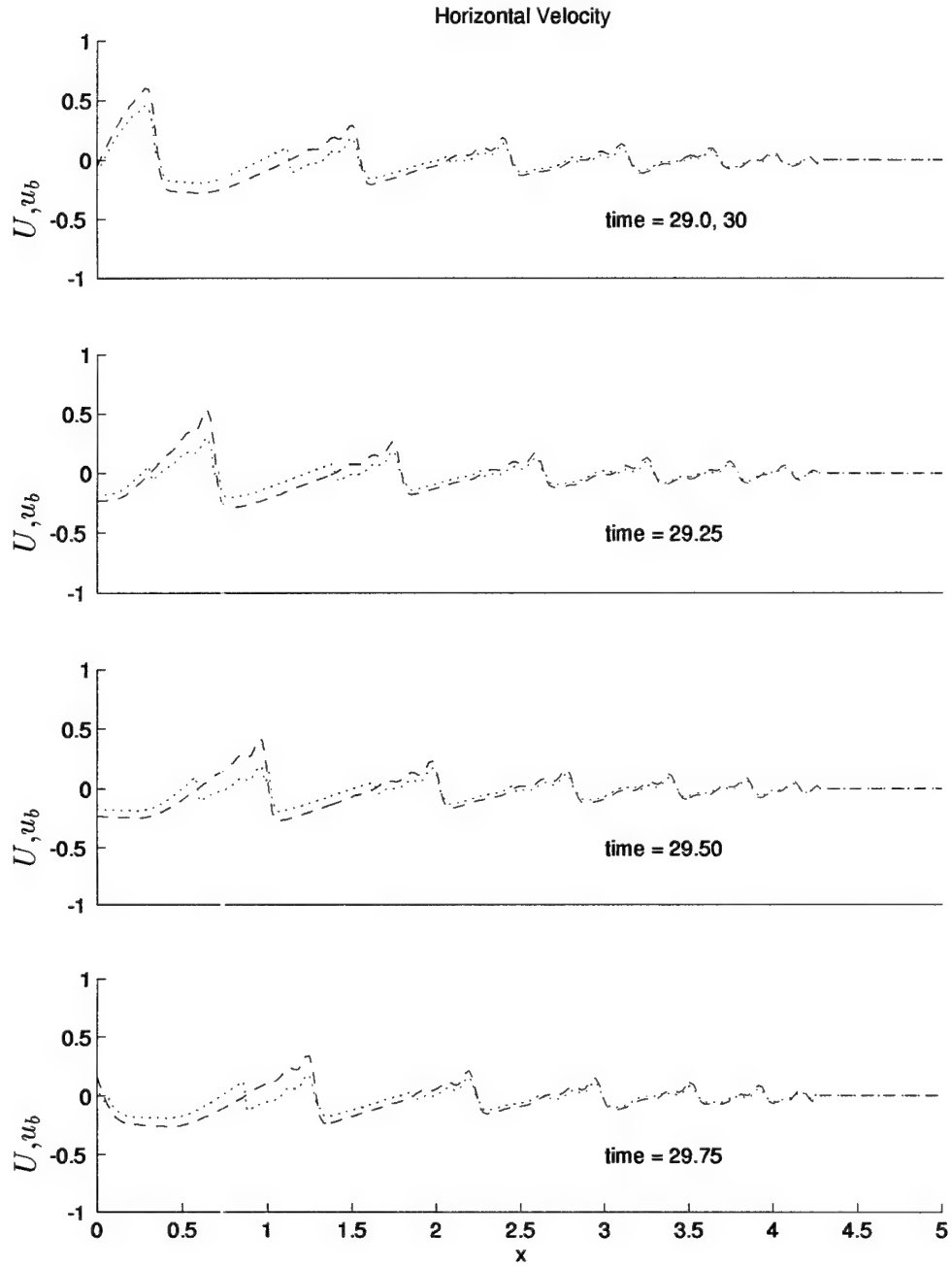

Figure 4.11: Computed cross-shore variation of normalized depth averaged velocity U and near bottom velocity u_b at 5 time levels, $t = 29.00$, 29.25, 29.50, 29.75, and 30.00: U (- - -); u_b ($\cdots$).

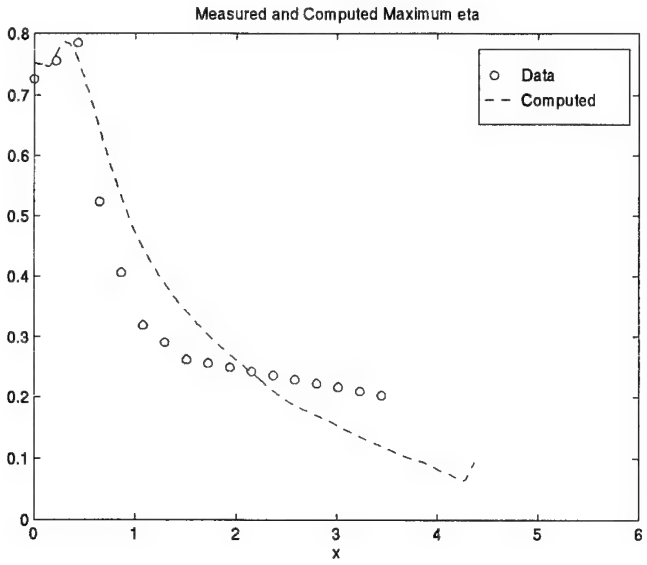

Figure 4.12: Cross-shore variation of the measured and computed maximum normalized free surface.

part, due to the cancellation of the overprediction and underprediction in the computed maximum and minimum elevations. The numerical model underpredicts the rapid decrease of the wave height immediately landward of the break point where the wave height is the largest.

The computed and measured time-averaged free surface elevation, set-down or setup, is depicted in Figure 4.15. The computed mean free surface is notably different in shape from that computed with IBREAK in Figure 11 of Kobayashi *et al.* (1989).

The maximum and minimum horizontal velocities at four spatial positions are depicted in Figure 4.16. In each panel the dashed line represents the computed horizontal velocity distribution and the solid line is the computed depth averaged velocity. The vertical axis is the ratio of z/d where z is the normalized vertical coordinate and d is the normalized still water depth. This is slightly different from the vertical axis of Figure 7 in Stive (1980) where the vertical coordinate equaled

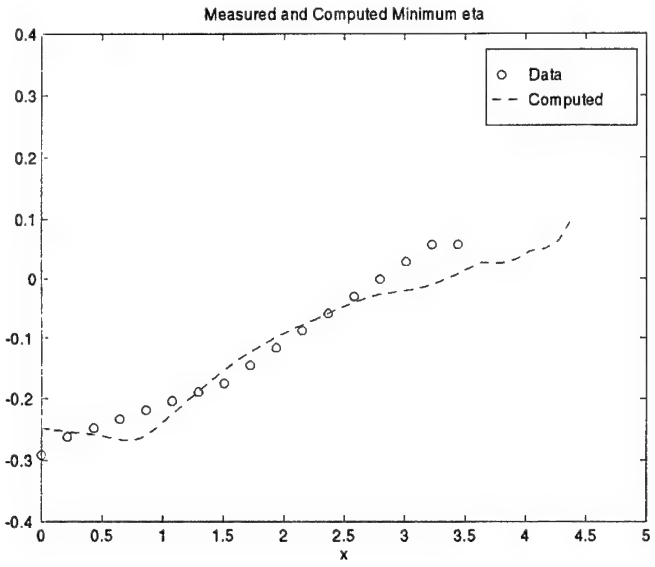

Figure 4.13: Cross-shore variation of the measured and computed minimum normalized free surface.

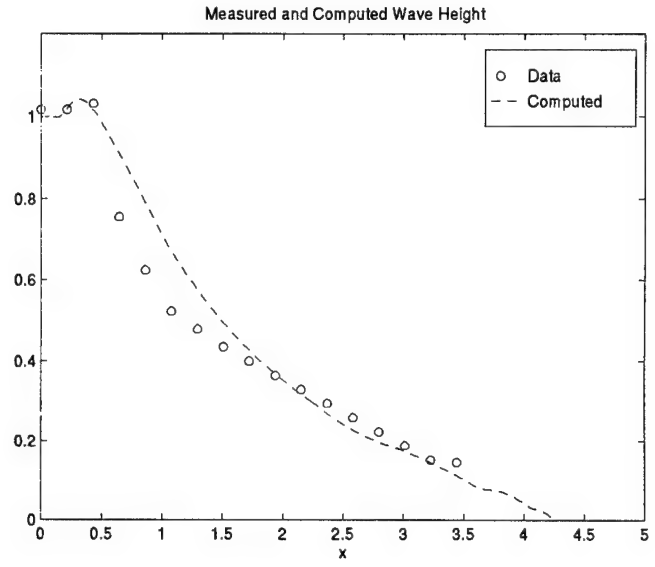

Figure 4.14: Cross-shore variation of the measured and computed normalized wave height.

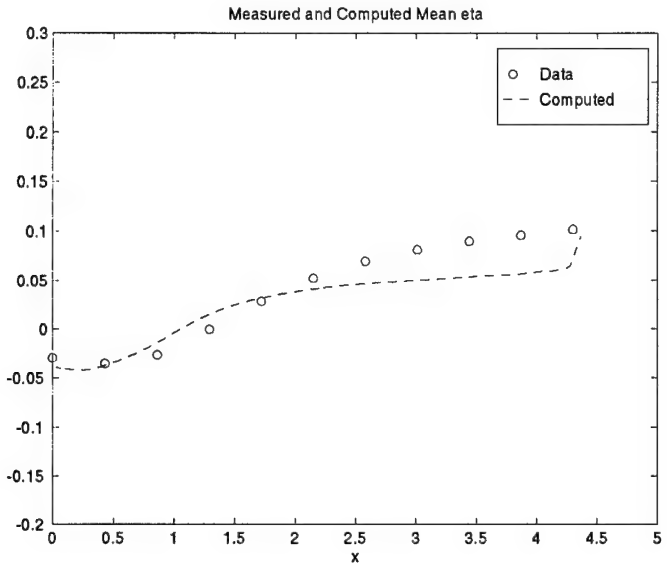

Figure 4.15: Cross-shore variation of the measured and computed mean normalized free surface.

zero at the mean water level. It is worth noting that the maximum and minimum values in Figure 4.16 are obtained at each elevation z without regard to the vertical phase differences. Panel one indicates that although the specified and measured free surface elevations match at the seaward boundary reasonably well, the maximum horizontal velocity is considerably overpredicted. Likewise, at the subsequent locations $x = 1.29$, 2.15, and 3.011 the predicted maximum velocity is larger than the measured. The greatest computed variation of the velocity over the depth occurs after breaking, at $x = 1.29$. This, however, does not correspond well to the measured data below the trough level that display virtually no variation with depth at $x = 1.29$.

The model VBREAK exhibits the small seaward oriented return current as explained by Kobayashi *et al.* (1989). Figure 4.17 shows the computed return current and the measured normalized undertow below the trough level at several locations throughout the water depth. The return current is calculated as the time

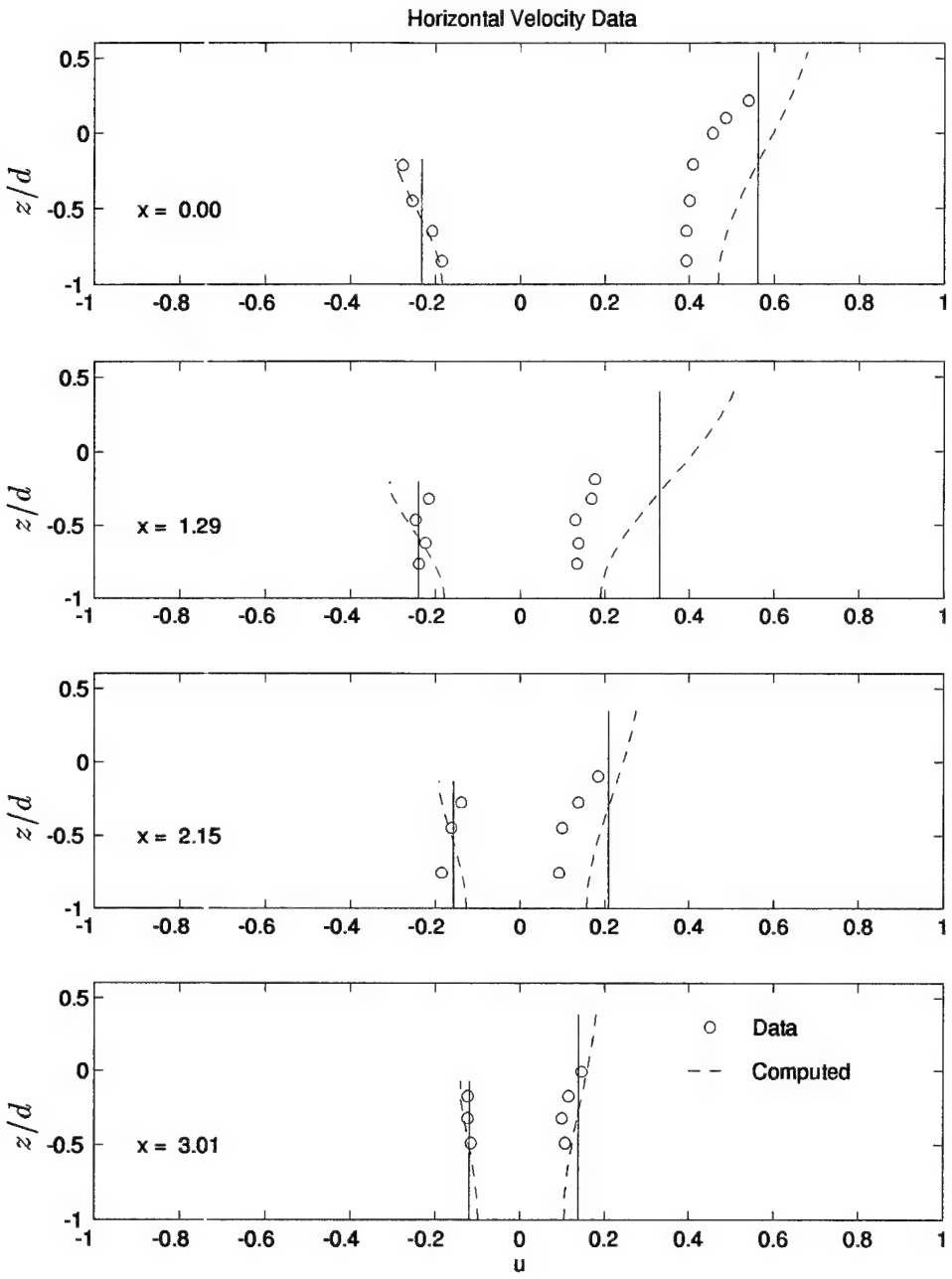

Figure 4.16: Measured and computed maximum and minimum normalized horizontal velocity at four locations, $x = 0$, 1.29, 2.15, and 3.01.

average of the horizontal velocity at a given elevation. The measured values are taken from Figure 8 based on Stive's data from Svendsen (1984). The numerical model predicts the order of magnitude of the undertow but does not predict its vertical variation well, perhaps because the model does not account for the landward mass flux caused by a roller above the trough.

For completeness, the cross-shore variations of the maximum, minimum and mean of the normalized free surface, the depth averaged velocity, and the near bottom velocity are depicted in Figure 4.18. The near bottom velocity is slightly smaller than the depth averaged velocity U as expected.

As in Section 4.1, the cross-shore variation of the time-averaged volume flux is used as an indicator of the computational accuracy. Figure 4.19 demonstrates that the computed flux is nearly zero to satisfy the no flux boundary condition into the impermeable beach.

The normalized energy quantities are shown in Figure 4.20. Notable is the fact that the numerical dissipation dominates over the physically tenable mechanisms such as breaking dissipation and bottom dissipation included explicitly in VBREAK . The value of the cubic velocity profile parameter a has been set to 3.0 in order to increase the breaking dissipation as explained in Section 2.2. However, the breaking dissipation is still small. The increase of the mixing length parameter C_l in 2.39 from 0.1 to 0.2 causes the decrease of $|\tilde{u}_b|$, resulting in little change in the breaking dissipation. This indicates that the velocity profile assumed in (2.33) does not describe well the wave energy dissipation due to breaking on the gentle slope. This probably derives from the fact that the wave front(roller) is not modeled specifically.

The measured and computed temporal variations of the free surface are compared at four spatial locations throughout the domain as shown in Figure 4.21. The variation of the free surface from the mean water level $\bar{\eta}$ for the last wave from

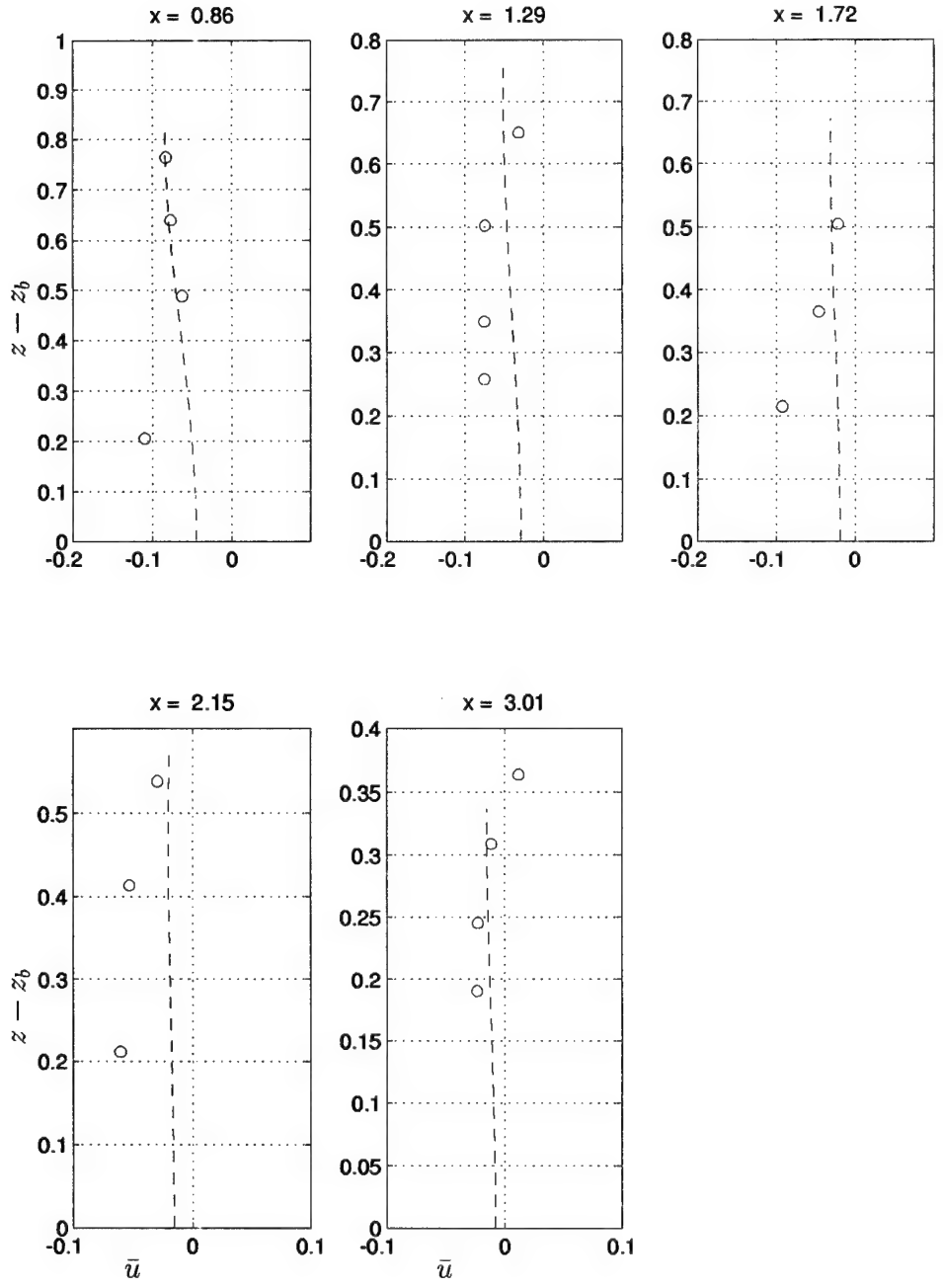

Figure 4.17: Measured and computed normalized undertow at five locations $x =$ 0.86, 1.29, 1.72, 2.15, and 3.01.

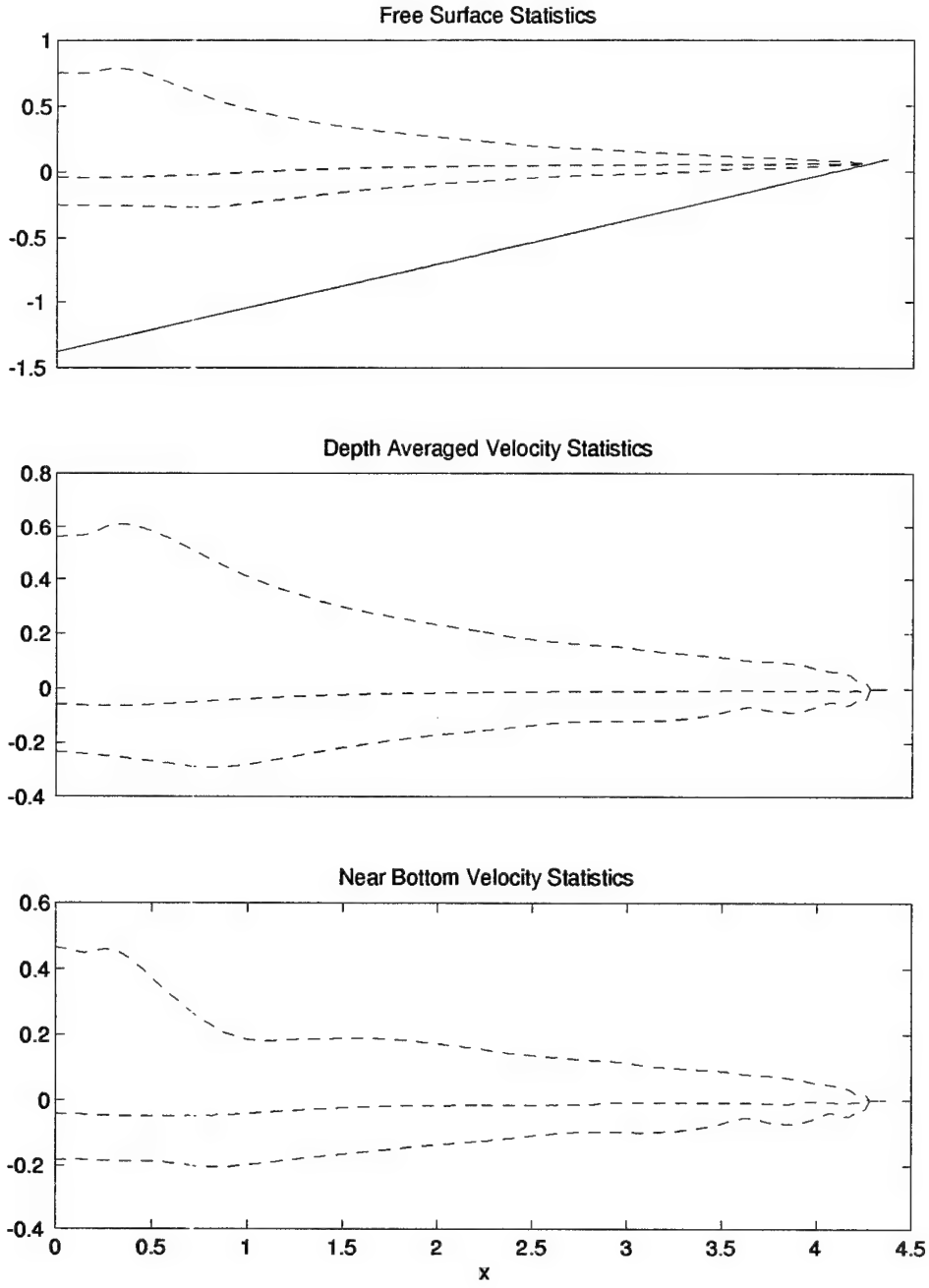

Figure 4.18: Computed cross-shore variation of maximum, minimum, and mean of the normalized free surface, depth averaged velocity, and near bottom velocity.

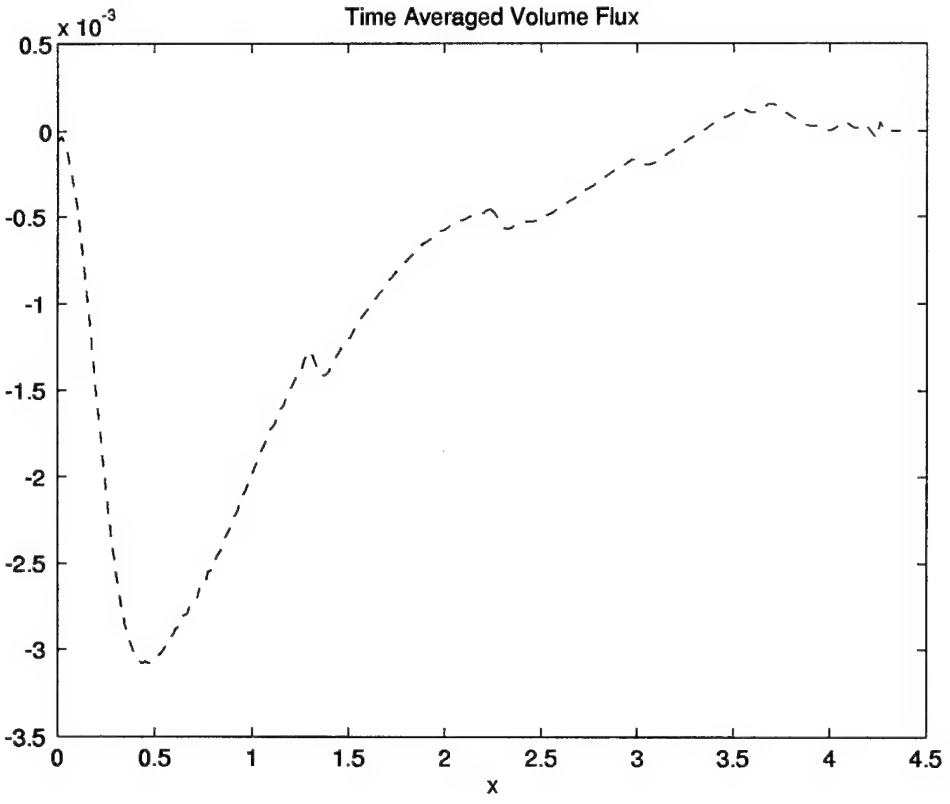

Figure 4.19: Computed cross-shore variation of normalized, time averaged volume flux .

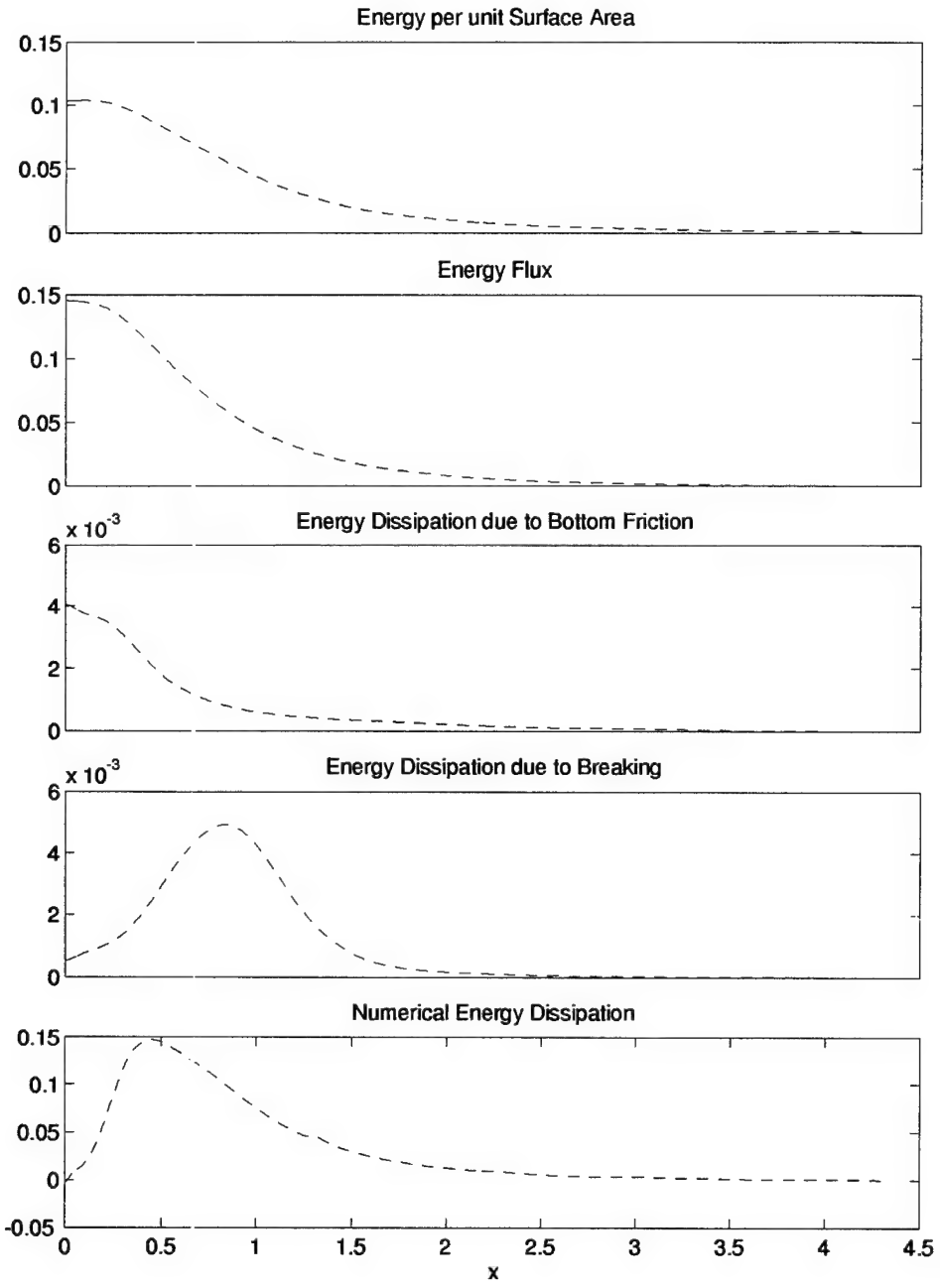

Figure 4.20: Computed cross-shore variation of normalized specific wave energy, energy flux, bottom dissipation, breaking dissipation, and numerical dissipation.

$t = 29.0$ to $t = 30.0$ is shown in each panel. The crest of the computed wave form has been matched by hand with the measured crest; therefore, Figure 4.21 should indicate only the comparison of the predicted and measured wave shapes. In fact, differences between the computed and actual phase speeds are expected, based on the comparison of VBREAK to the data set of Cox (1995) which preserved the phase information throughout the domain. Panel one shows the degree to which the specified incident cnoidal wave agrees with the measured data of Stive. Again, the high frequency oscillations following the wave crest are apparent in Figure 4.21.

4.3 Comparison of Model to Data of Cox *et al.* (1995)

The model VBREAK is finally compared with the data collected by Cox *et al.* (1995) that included detailed velocity profiles inside the surf zone. The experiment was performed in a wave flume. The 1:35 beach was constructed of Plexiglas and had a thin layer of sand glued to the surface to increase the bottom roughness. Figure 4.22 depicts the experimental setup and measurement locations. At each measuring line, water velocity measurements were taken at approximately twenty locations throughout the water column.

The constant wave period throughout the experiment was 2.2 s. The measuring line, L2 was located at the break point defined by Cox *et al.* (1995) as the point where aeration occurred in the tip of the wave crest. The spilling wave developed into a turbulent bore landward of measuring line 3.

The free surface and velocities were measured for the duration of the last 50 waves out of 300 at each location. The numerical model VBREAK is run with 300 waves in order to be consistent with the experimental procedure. The statistical measurements are based on the last 50 waves in the same way as the measured data.

The free surface and velocity characteristics have been found to be insensitive to the choice of the cubic velocity profile parameter a. In the following, the parameter a is set to 3.0 as in Sections 4.1 and 4.2.

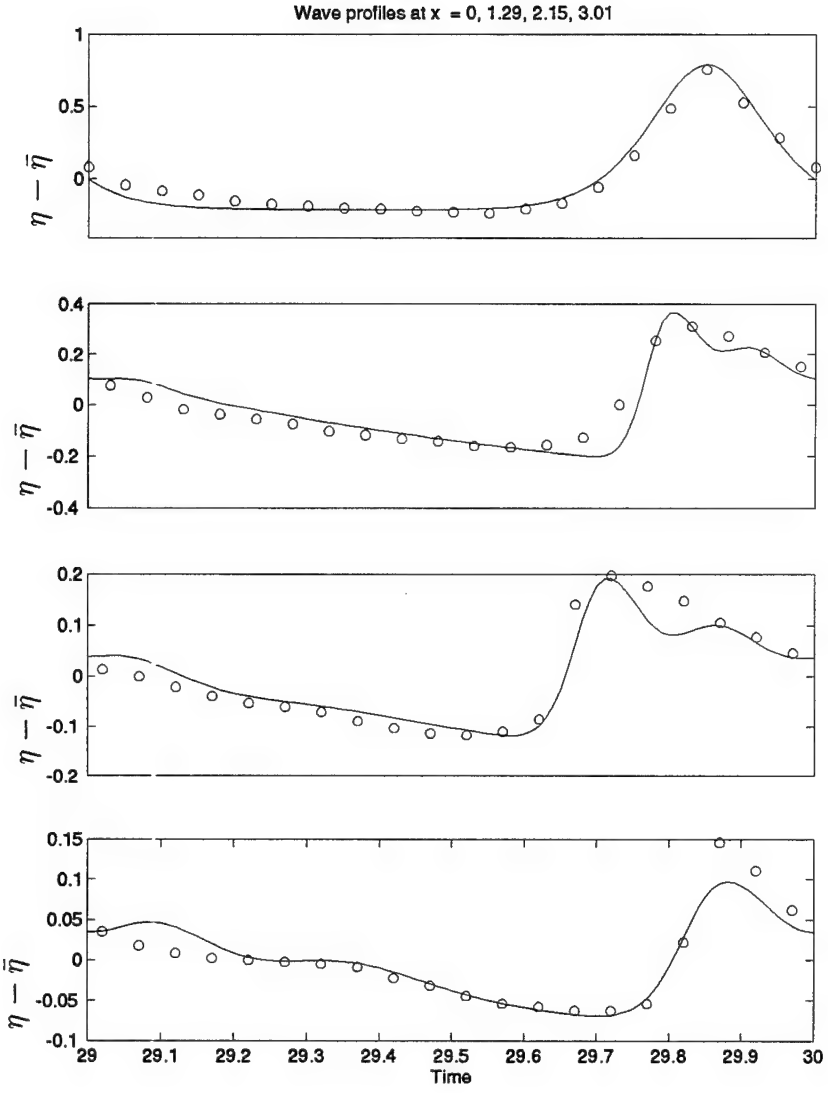

Figure 4.21: Computed and measured normalized wave profiles(with matched crest positions) at four locations, $x = 0$, 1.29, 2.15, and 3.01.

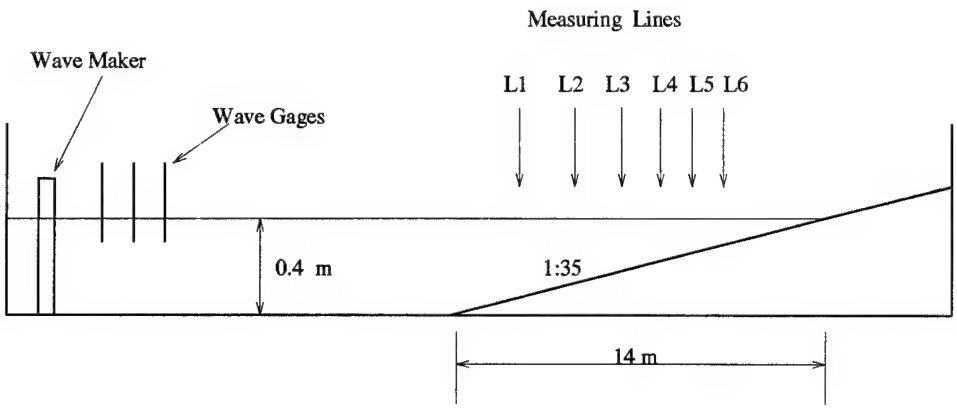

Figure 4.22: Experimental setup (Cox *et al.* 1995).

The friction factor $f'_w = 0.05$ is the same as that for the gentle slope specified in Section 4.2. An argument could be made that the friction factor for the quasi-two-dimensional model VBREAK would need to be recalibrated because the bottom friction is based on a near bottom velocity u_b rather than a depth averaged velocity U. However, the difference between the near bottom and depth averaged velocities is not large enough to warrant this effort. This is especially true considering that the bottom dissipation is secondary in the surf zone and that the constant friction factor is itself an approximation.

A Courant number of 0.4 maintained numerical stability and has been used in both of the following comparisons.

4.3.1 Model Initiation before Breaking

The model VBREAK is initially compared to the data with the seaward boundary at measuring line 1 depicted in Figure 4.22. The height of the incident regular waves at measuring line 1 was $H' = 13.22$ cm. The corresponding still water depth was 28.00 cm. Tables 4.6 and 4.7 represent the primary input and output from the model VBREAK. The resultant dimensionless parameters were: surf similarity

Table 4.5: Horizontal locations and still water depths at six measuring lines.

Line No.	x' (cm)	d (cm)
L1	0	28.00
L2	240	21.14
L3	360	17.71
L4	480	14.29
L5	600	10.86
L6	720	7.43

parameter $\xi = 0.216$; the ratio of horizontal to vertical length scales $\sigma = 19.0$; Ursell number = 74.0.

The normalized incident wave profile measured at line 1 is specified as input to VBREAK and is depicted in Figure 4.23. Only the last fifty waves are utilized in the model to data comparison and thus only those fifty waves are depicted in Figure 4.23. The total of the 300 waves is constructed through the repetition of six sets of the 50 waves depicted in Figure 4.23. The calculated reflected wave is insignificant relative to the incident wave. The computed wave reflection coefficient r = 0.01 is consistent with the small surf similarity parameter $\xi = 0.216$ for the 1:35 slope.

The runup computed based on a computational shoreline of water depth δ_r' = 0.5 cm, is depicted in Figure 4.24. As in the previous figure, only the last 50 of the 300 waves are shown. The computed runup Z is the shoreline elevation above the SWL and is plotted against the normalized time. The incident wave shown in Figure 4.23 is not breaking but is not perfectly periodic. The runup on the gentle slope amplifies the nonperiodic components of the incident waves shown in Figure 4.23. The runup consists of setup $\bar{\eta} \simeq 0.06$ and oscillatory components of amplitude $\simeq 0.02$. The runup was not measured in the experiment by Cox *et al.* (1995).

Table 4.6: Primary input data file (initiated before breaking) for Cox *et al.* (1995).

```
       5                                        --> NLINES
-----------------------------------------------------------------------
L13053                                                      BDJ June '95

SBC at L1; 300 waves input; f'=.05; and IWAVE=3
-----------------------------------------------------------------------
1                                                 <--ISYST
3                                                 <--IWAVE
1                                                 <--IBOT
1                                                 <--IENERG
1                                                 <--ITEMVA
1                                                 <--ISPAEU
I300                                              <--FINP2
250.                 300.                         <--TSTAT,TMAX
490                                               <--STILL
0.001              0.400              1.0         <--DELTA,COURNO,DKAPPA
.1322               2.2                           <--HREF,TREF
66001                                             <--NPINP
3.0                  .10                          <--APROFL,CMIXL
.28                0.028571                       <--DSEAP,SLSURF
1                                                 <--NBSEG
15.000           .028571        .05
66001                                             <--NPOUT
1                                                 <--NDELR
0.5
18                                                <--NONODS
1     2     3     120   121
122   180   181   182   240
241   242   300   301   302
360   361   362
5                                                 <--NOTIML
299.0       299.25      299.50      299.75       300.0      <--TIMSPA
```

Table 4.7: Primary output file (initiated before breaking) for Cox *et al.* (1995).

```
------------------------------------------------------------------
L13053                                                    BDJ June

SBC at L1; 300 waves input; f'=.05; and IWAVE=3
------------------------------------------------------------------

WAVE CONDITION

Measured Total Wave Profile at Seaward Boundary

Reference Wave Period          =     2.200000 sec.
Reference Wave Height          =     0.132200 meters
Depth at Seaward Boundary      =     0.280000 meters
Norm. Depth at Seaw. Bdr.      =     2.118
Included Correction Term   CT
0 = no; 1 = yes        INCLCT  =     0
Normalized Wave Length         =    12.515
"Sigma"                        =    18.951
Ursell Number                  =    73.951
Surf Similarity Parameter      =     0.216
Input Wave Train from Time=0 to TMAX
Computed or Read at Normalized Rate DELTI =     0.004545

Parameters of Vertical Velocity Variations
Cubic Profile Parameter     APROFL =     3.000000
Mixing Length Parameter     CMIXL  =     0.100000
Momentum Flux Coefficient   C2     =     0.548214
Kinetic Energy Flux Coeff.  C3     =    -0.069420
Energy Dissipation Coeff.   CB     =    15.163393
Coefficient of DB           CBL    =     2.873676


BOTTOM GEOMETRY

Norm. Horiz. Length of
      Computation Domain   =     5.979232
Number of Segments         =        1
-------------------------------------------
 SEGMENT    WBSEG(I)   TBSLOP(I)    BFFSEG(I)
       I      meters
-------------------------------------------
       1   15.000000    0.028571    0.050000
```

Table 4.7: – Continued

```
COMPUTATION PARAMETERS

Normalized DX                          =     0.798295D-02
Normalized DELTA                       =     0.100000E-02
Courant Number                         =     0.400
 Must not exceed unity
Numerical Damping Coefficient          =     1.0000
 Must be zero or positive
Normalized Computation Duration  TMAX =   300.000000
Statistical Calculations Start
 when Time is equal to           TSTAT=   250.000000
Total Number of Spatial Nodes    JMAX =      750
Number of Nodes Along Bottom Below SWL
                                 STILL =     490
Storing Temporal Variations from Time = 0
 to TMAX at Normalized Rate      DELTO =     0.004545
Wave Runup Time Series Stored for
                                  NDER =   1 Water Depths
Time Series of ETA, U, and UB
          Stored at              NONODS =      18 Nodes
Spacial Variations of ETA, U, and UB
         Stored at               NOTIML =      5 Time Levels

Maximum time step       =    0.21941E-02
Minimum time step       =    0.13309E-02

REFLECTION COEFFICIENT

ETARRMS/ETAIRMS =     0.010

INCIDENT AND REFLECTED WAVES

            Max          Min          Mean          RMS
Inc.      0.7186      -0.3113      -0.0277       0.3057
Ref.      0.0098      -0.0012       0.0050       0.0029

SHORELINE OSCILLATIONS

Largest Node Number Reached by Computational Shoreline
                                          SMAX =      523
-------------------------------------------------------------------
      I   DELTAR(I)    RUNUP(I)  RUNDOWN(I)  SETUP(I) RMS(I)
            [cm]         Ru          Rd          Zr       Rrms
-------------------------------------------------------------------
      1     0.500      0.099       0.028       0.060      0.015
```

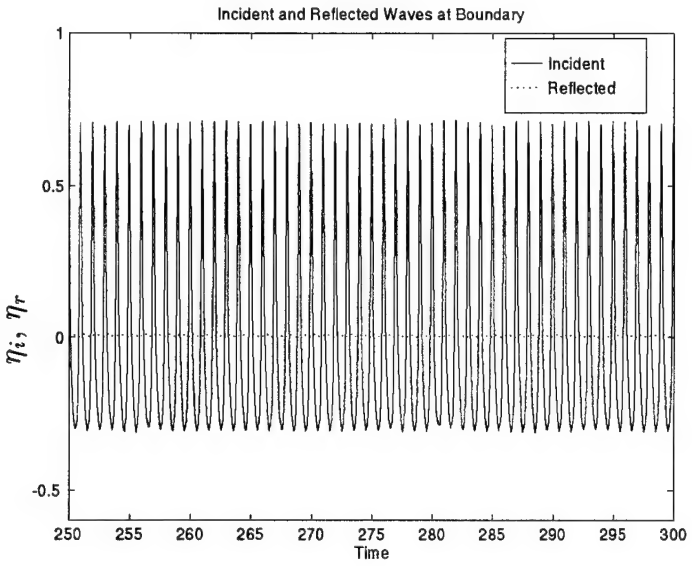

Figure 4.23: The last 50 normalized incident and reflected waves at seaward boundary, measuring line 1.

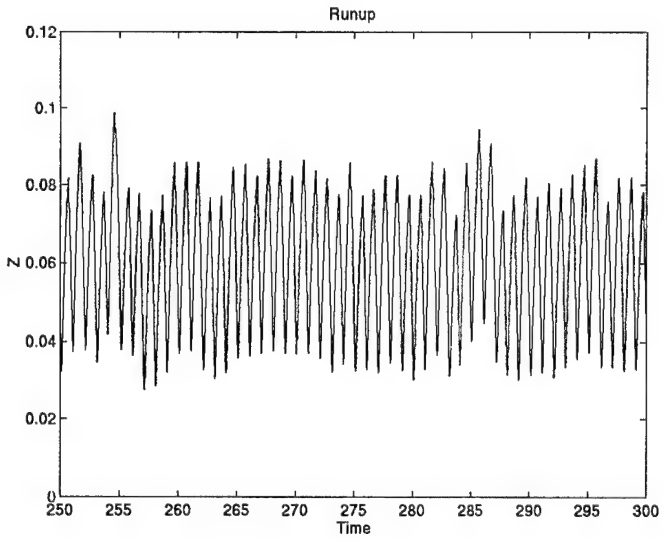

Figure 4.24: Computed normalized time series of runup with $\delta_r' = 0.5$ cm.

Figures 4.25 and 4.26 depict the computed spatial variation of the normalized free surface η and the depth averaged velocity U as well as the near bottom velocity u_b at five times throughout the final wave period. Because the input waves specified at the seaward boundary are not exactly periodic, panel one of Figure 4.25 exposes the slight difference between the free surfaces at times $t = 299$ and $t = 300$. The wave shape changes as it propagates shoreward. The nonlinear terms in the shallow water equations are responsible for the steepening of the wave front that is most apparent in panel one of Figure 4.25. The magnitude of the near bottom velocity shown in Figure 4.26 is smaller than that of the depth averaged velocity because of the assumption made in (2.44). The near bottom velocity has an implausible discontinuity at the zero crossings of the depth averaged velocity caused by the abrupt change of the near bottom velocity correction based on (2.44a) and (2.44b). If the computed momentum flux correction m does not approach zero as the depth averaged velocity U approaches zero, a discontinuity will occur in the horizontal velocity as the depth averaged velocity changes sign.

The comparison of the computed and measured time series of the normalized free surface for the last ten waves is depicted in Figure 4.27. The free surface shown in panel one is used as the boundary condition for the computation. Subsequent panels show the agreement in phase and shape at five measuring lines. Initially, VBREAK overpredicts the phase speed as seen in the second panel at measuring line 2. After wave breaking, the model underpredicts the phase speed. The greatest accumulative error is apparent in the last panel, at measuring line 6. Additionally, the wave height is underpredicted at the measuring lines 2–6.

Because the input wave is measured data, the model output is not perfectly periodic; comparisons are therefore made of the hydrodynamic quantities phase-averaged over the last 50 waves. The comparison of the phase-averaged free surface is made in Figure 4.28. Because the nonperiodic components are relatively small,

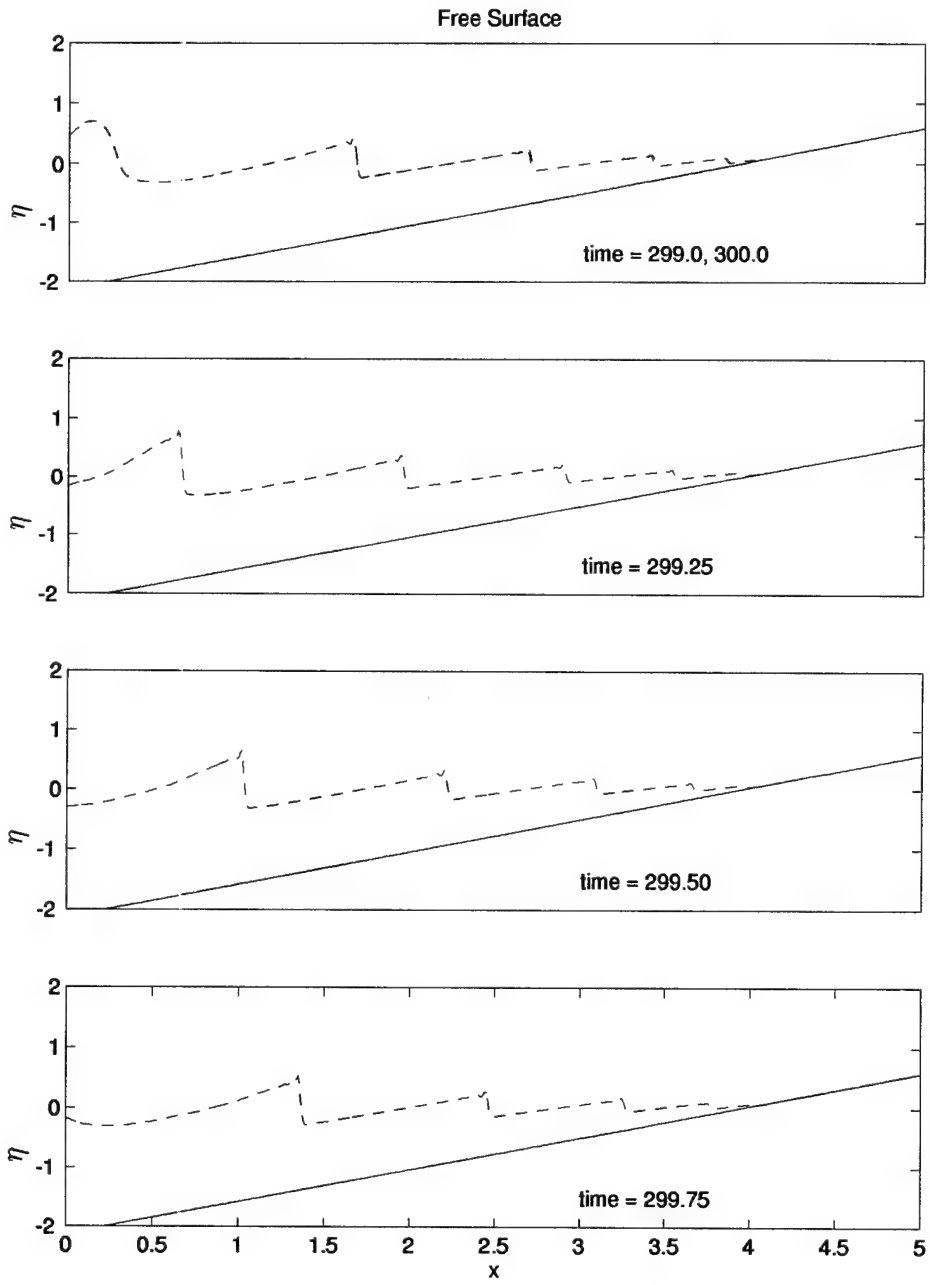

Figure 4.25: Computed cross-shore variation of normalized free surface η at 5 time levels, $t = 299.00$, 299.25, 299.50, 299.75, and 300.

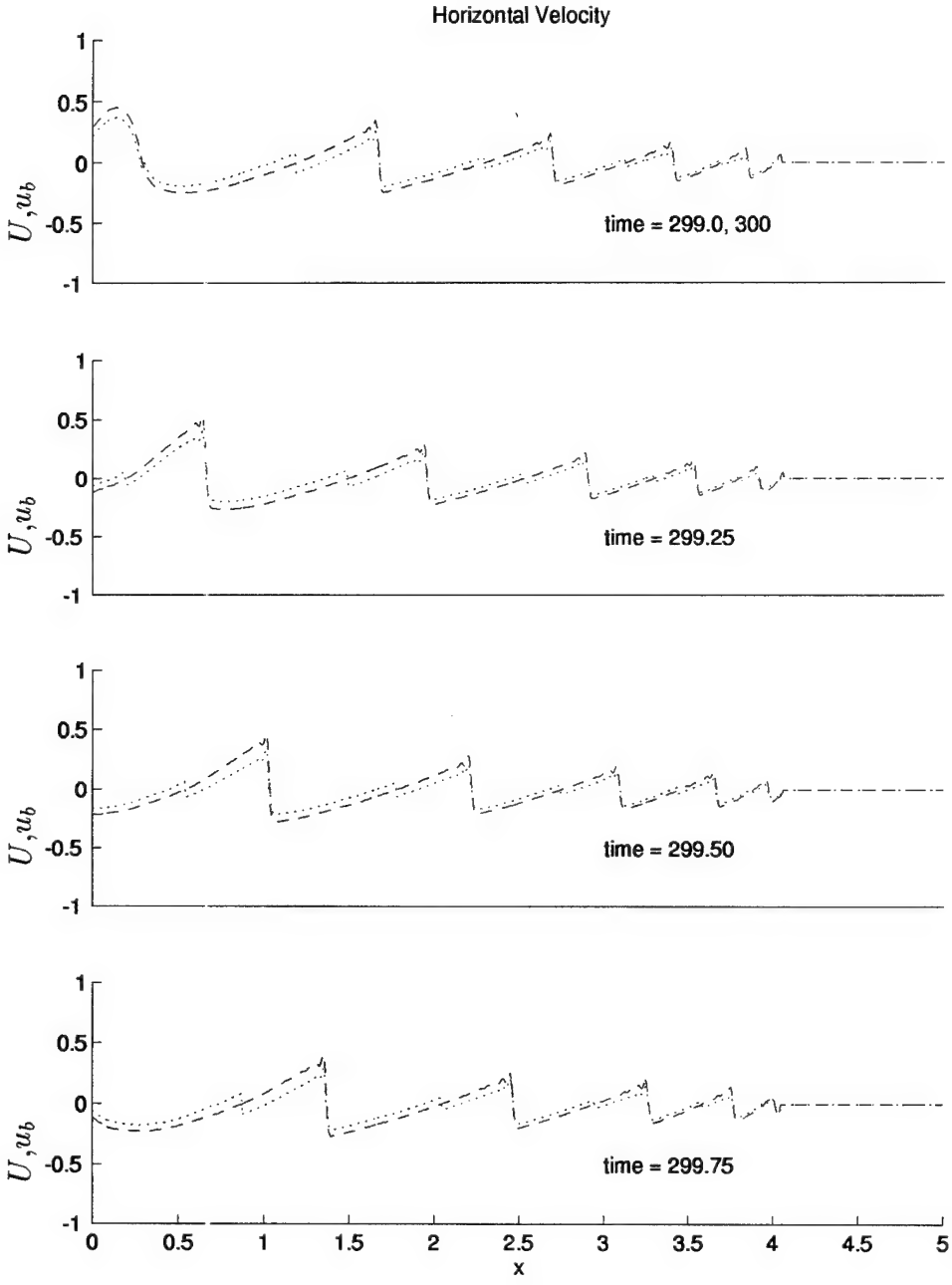

Figure 4.26: Computed normalized cross-shore depth averaged velocity U and near bottom velocity u_b at 5 time levels, $t = 299.00$, 299.25, 299.50, 299.75, and 300: U (- - -); u_b ($\cdots$).

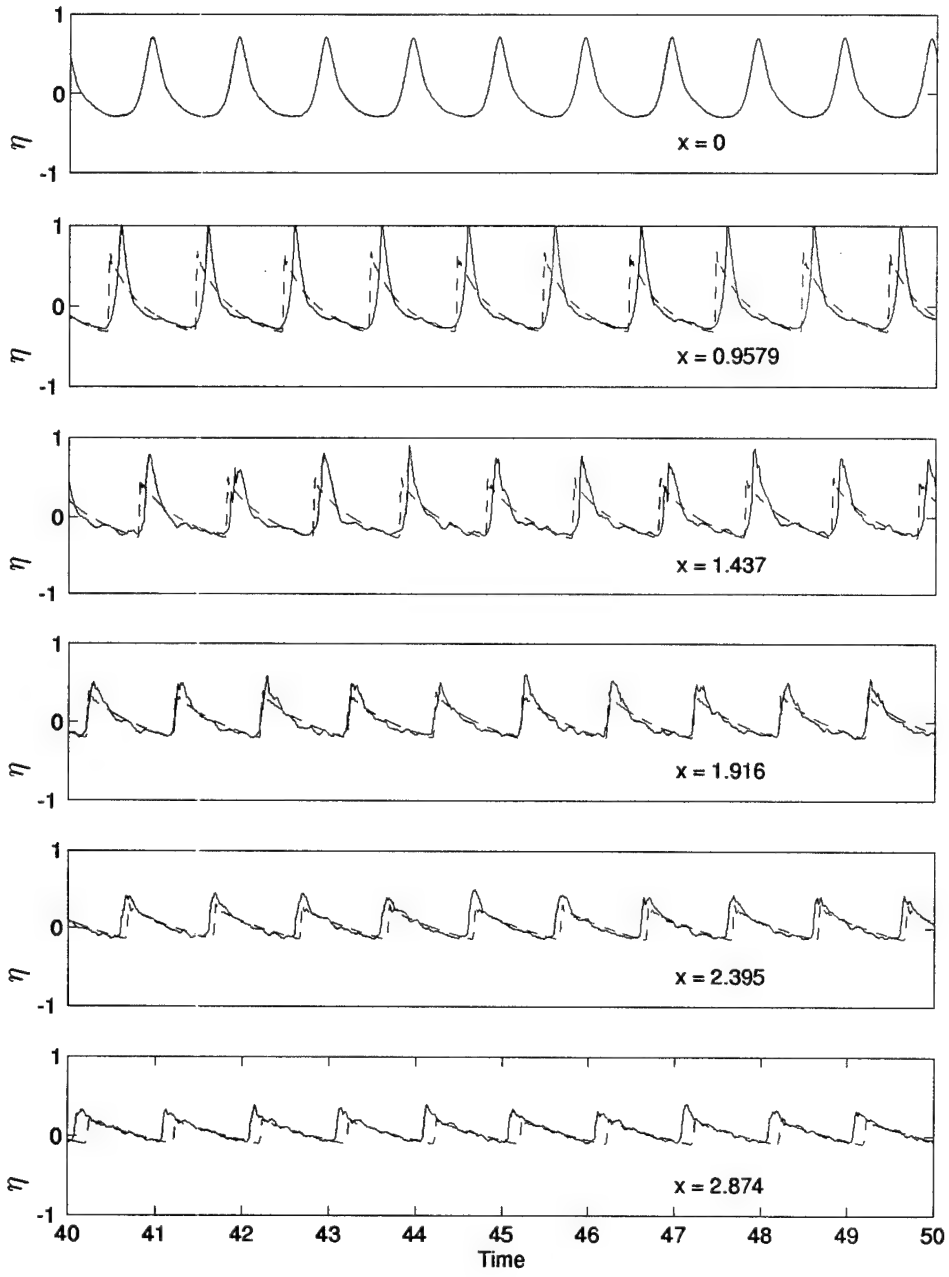

Figure 4.27: Measured and computed time series for the last ten waves of the normalized free surface at six measuring lines: Measured(—); Computed(- - -).

the phase-averaged free surface exhibits the same characteristics as the individual waves shown in Figure 4.27.

The horizontal velocity data was taken at approximately twenty elevations throughout the water depth. Figures 4.29 through 4.34 compare the model VBREAK output with the phase-averaged measured velocity at three vertical elevations. The first panel shows the comparison near the wave trough level. The plot of the measured phase-averaged u is discontinuous due to dropouts in the measured data. Only the reliable data near the trough has been plotted in Figure 4.29 through 4.34. The second panel of each figure is at a vertical location near mid-depth. Finally, the last is a comparison of the near bottom velocities at a distance of 1.1 cm above the bottom. Obviously, the disagreement in the measured and computed velocity variations is exacerbated through the inaccurate prediction of the phase speed. For instance, at measuring line 6, the velocities are predicted reasonably well except for the mismatch in the phase between the computed and measured data. The irregularities in each of the velocity plots, as previously seen in Sections 4.1 and 4.2, are due to the sign change in the bottom velocity correction. The discontinuity in the bottom velocity correction accompanies the sign change in the depth averaged velocity U. It is most apparent near the bottom and free surface where the values of F in (2.33) is the largest as shown in Figure 2.2.

The vertical velocity variations at six phases are shown in Figures 4.35 through 4.40. In each figure, the first panel depicts the computed and measured horizontal velocity as a function of the normalized vertical distance $(z - z_b)$ above the bottom. The computed and measured free surfaces are shown as an empty circle and as a horizontal line, respectively. The measured velocity data is plotted as a solid line, excluding the data points that are deemed unreliable due to the proximity of the free surface. The second panel depicts the comparison of the vertical variation of the measured vertical velocity with the value computed using (2.45). The

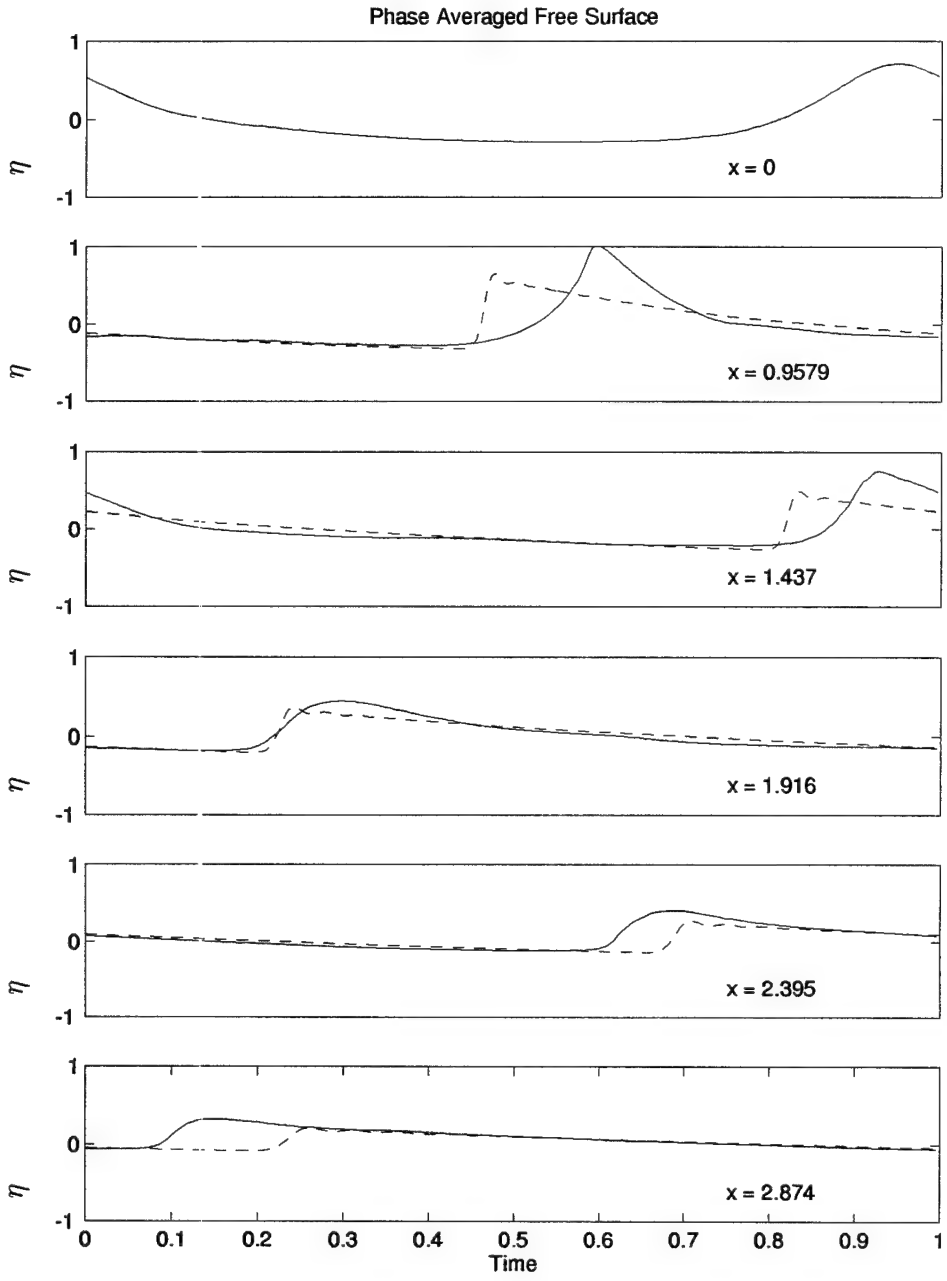

Figure 4.28: Time series of the phase-averaged, normalized free surface at six measuring lines: Measured(—); Computed(- - -).

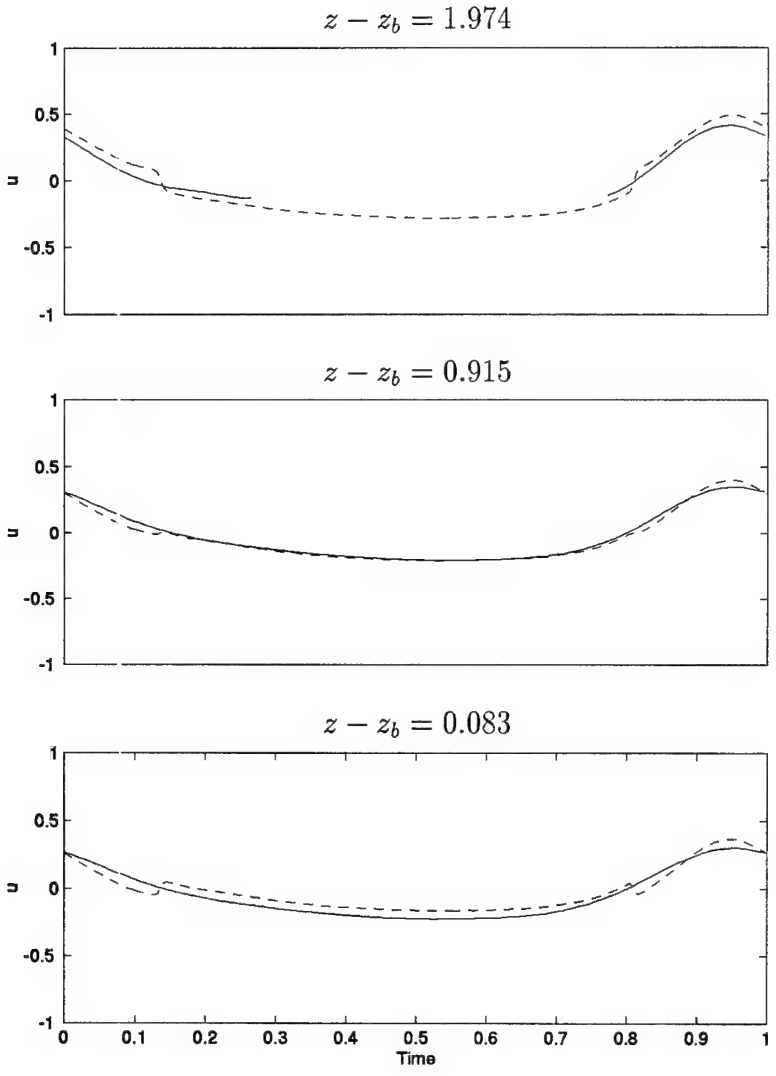

Figure 4.29: Normalized phase-averaged horizontal velocity u at three elevations at measuring line 1; $(z' - z'_b) = 1.1$, 12.1, 26.1 cm.: Measured(—); Computed(- - -).

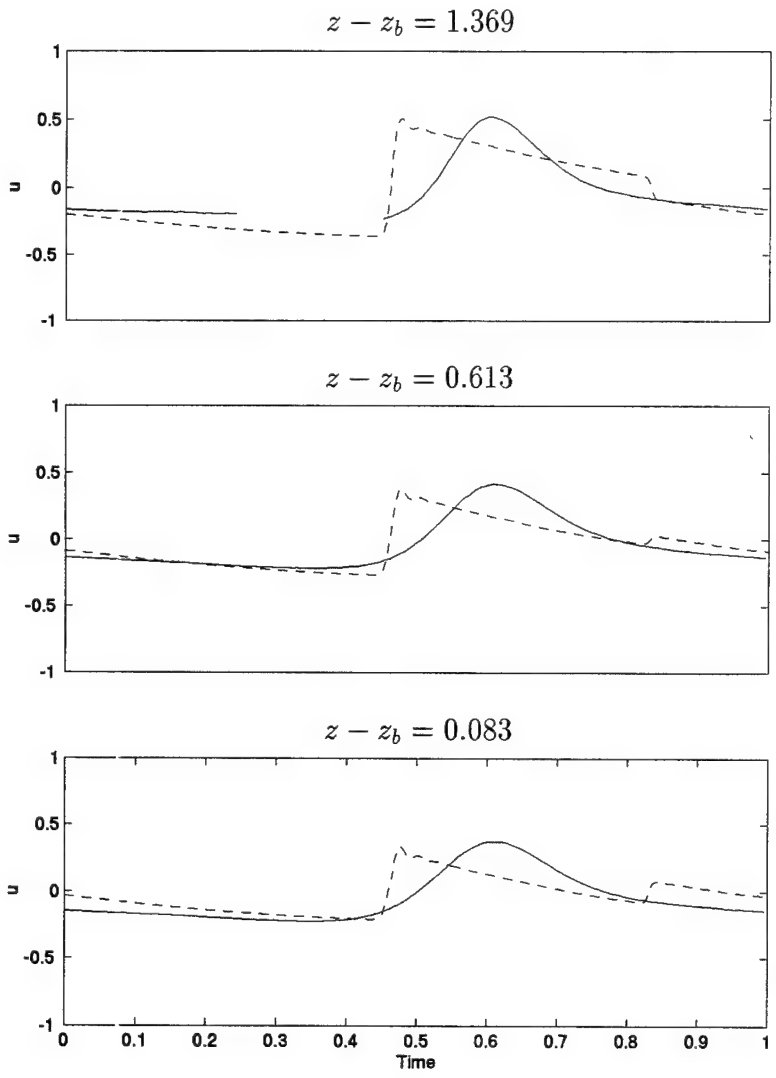

Figure 4.30: Normalized phase-averaged horizontal velocity u at three elevations at measuring line 2; $(z' - z'_b)$ = 1.1, 8.1, 18.1 cm.: Measured(—); Computed(- - -).

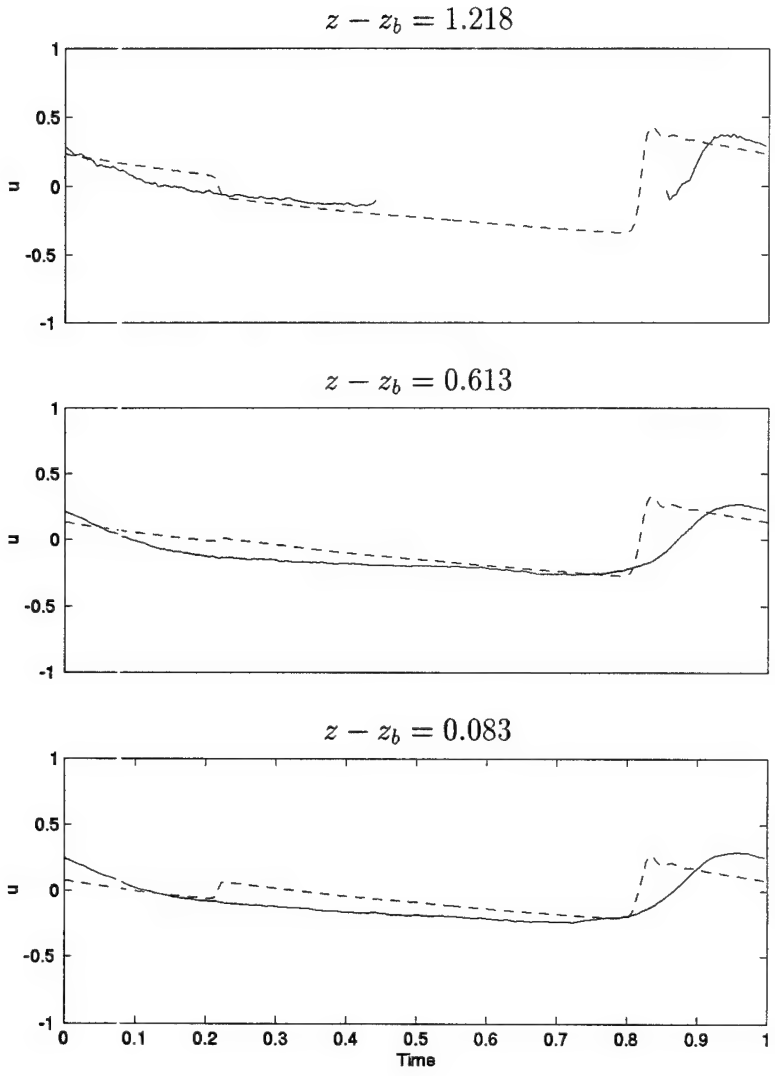

Figure 4.31: Normalized phase-averaged horizontal velocity u at three elevations at measuring line 3; $(z' - z_b') = 1.1$, 8.1, 16.1 cm.: Measured(—); Computed(- - -).

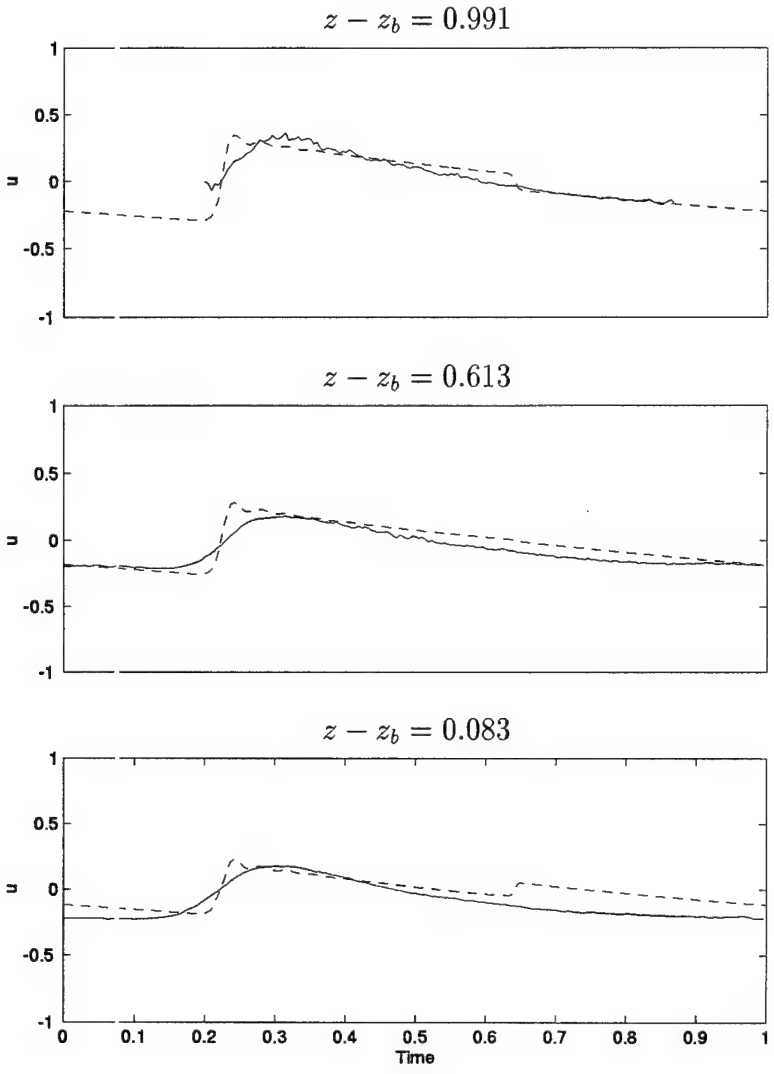

Figure 4.32: Normalized phase-averaged horizontal velocity u at three elevations at measuring line 4; $(z' - z'_b)$ = 1.1, 8.1, 13.1 cm.: Measured(—); Computed(- - -).

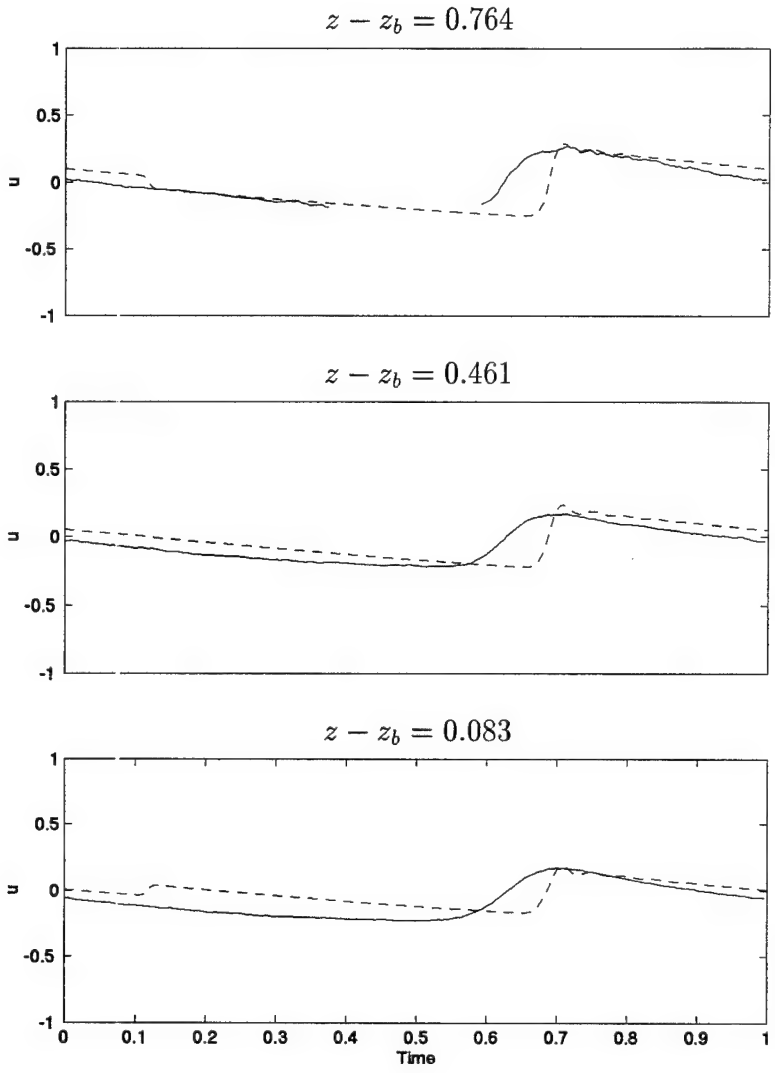

Figure 4.33: Normalized phase-averaged horizontal velocity u at three elevations at measuring line 5; $(z' - z'_b)$ = 1.1, 6.1, 10.1 cm.: Measured(—); Computed(- - -).

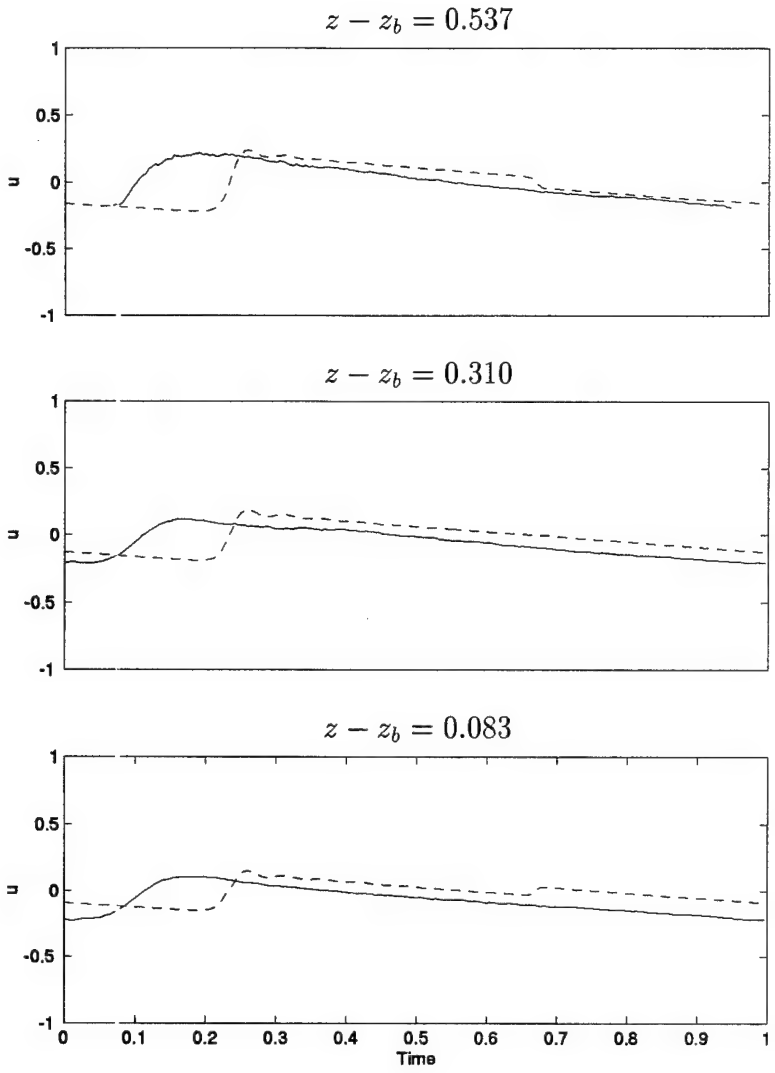

Figure 4.34: Normalized phase-averaged horizontal velocity u at three elevations at measuring line 6; $(z' - z'_b)$ = 1.1, 4.1, 7.1 cm.: Measured(—); Computed(- - -).

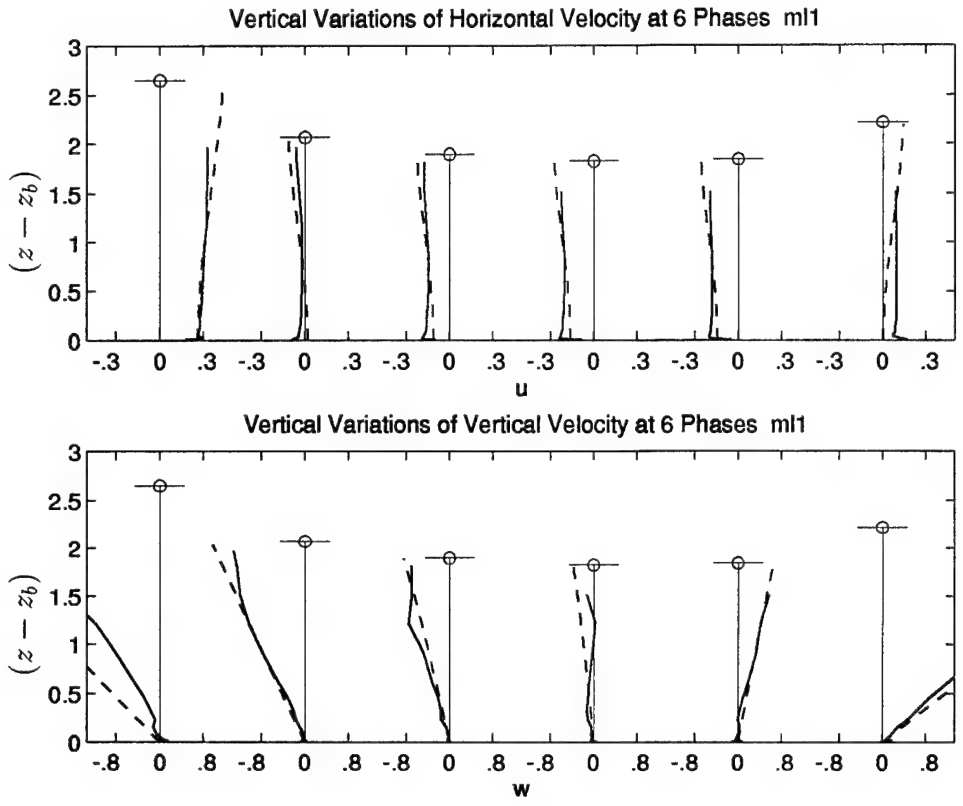

Figure 4.35: Vertical variations of normalized horizontal and vertical velocity at six phases at measuring line 1: Measured(—); Computed(- - -).

discrepiency between the measured and computed vertical variations are caused, in part, by the aforementioned phase mismatch. As a whole, the agreement is reasonable in spite of the simple vertical velocity profile assumed in (2.33) with (2.40). This is probably because the comparison is limited below the wave trough level where the energy dissipation due to wave breaking is expected to occur above the trough level.

For completeness, the cross-shore variation of the maximum, minimum and mean of the free surface, the depth averaged velocity, and the near bottom velocity is depicted in Figure 4.41.

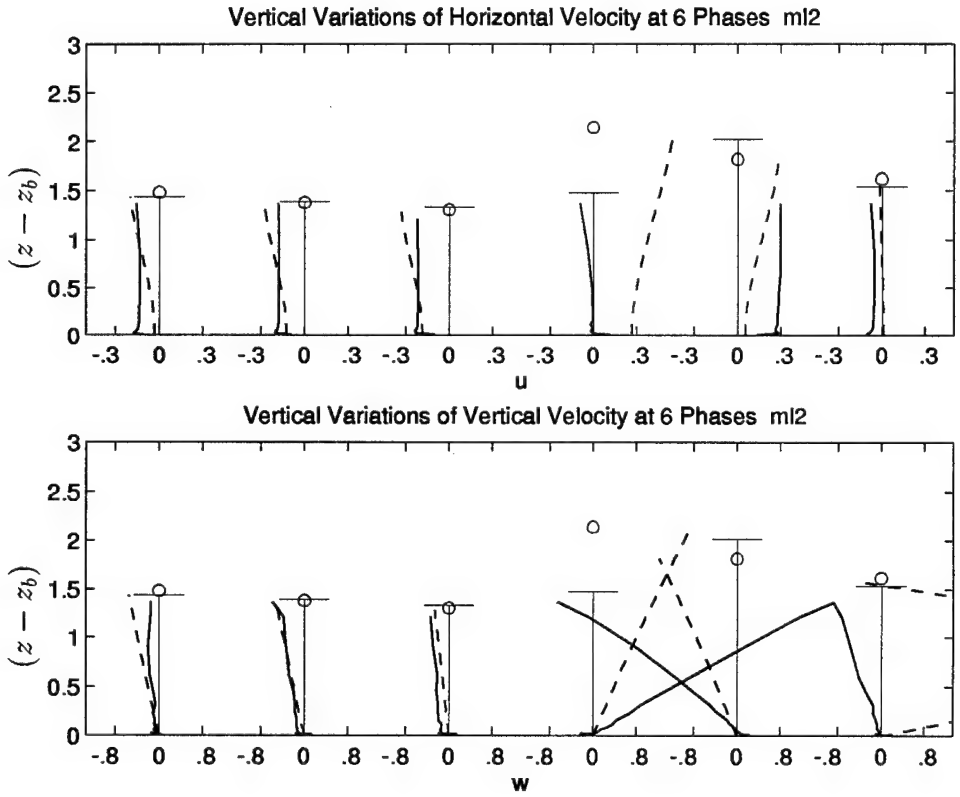

Figure 4.36: Vertical variations of normalized horizontal and vertical velocity at six phases at measuring line 2: Measured(—); Computed(- - -).

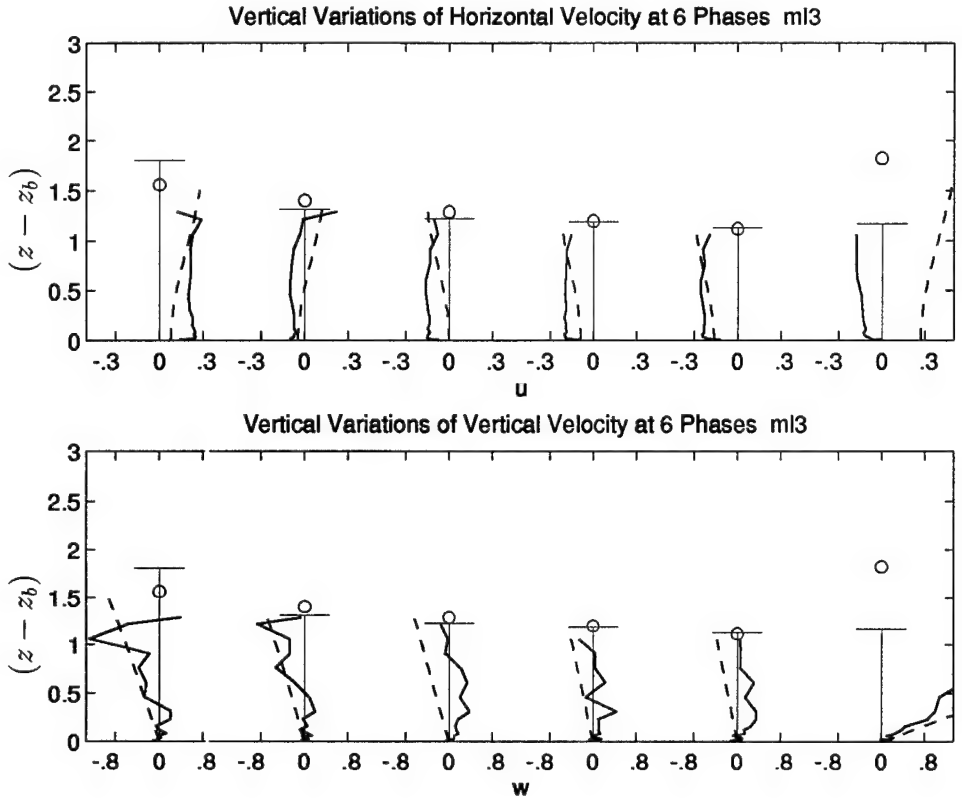

Figure 4.37: Vertical variations of normalized horizontal and vertical velocity at six phases at measuring line 3: Measured(—); Computed(- - -).

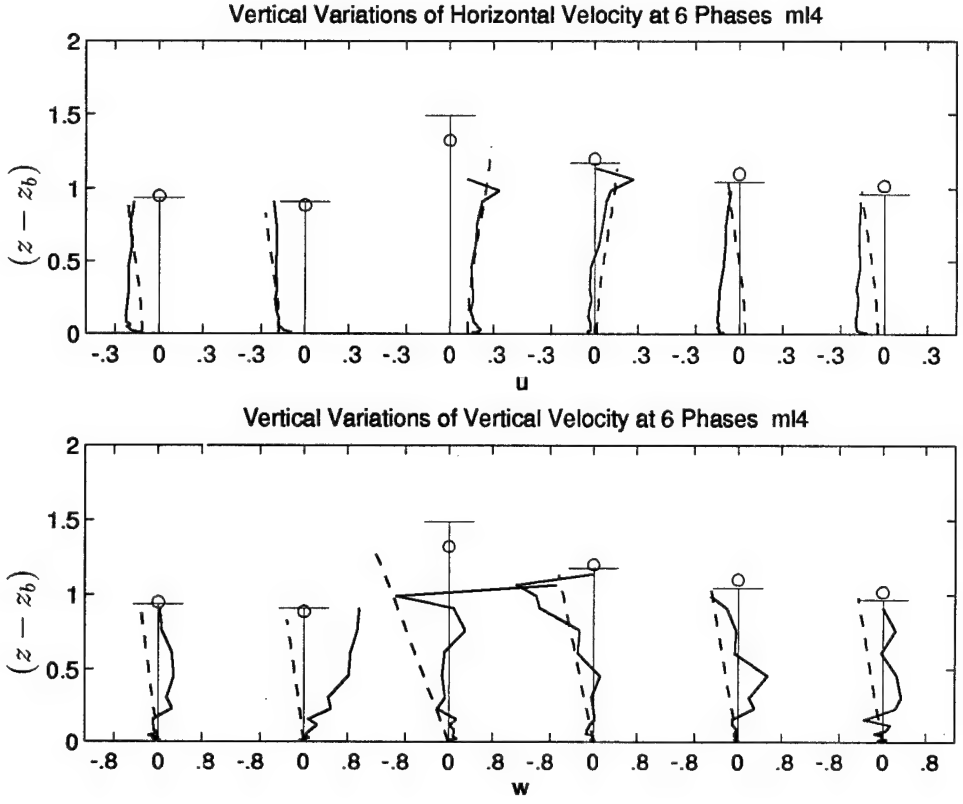

Figure 4.38: Vertical variations of normalized horizontal and vertical velocity at six phases at measuring line 4: Measured(—); Computed(- - -).

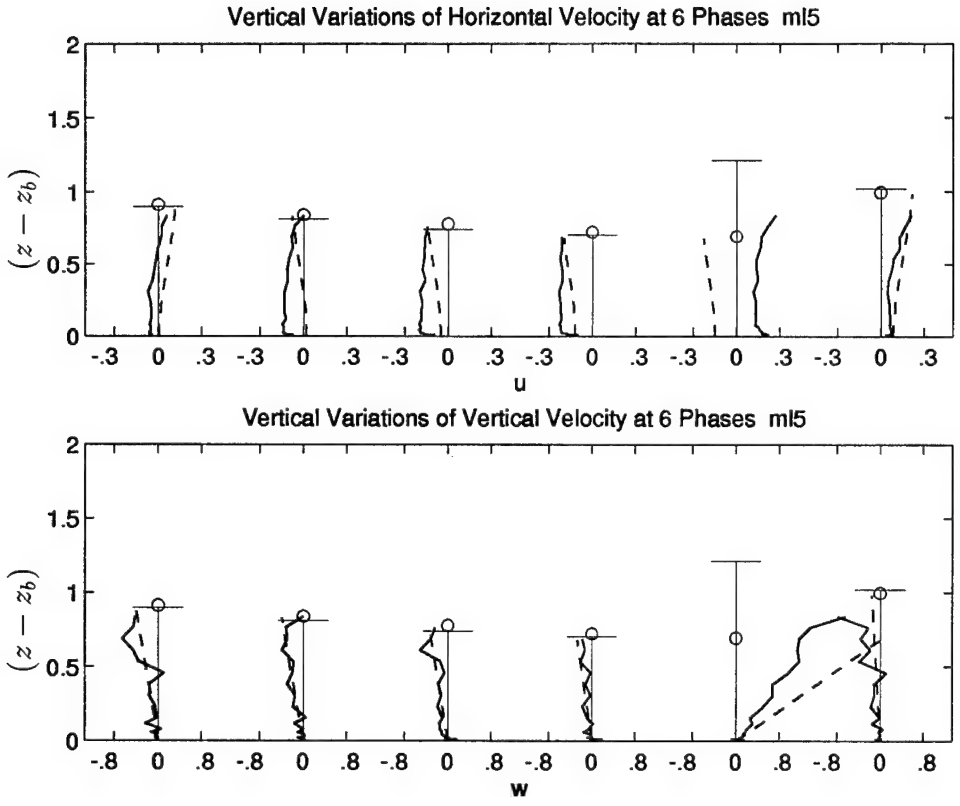

Figure 4.39: Vertical variations of normalized horizontal and vertical velocity at six phases at measuring line 5: Measured(—); Computed(- - -).

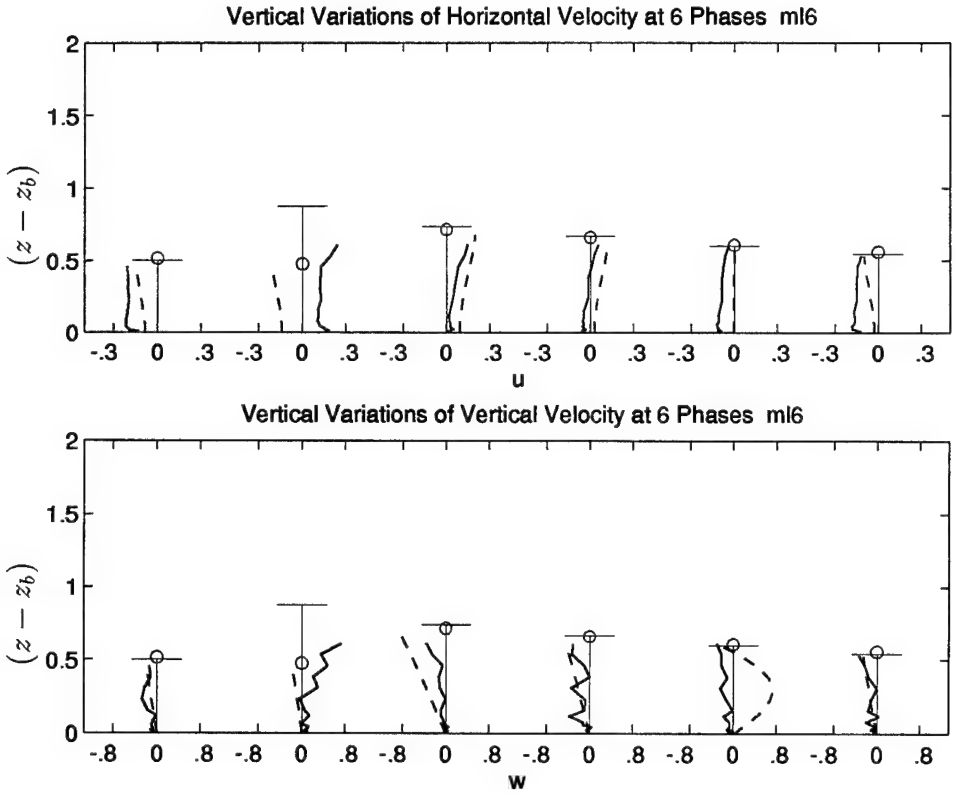

Figure 4.40: Vertical variations of normalized horizontal and vertical velocity at six phases at measuring line 6: Measured(—); Computed(- - -).

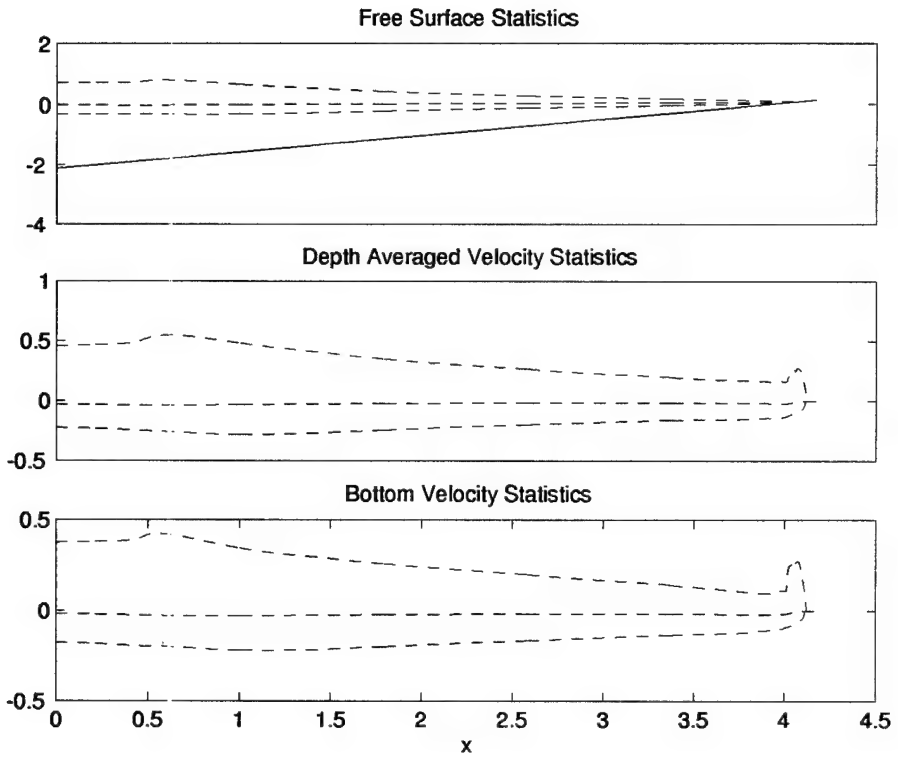

Figure 4.41: Computed cross-shore variation of maximum, minimum, and mean of the normalized free surface elevation, depth averaged velocity, and near bottom velocity.

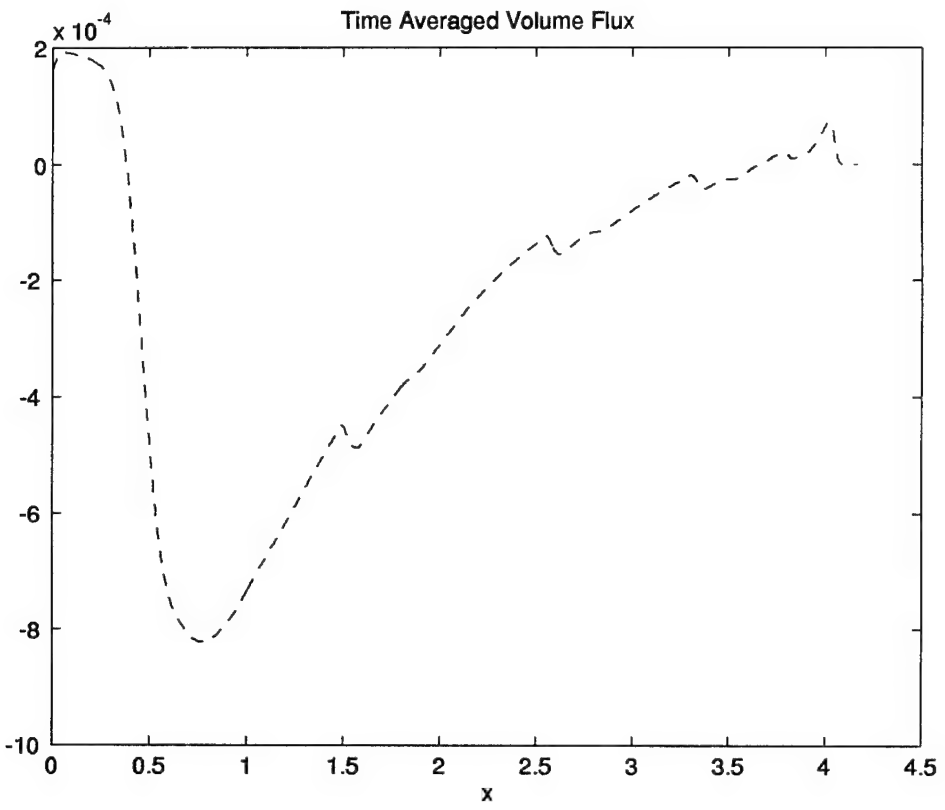

Figure 4.42: Computed cross-shore variation of normalized, time averaged volume flux .

The cross-shore variation of the time averaged volume flux is again used as an indicator of the computational accuracy. Figure 4.42 demonstrates that this flux is zero almost exactly.

The normalized energy quantities are shown in Figure 4.43. The numerical dissipation dominates over the dissipation due to bottom friction and wave breaking as in Section 4.2. This clearly indicates the shortcoming of the assumed velocity profile in (2.33) which may be reasonable below the trough level but can not account for the much larger dissipation occurring above the trough level.

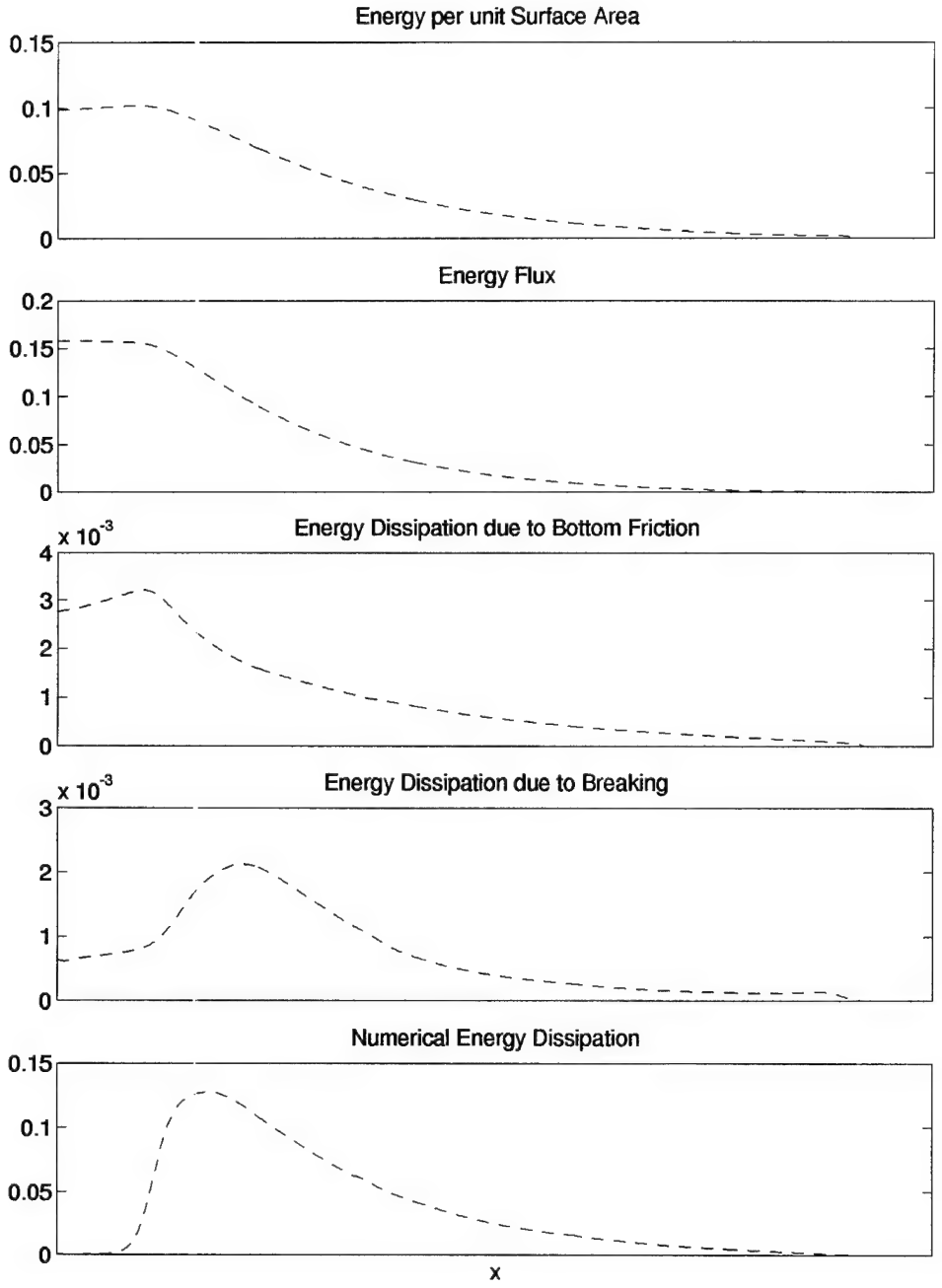

Figure 4.43: Computed cross-shore variation of normalized specific wave energy, energy flux, bottom dissipation, breaking dissipation, and numerical dissipation.

4.3.2 Model Initiation after Breaking

The model VBREAK is compared to the identical set of data as in Section 4.3.1 except with the seaward boundary located at measuring line 3 as depicted in Figure 4.22. The height of the incident regular waves at measuring line 3 was $H' = 12.71$ cm. The corresponding still water depth was 17.71 cm. The Tables 4.8 and 4.9 represent the primary input and output files from the model VBREAK . The resultant dimensionless parameters were: surf similarity parameter $\xi = 0.22$; the ratio of horizontal to vertical length scales $\sigma = 19.3$; Ursell number = 183.0.

Figures 4.44 through 4.60 may be compared with the corresponding figure is Section 4.3.1. As a whole, the agreement between the measured and computed free surface and velocities is somewhat better because VBREAK is initiated at a measuring line landward of the break point and closer to measuring lines 4, 5, and 6. The vertical variation of the horizontal velocity given by (2.33) with (2.40) is assumed to be caused by wave breaking and it is hence more appropriate to take the seaward boundary of VBREAK inside the surf zone.

Table 4.8: Primary input data file (initiated after breaking) for Cox *et al.* (1995).

```
       5                                        --> NLINES
-------------------------------------------------------------------------
L33053                                                        BDJ June '95

SBC at L3; 300 waves input; f'=.05; and IWAVE=3
-------------------------------------------------------------------------
1                                              <--ISYST
3                                              <--IWAVE
1                                              <--IBOT
1                                              <--IENERG
1                                              <--ITEMVA
1                                              <--ISPAEU
J300                                           <--FINP2
250.                 300.                      <--TSTAT,TMAX
310                                            <--STILL
0.001              0.400              1.0      <--DELTA,COURNO,DKAPPA
.1271               2.2                       <--HREF,TREF
66001                                          <--NPINP
3.0                 .10                        <--APROFL,CMIXL
.177143             0.028571                   <--DSEAP,SLSURF
1                                              <--NBSEG
11.400           .028571        .05
66001                                          <--NPOUT
1                                              <--NDELR
0.5
12                                              <--NONODS
1     2     3     60    61
62    120   121   122   180
181   182
5                                              <--NOTIML
299.0       299.25       299.50       299.75       300.0       <--TIMSPA
```

Table 4.9: Primary output file (initiated after breaking) for Cox *et al.* (1995).

```
------------------------------------------------------------------------
L33053                                                          BDJ June

SBC at L3; 300 waves input; f'=.05; and IWAVE=3
------------------------------------------------------------------------

WAVE CONDITION

Measured Total Wave Profile at Seaward Boundary

Reference Wave Period          =     2.200000 sec.
Reference Wave Height          =     0.127100 meters
Depth at Seaward Boundary      =     0.177143 meters
Norm. Depth at Seaw. Bdr.      =     1.394
Included Correction Term   CT
0 = no; 1 = yes        INCLCT  =     0
Normalized Wave Length         =    15.969
"Sigma"                        =    19.328
Ursell Number                  =   182.968
Surf Similarity Parameter      =     0.220
Input Wave Train from Time=0 to TMAX
Computed or Read at Normalized Rate DELTI =     0.004545

Parameters of Vertical Velocity Variations
Cubic Profile Parameter     APROFL =     3.000000
Mixing Length Parameter     CMIXL  =     0.100000
Momentum Flux Coefficient   C2     =     0.548214
Kinetic Energy Flux Coeff.  C3     =    -0.069420
Energy Dissipation Coeff.   CB     =    15.163393
Coefficient of DB           CBL    =     2.930764


BOTTOM GEOMETRY

Norm. Horiz. Length of
      Computation Domain   =     4.632540
Number of Segments         =        1
-------------------------------------------
 SEGMENT    WBSEG(I)   TBSLOP(I)    BFFSEG(I)
       I      meters
-------------------------------------------
       1   11.400000    0.028571    0.050000
```

Table 4.9: – Continued

```
COMPUTATION PARAMETERS

Normalized DX                          =     0.814155D-02
Normalized DELTA                       =     0.100000E-02
Courant Number                         =     0.400
 Must not exceed unity
Numerical Damping Coefficient          =     1.0000
 Must be zero or positive
Normalized Computation Duration  TMAX =   300.000000
Statistical Calculations Start
 when Time is equal to           TSTAT=   250.000000
Total Number of Spatial Nodes    JMAX =      570
Number of Nodes Along Bottom Below SWL
                                 STILL =     310
Storing Temporal Variations from Time = 0
 to TMAX at Normalized Rate     DELTO =     0.004545
Wave Runup Time Series Stored for
                                  NDER =   1 Water Depths
Time Series of ETA, U, and UB
          Stored at             NONODS =      12 Nodes
Spacial Variations of ETA, U, and UB
         Stored at              NOTIML =      5 Time Levels

Maximum time step       =    0.27585E-02
Minimum time step       =    0.14089E-02

REFLECTION COEFFICIENT

ETARRMS/ETAIRMS =     0.019

INCIDENT AND REFLECTED WAVES

            Max           Min          Mean          RMS
Inc.      0.9450       -0.2849       -0.0211       0.2714
Ref.      0.0320        0.0007        0.0169       0.0052

SHORELINE OSCILLATIONS

Largest Node Number Reached by Computational Shoreline
                                          SMAX =      364
-------------------------------------------------------------
      I   DELTAR(I)    RUNUP(I)  RUNDOWN(I)  SETUP(I) RMS(I)
            [cm]         Ru          Rd          Zr      Rrms
-------------------------------------------------------------
      1     0.500       0.165       0.014       0.090      0.031
```

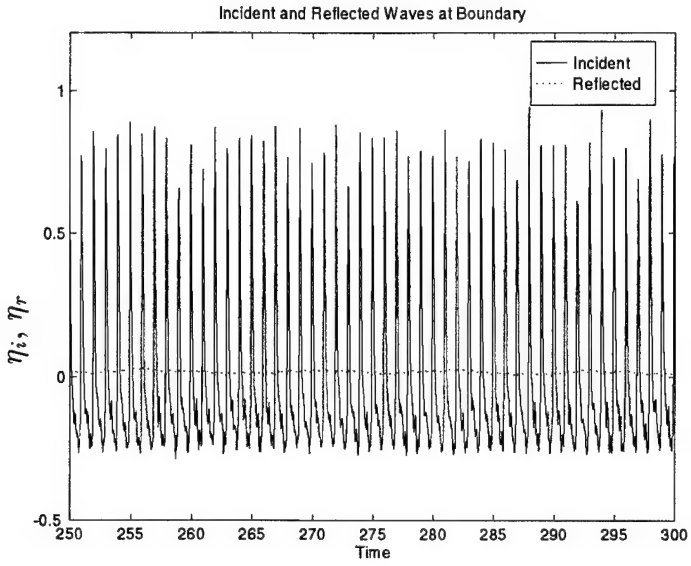

Figure 4.44: The last 50 normalized incident and reflected waves at seaward boundary, measuring line 3.

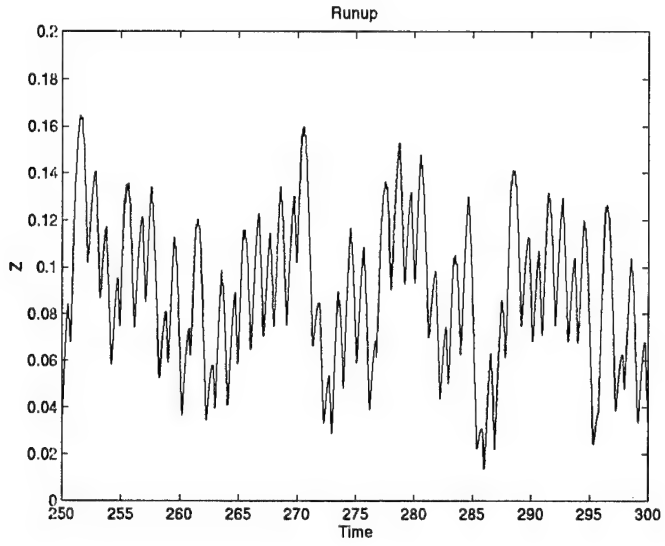

Figure 4.45: Computed normalized time series of runup with $\delta_r' = 0.5$ cm.

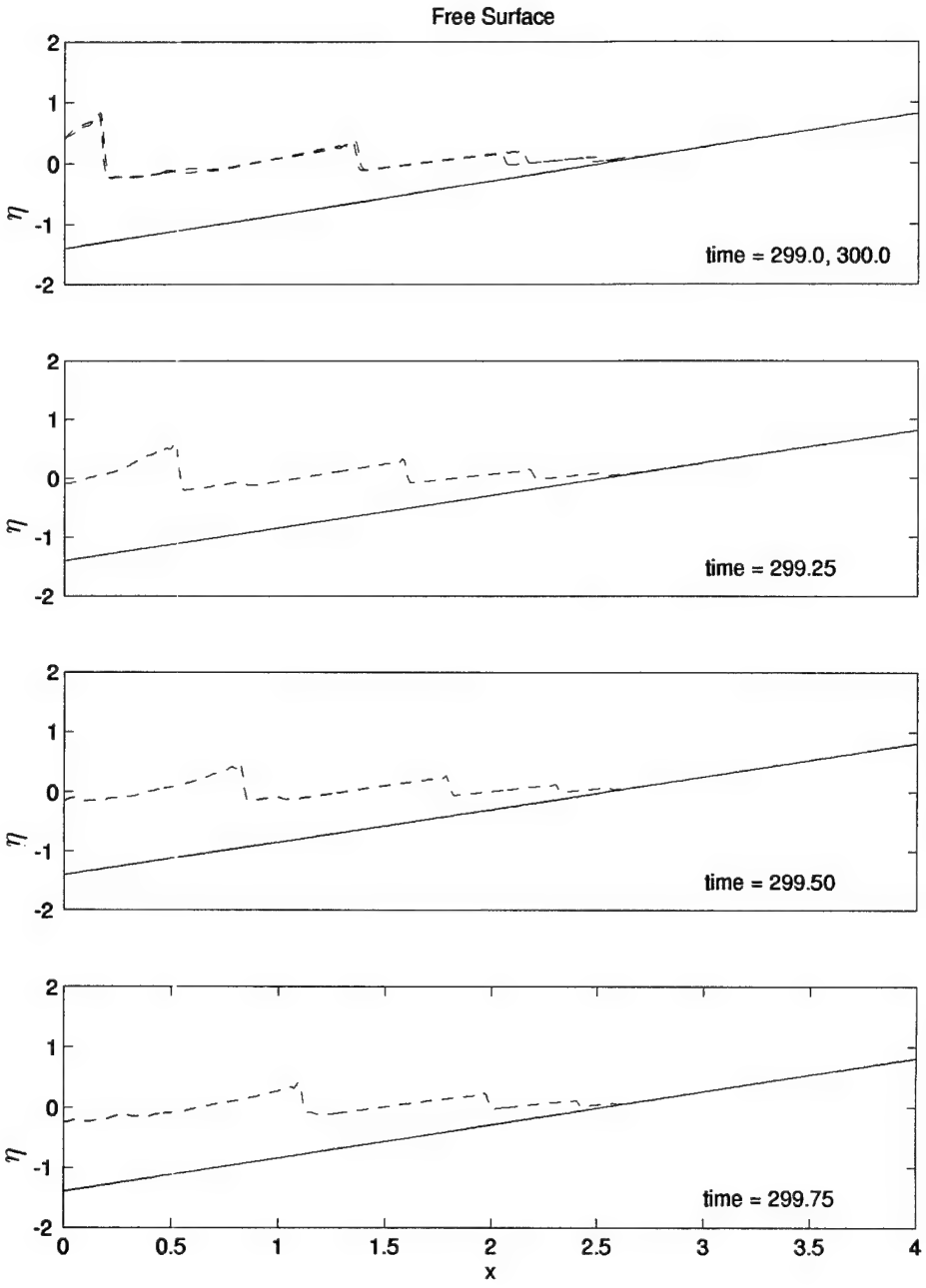

Figure 4.46: Computed cross-shore variation of normalized free surface η at 5 time levels, $t = 299.00$, 299.25, 299.50, 299.75, and 300.

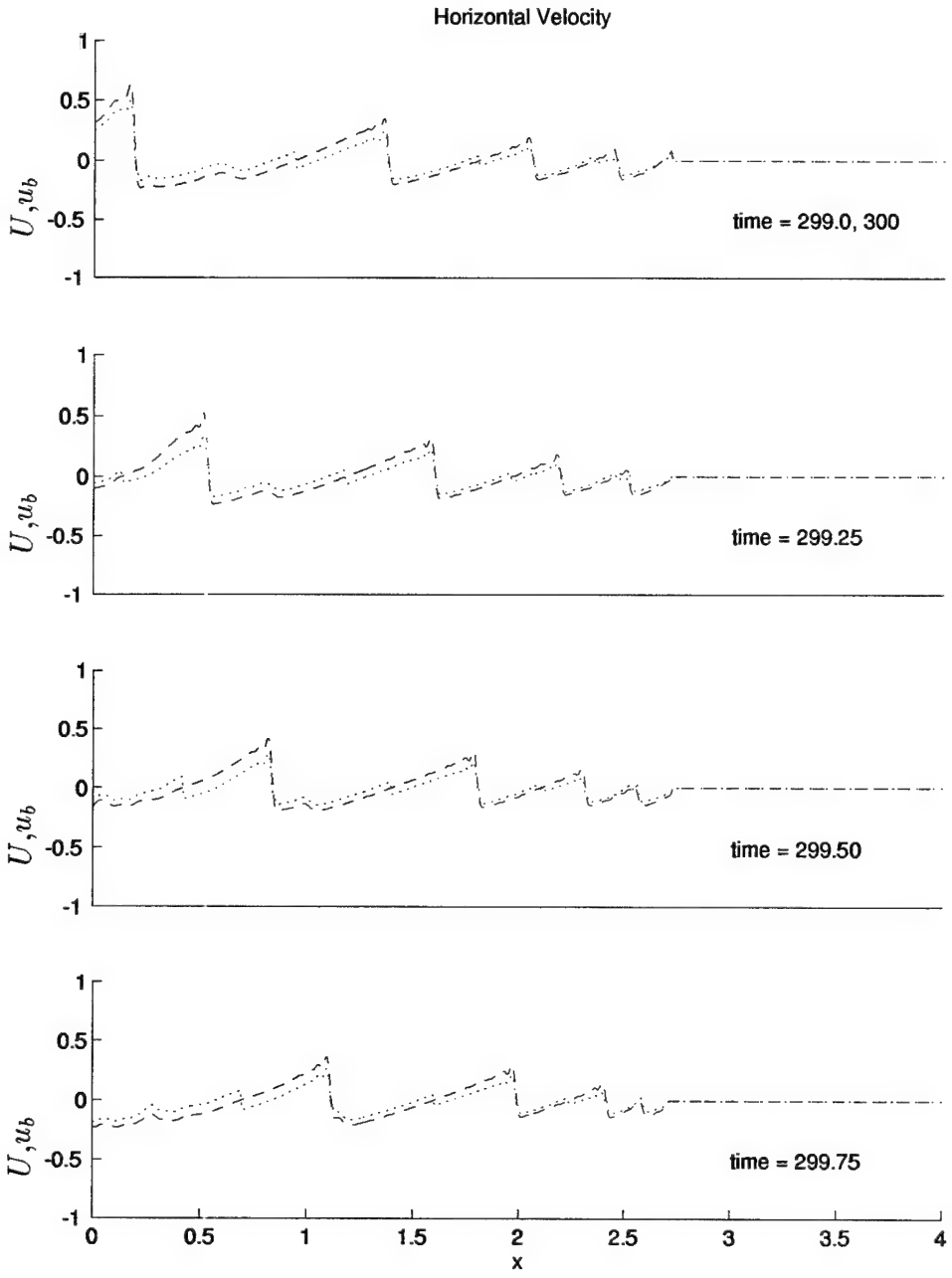

Figure 4.47: Computed normalized cross-shore depth averaged velocity U and near bottom velocity u_b at 5 time levels, $t = 299.00$, 299.25, 299.50, 299.75, and 300: U (- - -); u_b ($\cdots$).

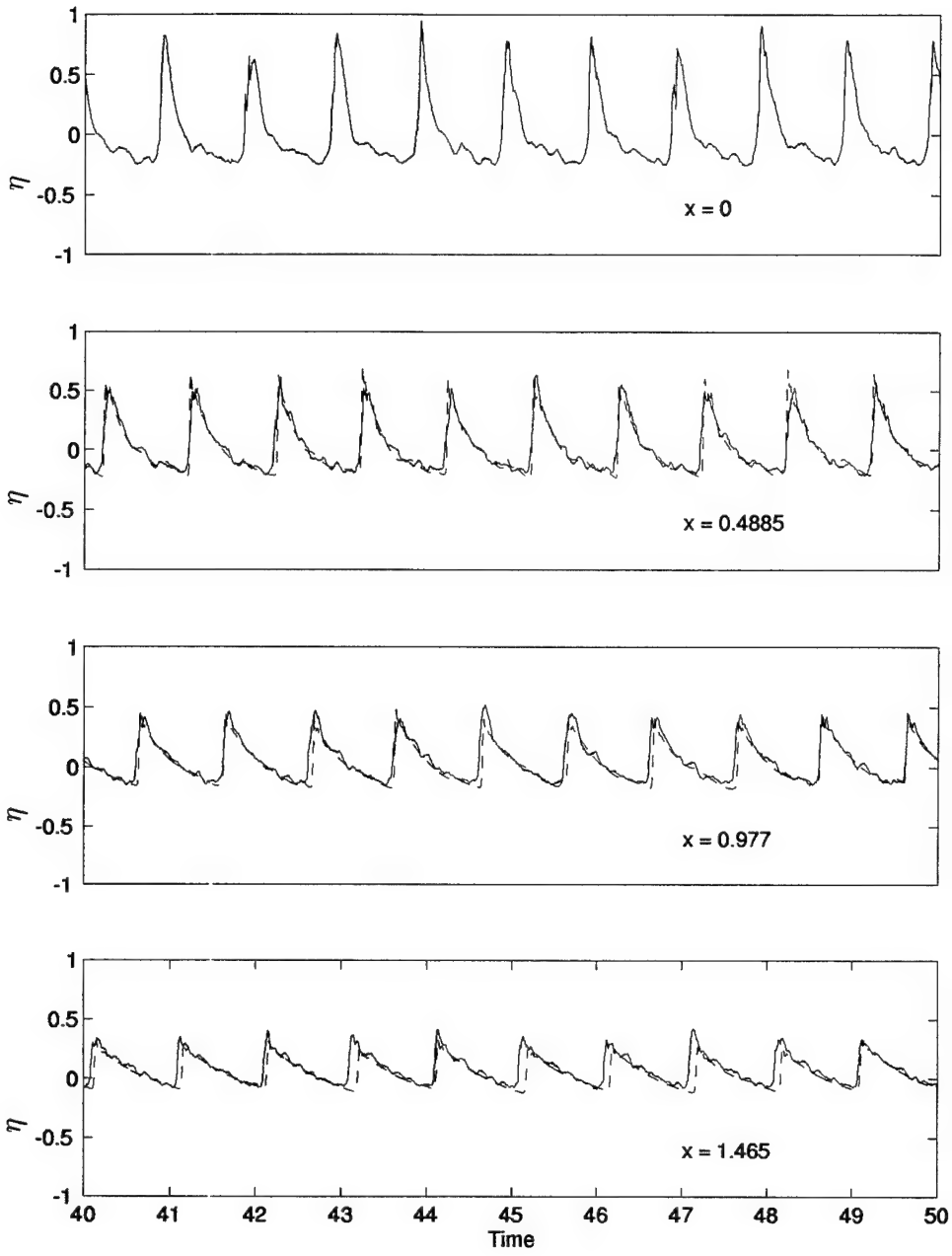

Figure 4.48: Measured and computed time series for the last ten waves of the normalized free surface at four measuring lines: Measured(—); Computed(- - -).

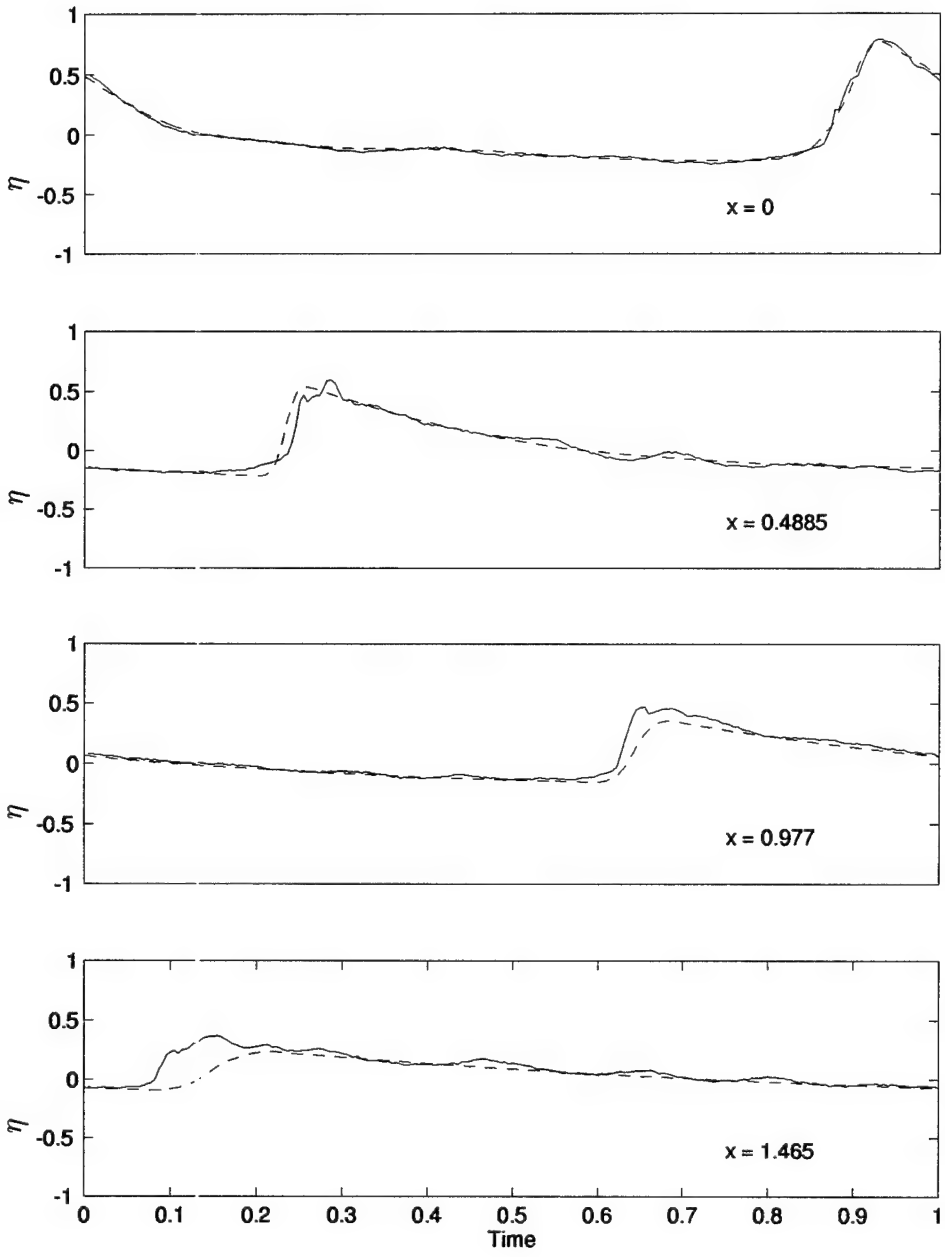

Figure 4.49: Time series of the phase-averaged, normalized free surface at four measuring lines: Measured(—); Computed(- - -).

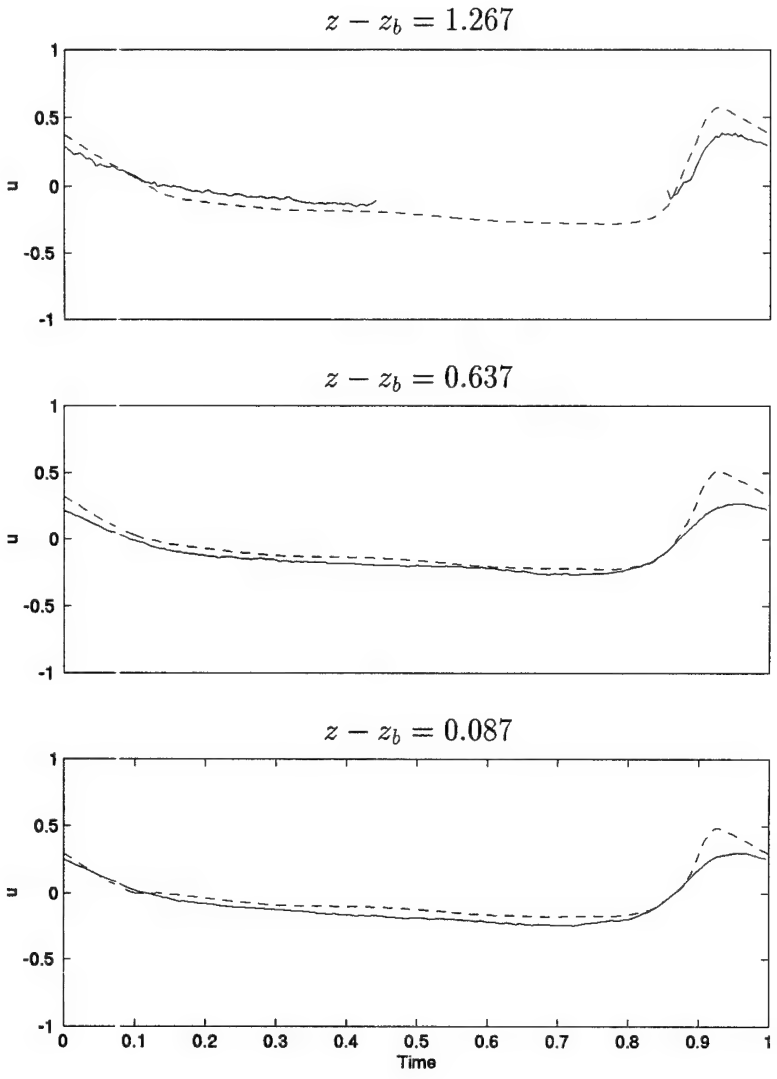

Figure 4.50: Normalized phase-averaged horizontal velocity u at three elevations at measuring line 3; $(z' - z'_b) = 1.1$, 8.1, 16.1 cm.: Measured(—); Computed(- - -).

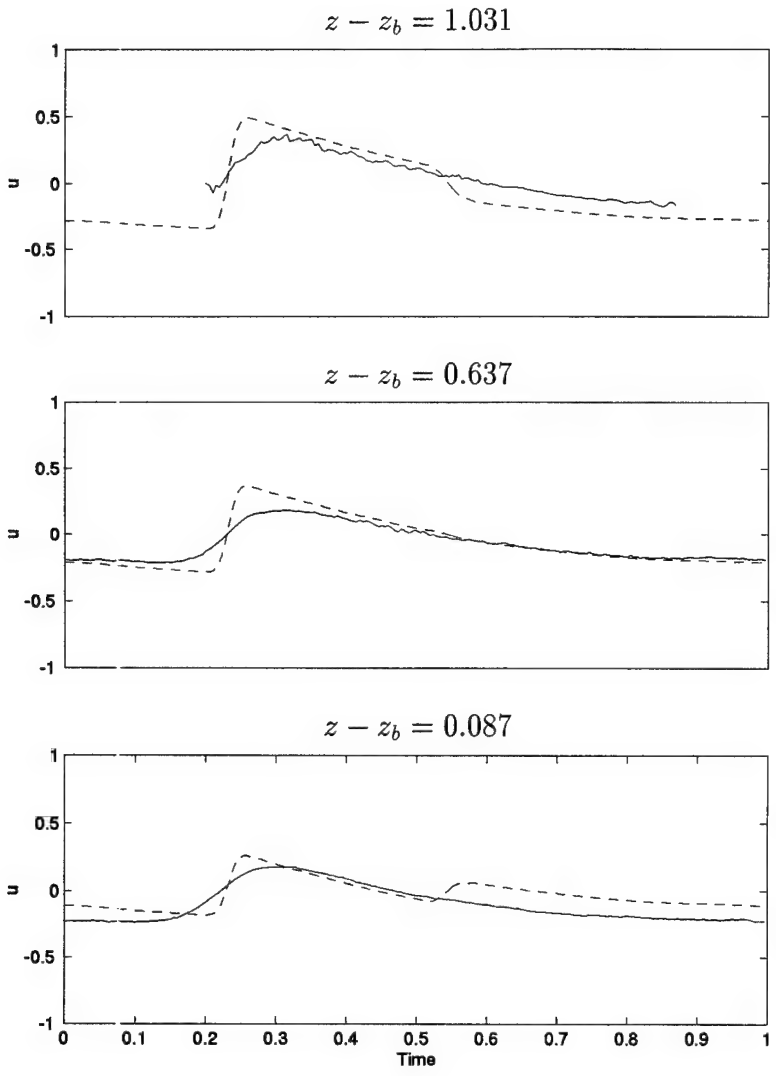

Figure 4.51: Normalized phase-averaged horizontal velocity u at three elevations at measuring line 4; $(z' - z'_b) = 1.1$, 8.1, 13.1 cm.: Measured(—); Computed(- - -).

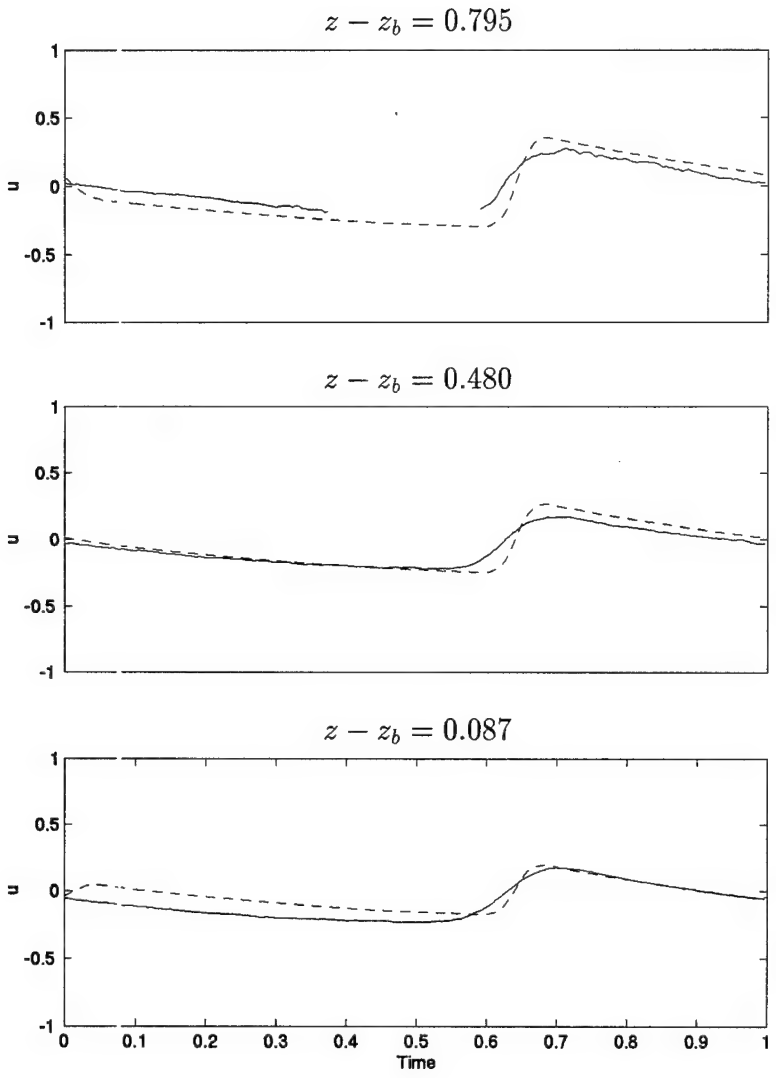

Figure 4.52: Normalized phase-averaged horizontal velocity u at three elevations at measuring line 5; $(z' - z_b') = 1.1$, 6.1, 10.1 cm.: Measured(—); Computed(- - -).

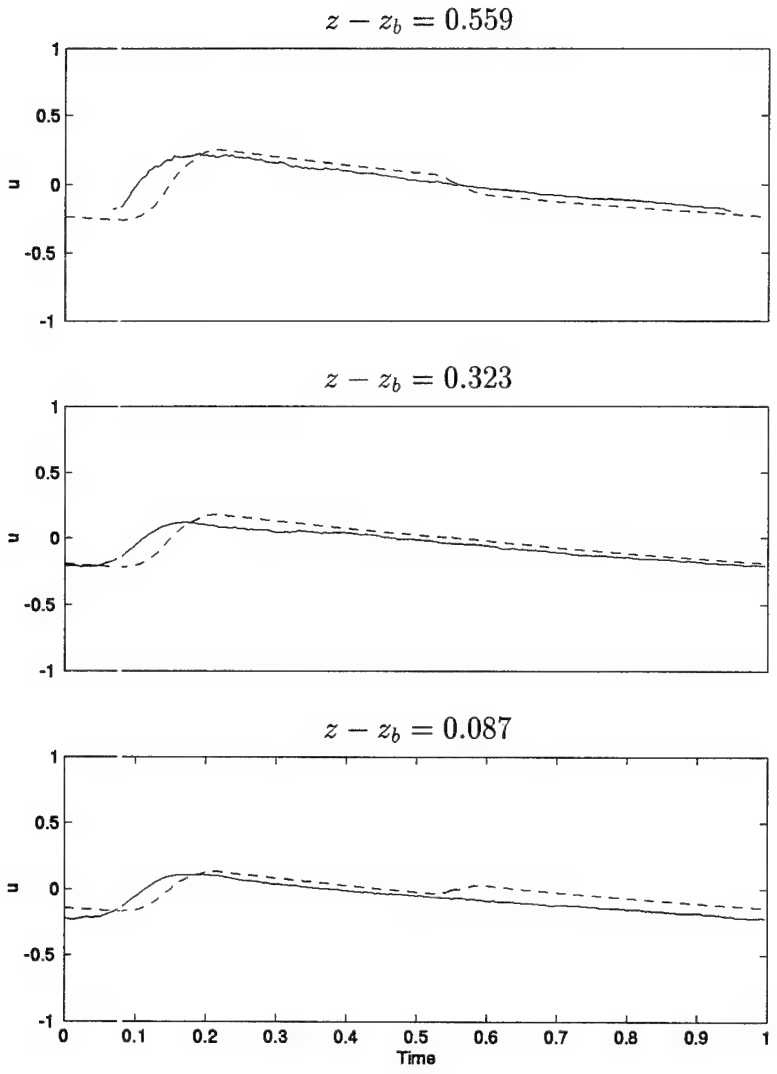

Figure 4.53: Normalized phase-averaged horizontal velocity u at three elevations at measuring line 6; $(z' - z'_b) = 1.1,\ 4.1,\ 7.1$ cm.: Measured(—); Computed(- - -).

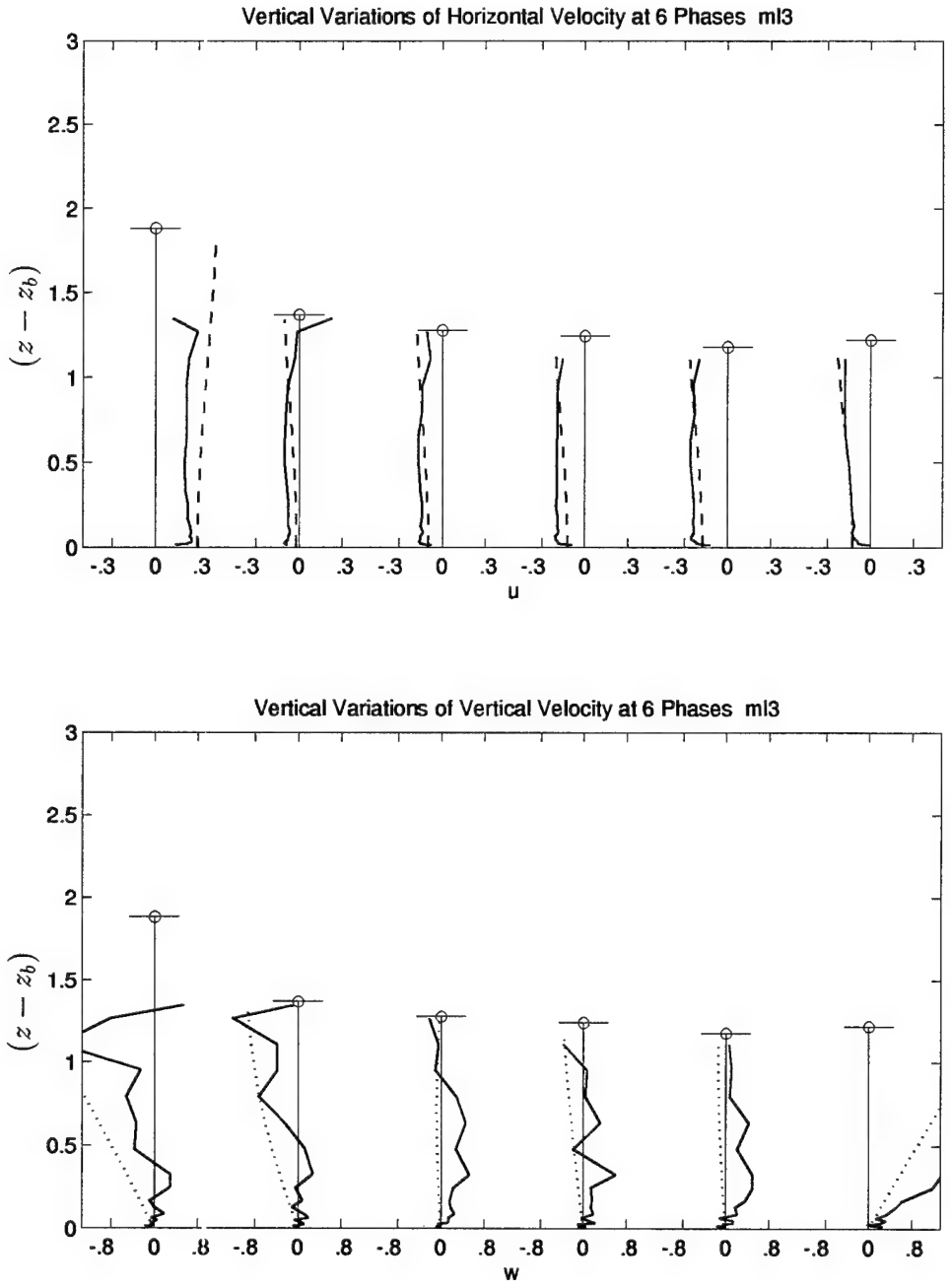

Figure 4.54: Vertical variations of normalized horizontal and vertical velocity at six phases at measuring line 3: Measured(—); Computed(- - -).

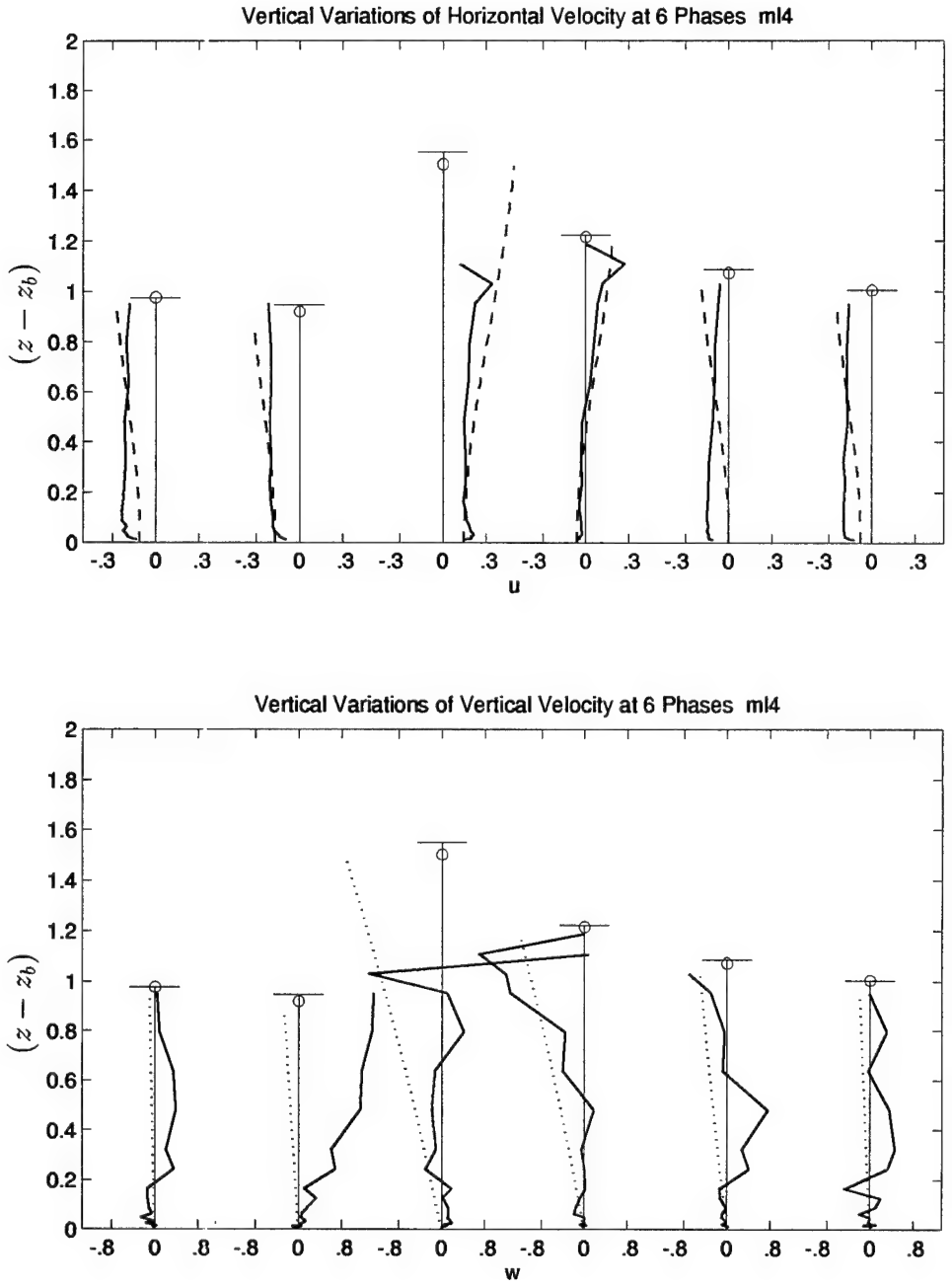

Figure 4.55: Vertical variations of normalized horizontal and vertical velocity at six phases at measuring line 4: Measured(—); Computed(- - -).

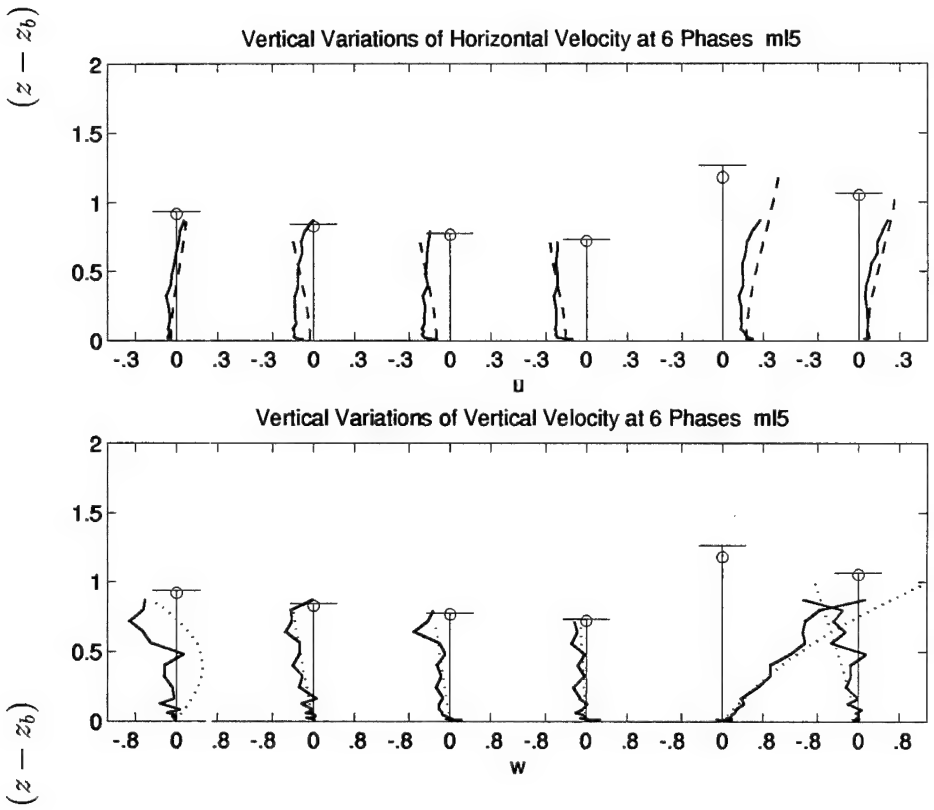

Figure 4.56: Vertical variations of normalized horizontal and vertical velocity at six phases at measuring line 5: Measured(—); Computed(- - -).

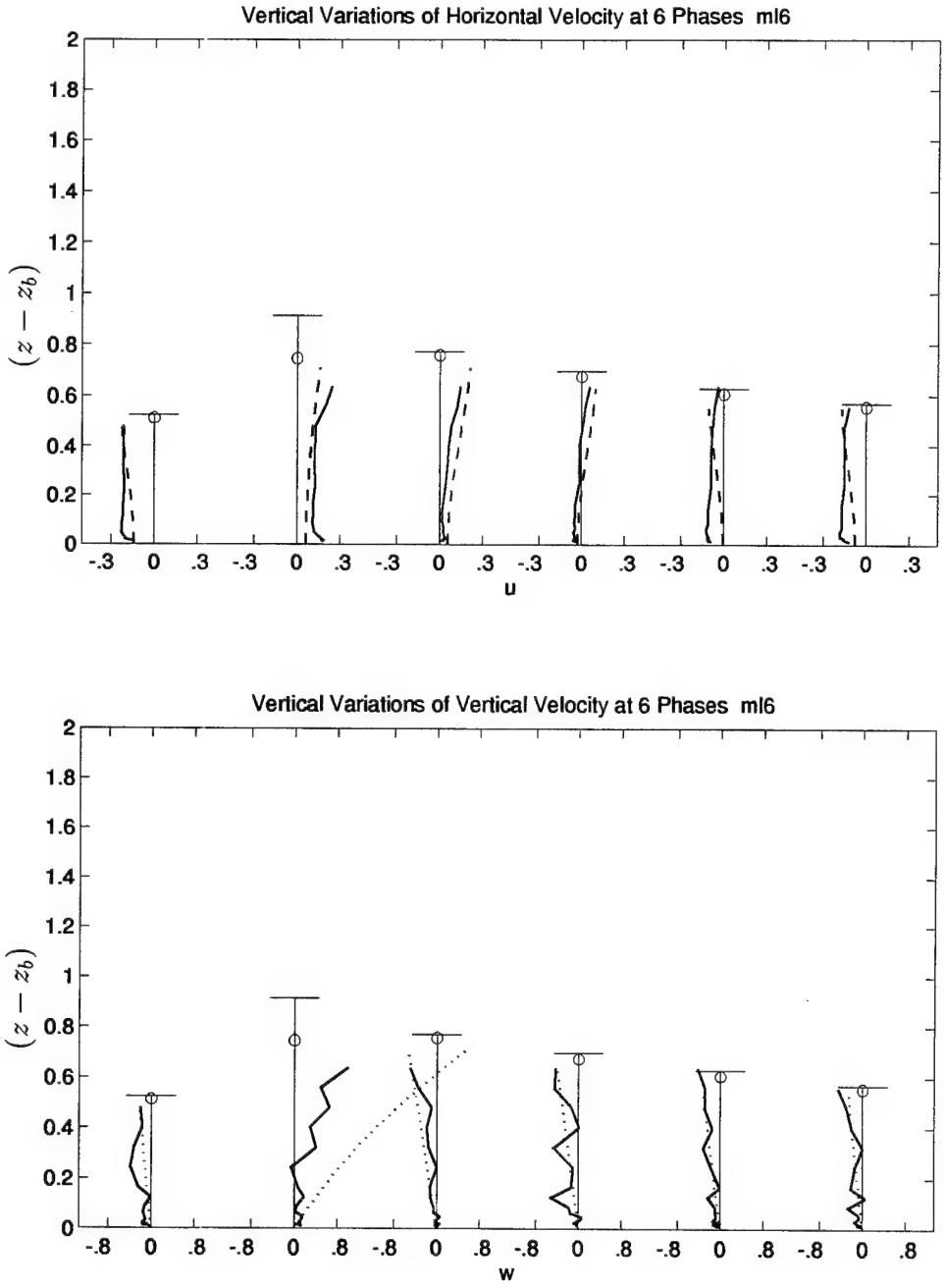

Figure 4.57: Vertical variations of normalized horizontal and vertical velocity at six phases at measuring line 6: Measured(—); Computed(- - -).

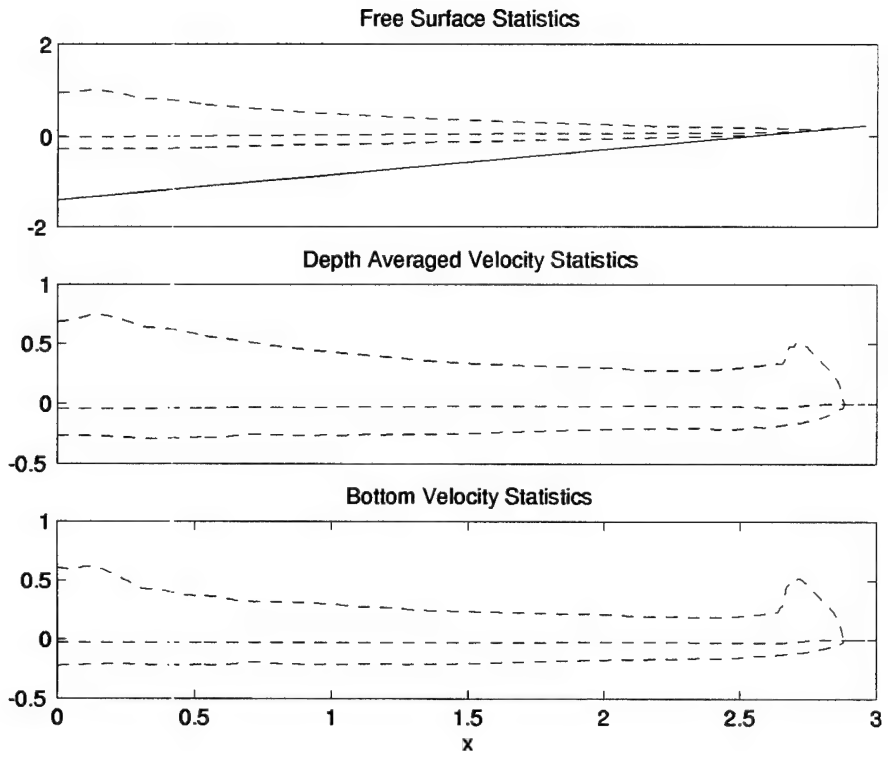

Figure 4.58: Computed cross-shore variation of maximum, minimum, and mean of the normalized free surface elevation, depth averaged velocity, and near bottom velocity.

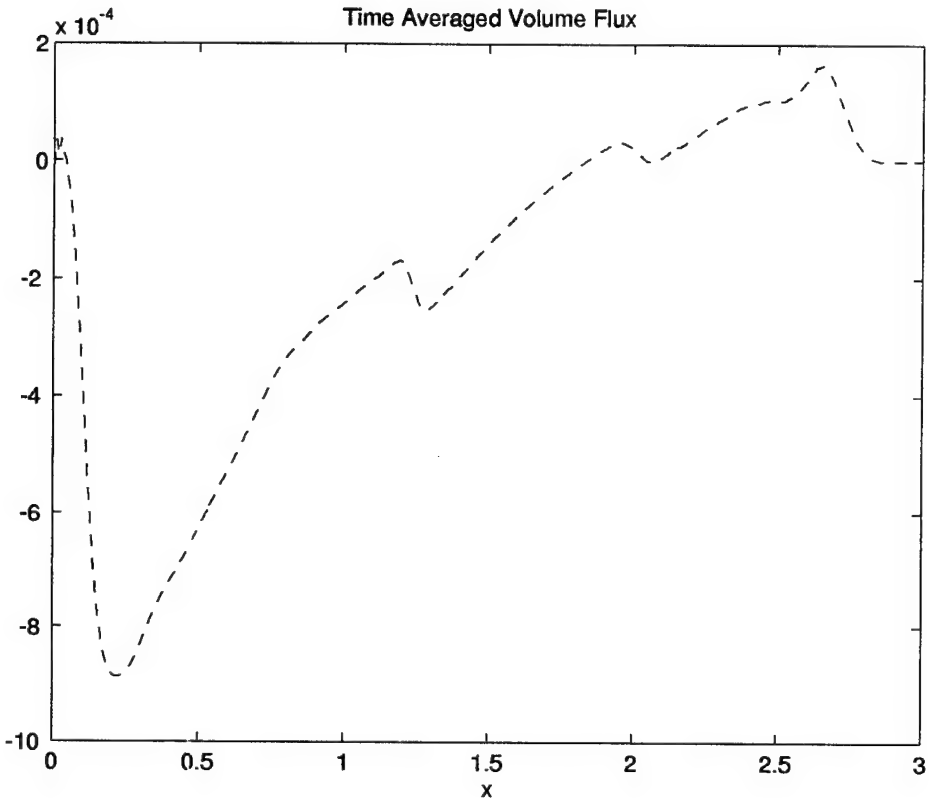

Figure 4.59: Computed cross-shore variation of normalized, time averaged volume flux .

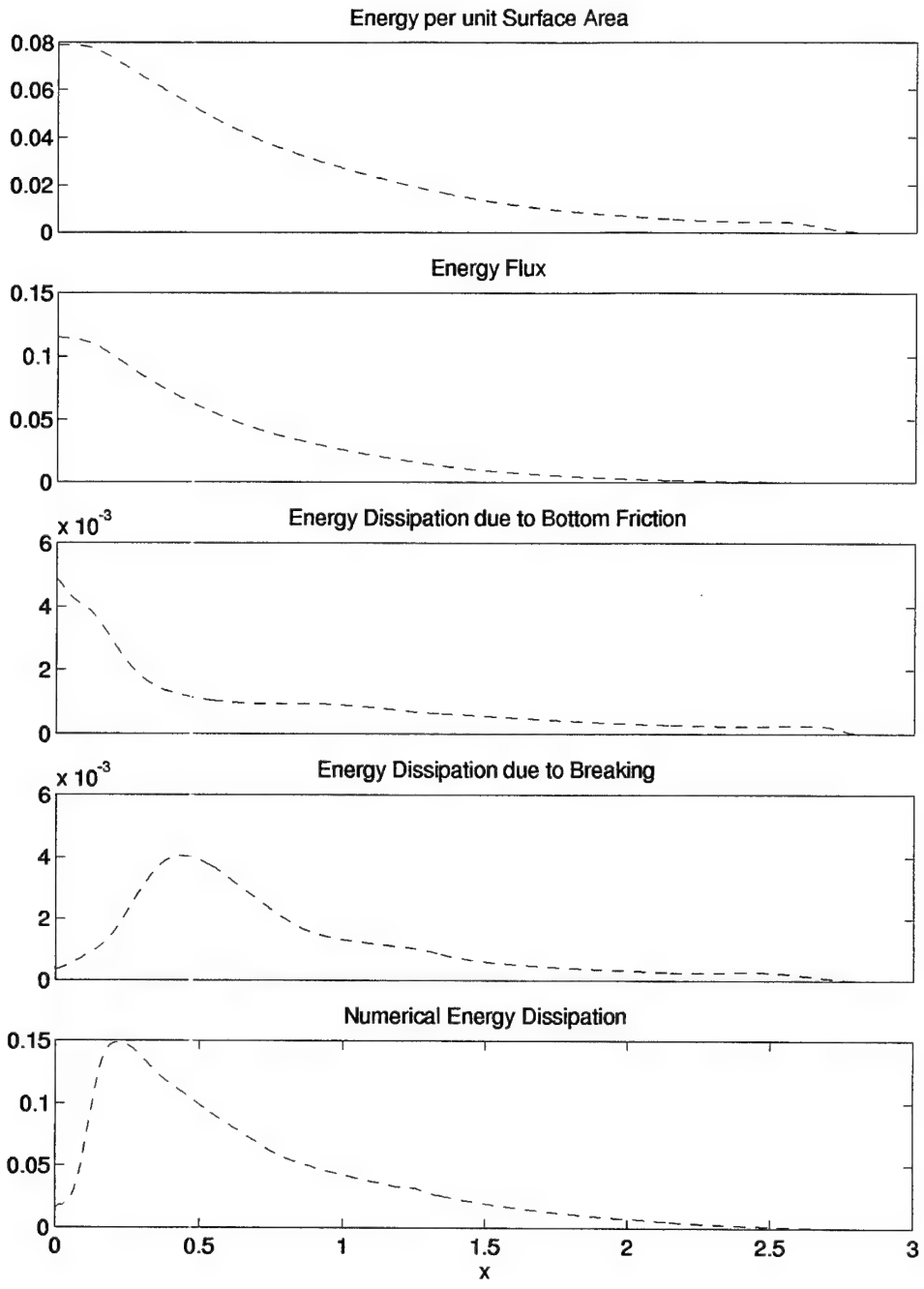

Figure 4.60: Computed cross-shore variation of normalized specific wave energy, energy flux, bottom dissipation, breaking dissipation, and numerical dissipation.

Chapter 5

CONCLUSIONS

The numerical model VBREAK is developed to predict the cross-shore and temporal variations of the free surface elevation η, the depth-averaged horizontal velocity U, and the near-bottom horizontal velocity correction $\tilde{u}_b$ associated with the momentum flux correction m due to the vertical variation of the horizontal velocity u under the action of normally incident breaking waves. The three governing equations required for the computation of the three unknown variables are the depth-integrated continuity and horizontal momentum equations together with the new equation for the momentum flux correction m derived from the depth-integrated wave energy equation.

The normalized vertical profile of the horizontal velocity u outside the thin wave boundary layer is assumed to be cubic on the basis of limited available data. The turbulent shear stress outside the wave boundary layer is assumed to be expressed using the turbulent eddy viscosity whose mixing length is proportional to the instantaneous water depth. Although two additional empirical parameters are introduced in relation to these assumptions, the computed vertical profiles of the horizontal velocity are found to be fairly insensitive to these empirical parameters in their ranges expected from limited available data.

The numerical model VBREAK is reduced to a one-dimensional model and compared to the previously developed model IBREAK. With appropriate simplification of the seaward boundary condition, the momentum flux correction equals

zero identically throughout the computation domain for all times. The computed results of the one-dimensional model corresponding to VBREAK are essentially the same as the results of IBREAK for the steep slope case. The comparison of the models demonstrates the efficiency and accuracy of the MacCormack method in the solution of the finite-amplitude shallow-water equations.

The model VBREAK is compared with the laboratory data presented by Stive (1980) and Stive and Wind (1982). The free surface statistics are predicted reasonably accurately. The computed minimum horizontal velocities at several vertical locations under the wave trough compare well with the measured data. The maximum horizontal velocities, however, are consistently overpredicted. The time-averaged seaward return current is predicted to within the order of magnitude only. Despite the explicit modeling of energy dissipation due to wave breaking, most of the energy is dissipated numerically. The assumed velocity profile does not describe well the wave energy dissipation due to breaking on a gentle slope. This is probably due to the absence of a surface roller in the model VBREAK to increase the energy dissipation due to wave breaking and the shoreward mass flux above the trough level.

The model VBREAK is compared with the detailed fluid velocity measurements of Cox *et al.* (1995). VBREAK predicts the general free surface characteristics well. The laboratory data of Cox included phase information and is used to asses the phase speed predictions of VBREAK. The computed phase speed exceeds the measured speed seaward of the break point. Following wave breaking, however, VBREAK underpredicts the phase speed. The computed horizontal velocities compare reasonably well with the data except that differences in phase generate errors, especially near the wave crest. The agreement with the data improves somewhat when the seaward boundary of VBREAK is taken to be landward of the break point because the vertical horizontal velocity variation in VBREAK is assumed to

be caused by wave breaking. The discontinuity in the bottom velocity correction that accompanies the sign change in the depth averaged velocity generates an unrealistic kink in the time series of the horizontal velocity. As a whole, the agreement is reasonable considering the assumed simple vertical velocity profile.

REFERENCES

Ahrens, J.P., 1975. "Large wave tank tests of riprap stability." *Technical Memo No. 51*, U.S. Army Coastal Engineering Research Center, Ft. Belvoir, VA

Anderson, D.A., Tannehill, J.C., and Pletcher, R.H., 1984. *Computational fluid mechanics and heat transfer.* Hemisphere, New York, NY

Battjes, J.A., 1974. "Surf similarity." *Proc. 14th Coast. Engrg. Conf.*, ASCE, 466–480.

Chaudhry, M.H., 1993. *Open-channel flow.* Prentice Hall, Englewood Cliffs, NJ

Cox, D.T., Kobayashi, N., and Okayasu, A., 1994. "Vertical variations of fluid velocities and shear stress in surf zones." *Proc. 23rd Coast. Engrg. Conf.*, ASCE, 98–112.

Cox, D.T., Kobayashi, N., and Okayasu, A., 1995. "Experimental and numerical modeling of surf zone hydrodynamics." *Res. Rept. No. CACR-95-07*, Ctr. for Applied Coast. Res., Univ. of Delaware, Newark, DE.

Fennema, R.J., and Chaudhry, M.H., 1986. "Explicit numerical schemes for unsteady free-surface flows with shocks." *Water Resources Res.*, **22**(13), 1923–1930.

Gharangik, A.M., and Chaudhry, M.H., 1991. "Numerical simulation of hydraulic jump." *J. Hydraulic Engrg.*, ASCE, **117**(9), 1195–1211.

Heitner, K.L., and Housner, G.W., 1970. "Numerical model for tsunami run-up." *J. Wtrwy. Port, Coast. and Oc. Engrg.*, ASCE, **96**(3), 701–719.

Jameson, A., Schmidt, W., and Turkel, E., 1981. "Numerical solutions of the Euler equations by finite volume methods using Runge-Kutta time-stepping schemes." *Proc. AIAA 14th Fluid and Plasma Dynamics Conf.*, Am. Inst. Aeronaut. and Astronaut., 81–1259.

Johnson, B.D., 1996. "Formulation and validation of vertically two-dimensional shallow-water wave model." *Master's thesis, University of Delaware.*

Johnson, B.D., Koyayashi, N., and Cox, D.T., 1996. "Formulation and validation of vertically two-dimensional shallow-water wave model." *Proc. 25rd Coast. Engrg. Conf.*, ASCE, (accepted)

Jonsson, I.G., 1966. "Wave boundary layers and friction factors." *Proc. 10th Coast. Engrg. Conf.*, ASCE, **1**, 127–148.

Jonsson, I.G., and Carlsen, N.A., 1976. "Experimental and theoretical investigations in an oscillatory turbulent boundary layer." *J. Hydraul. Res.*, **14**, 45–60.

Kobayashi, N., and Otta, A.K., 1987. "Hydraulic stability analysis of armor units." *J. Wtrwy. Port, Coast. and Oc. Engrg.*, ASCE, **113**(2), 171–186.

Kobayashi, N., Otta, A.K., and Roy, I., 1987. "Wave reflection and run-up on rough slopes." *J. Wtrwy. Port, Coast. and Oc. Engrg.*, ASCE, **113**(3), 282–298.

Kobayashi, N., DeSilva, G.S., and Watson, K.D., 1989. "Wave transformation and swash oscillation on gentle and steep slopes." *J. Geophys. Res.*, **94**(C1), 951–966.

Kobayashi, N., and Wurjanto, A., 1989. "Numerical model for design of impermeable coastal structures." *Res. Rept. No. CE-89-75*, Ctr. for Applied Coast. Res., Univ. of Delaware, Newark, DE.

Kobayashi, N., Cox, D.T., and Wurjanto, A., 1990. "Irregular wave reflection and run-up on rough impermeable slopes." *J. Wtrwy. Port, Coast. and Oc. Engrg.*, ASCE, **116**(6), 708–726.

Kobayashi, N., and Wurjanto, A., 1992. "Irregular wave setup and run-up on beaches." *J. Wtrwy. Port, Coast. and Oc. Engrg.*, ASCE, **118**(4), 368–386.

Kobayashi, N., and Raichle, A.W., 1994. "Irregular wave overtopping of revetments in surf zones." *J. Wtrwy. Port, Coast. and Oc. Engrg.*, ASCE, **120**(1), 56–73.

Kobayashi, N., and Poff, M.T., 1994. "Numerical model RBREAK2 for random waves on impermeable coastal structures and beaches." *Res. Rept. No. CACR-94-12*, Ctr. for Applied Coast. Res., Univ. of Delaware, Newark, DE.

Kobayashi, N., and Karjadi, E.A., 1994. "Swash dynamics under obliquely incident waves." *Proc. 24th Coast. Engrg. Conf.*, ASCE, 2155–2169.

Kobayashi, N., and Karjadi, E.A., 1995. "Obliquely incident irregular waves in surf and swash zones." *J. Geophys. Res.*, **101**(C3), 6527–6542.

MacCormack, R.W., 1969. "The effect of viscosity in hypervelocity impact cratering." *Paper 69-354*, Am. Inst. of Aeronaut. and Astronaut., New York.

Madsen, P.A., and Svendsen, I.A., 1983. "Turbulent bores and hydraulic jumps." *J. Fluid Mech.*, **129**, 1–25.

Press, W.H., Flannery, B.P., Teukolsky, S.A., and Vetterling, W.T., 1986. *Numerical recipes: The art of scientific computing.* Cambridge Univ. Press, Cambridge, U.K.

Raubenheimer, B., Guza, R.T., Elgar, S., and Kobayashi, N., 1995. "Swash on a gently sloping beach." *J. Geophys. Res.*, **100**(C5), 8751–8760.

Rodi, W., 1980. "Turbulence models and their application in hydraulics." *Intl. Assoc. Hydraul. Res.*, Delft, the Netherlands.

Schäffer, H.A., Deigaard, R., and Madsen, P., 1992. "A two-dimensional surf zone model based on the Boussinesq equations." *Proc. 23rd Coast. Engrg. Conf.*, ASCE, **1**, 576–589.

Stive, M.J.F., 1980. "Velocity and pressure field of spilling breakers." *Proc. 17th Coast. Engrg. Conf.*, ASCE, 547–566.

Stive, M.J.F., and Wind, H.G., 1982. "A study of radiation stress and set-up in the nearshore region." *J. Coast. Engrg.*, **6**, 1–25.

Svendsen, I.A., 1984. "Mass flux and undertow in a surf zone." *J. Coast. Engrg.*, **8**, 347–365.

Svendsen, I.A., and Madsen, P.A., 1984. "A turbulent bore on a beach." *J. Fluid Mech.*, **148**, 73–96.

Tørum, A., 1994. "Wave-induced forces on armor unit on berm breakwaters." *J. Wtrwy. Port, Coast. and Oc. Engrg.*, ASCE, **120**(3), 251–268.

Wurjanto, A., and Kobayashi, N., 1991. "Numerical model for random waves on impermeable coastal structures and beaches." *Res. Rept. No. CACR-91-05*, Ctr. for Applied Coast. Res., Univ. of Delaware, Newark, DE.

Zelt, J.A., 1991. "The run-up of nonbreaking and breaking solitary waves." *J. Coast. Engrg.*, **15**, 205–246.